

**ATOMIC PROCESSES IN HOT PLASMAS
AND X-RAY EMISSION**

T. KATO

**INSTITUTE OF PLASMA PHYSICS
NAGOYA UNIVERSITY**

NAGOYA, JAPAN

This document is prepared as a preprint or compilation of atomic data for fusion research sponsored fully or partly by the IPP/Nagoya University. This is intended for future publication in a journal or will be included in a data book after some evaluations or rearrangements of its contents. Extracts or references of this documents should not be published prior to publication of the original, without the agreement of the authors.

IPPJ-AM-4

ATOMIC PROCESSES IN HOT PLASMAS AND X-RAY EMISSION

Takako Kato

Institute of Plasma Physics, Nagoya University, Nagoya

April 1978

Equiries about copyright and reproduction should be addressed to
Research Information Center, IPP/Nagoya University, Nagoya, Japan.

Table of Contents

1.	Introduction	1
2.	Continuous Emission Mechanisms for a Thin, Hot Plasma	2
2.1.	Thermal bremsstrahlung	2
2.2.	Recombination radiation	3
2.3.	Two photon decays	4
3.	Rate Coefficients	5
3.1.	Collisional excitation rate coefficient	5
3.2.	Ionization	7
(1)	Direct collisional ionization	7
(2)	Autoionization	8
3.3.	Recombination	9
(1)	Radiative recombination	9
(2)	Dielectronic recombination	10
(3)	Two-electron recombination (Three body recombination)	14
4.	Line Intensities from a Thin, Hot Plasma	15
4.1.	Ionization equilibrium	15
4.2.	Level population density	18
4.3.	Line intensity	20
4.4.	Satellite line	20
5.	Calculated Results	24
5.1.	Assumption and applicability	24
5.2.	Prominent lines	26
5.3.	Comparison with other results	28
5.4.	Radiation losses	30
6.	Observed X-Ray Spectrum	32
6.1.	Proportional Counter	32
6.2.	Pulse height spectrum	36

1. Introduction

X-ray emission has been observed from both celestial objects and laboratory plasmas, and physical properties of the plasmas are obtained by analyzing X-ray spectra. Plasma parameters are obtained by comparison of the observed spectra with theoretical ones.

We review here the rate coefficients of relevant processes and the calculated spectra by several authors, and give useful formulae of practical convenience. We recommend the formulae by Lots (1967, 1968) for direct collisional ionization, by Jordan (1969) for autoionization, by Aldrovandi and Péquignot (1973, 1974) for radiative recombination, and by Jacobs et al (1977) for dielectronic recombination. Burgess (1965) gave a simple formula for dielectronic recombination, but Jacobs et al (1977) have calculated the dielectronic recombination rate including autoionization into an excited state of the recombining ion, and their results give smaller values than those by Burgess (1965). For the collisional excitation rate, the formula with use of the gaunt factor proposed by Mewe (1972a) with classification of $\Delta n = 0$ and $\Delta n \neq 0$ for allowed transitions (Kato, 1977) is recommended.

Landini and Fossi (1970), Tucker and Koren (1971), Mewe (1972b, 1975) and Kato (1976) have calculated line intensities for solar coronal conditions with the density effect discussed in 5.1, whereas Raymond and Smith (1977) and Stern et al (1978) gave the results for interstellar conditions without the density effect. We show the calculated

results based on atomic data by Kato (1976) in this article for a thin plasma of interstellar abundances. The ion abundances given by Jordan (1969) for C through S and by Jacobs et al (1977) for Fe are used for the ionization equilibrium. This model assumes a thin plasma where the density effect for dielectronic recombination is negligible, and this assumption is valid for $n_e < 10^{14} \text{ cm}^{-3}$ at 100 eV for ions of charge $z = 10$. The calculated results are shown to be useful for analyzing observations.

X-ray spectra to be observed by representative detectors with various thicknesses ^{of} the window are shown. They are used to determine the temperature, the abundances of elements, the interstellar absorption and the emission measure.

2. Continuous Emission Mechanism from a Thin Hot Plasma

2.1. Thermal bremsstrahlung

The spectrum of thermal bremsstrahlung from electrons which obey a Maxwellian distribution is written as

$$\frac{dP_{ff}}{dK} = \frac{3.0 \times 10^{-15}}{k(KT)^{1/2}} z^2 \bar{g}_{ff}(k, KT) e^{-k/KT} n_e n_z \text{ photons} \\ (\text{cm}^3 \text{ sec keV})^{-1}, \quad (2.1)$$

where k and KT are the energy of an emitted photon and the electron temperature in keV, respectively, n_e and n_z are

the electron density and the ion density, respectively, z is the ionic charge, and g_{ff} is the average gaunt factor. The values of $\bar{g}_{ff}(k, KT)$ are calculated numerically by Karzas and Latter (1961). Simple approximate analytic expressions for \bar{g}_{ff} are given in Table 1.

The energy generation rate by thermal bremsstrahlung is obtained by integrating eq. (2.1)

$$U = 4.8 \times 10^{-24} (KT)^{1/2} \langle g_{ff}(KT) \rangle z^2 n_e n_z \text{ erg (cm}^3 \text{ sec)}^{-1}, \quad (2.2)$$

where $\langle g_{ff}(KT) \rangle$ takes the value between 1.15 and 1.45 for the temperature range of $KT < 13.6z^2$ keV.

The detailed explanation is given in Kato (1978).

2.2 Recombination radiation

Recombination radiation is emitted when a free electron is trapped by an ion into a shell of principal quantum number n and with \bar{s} holes. The spectrum by recombination radiation for a Maxwellian electron gas with a temperature KT , is given by

$$\frac{dP_{fb}^n}{dk} = \frac{8.4 \times 10^{-17}}{k(KT)^{3/2}} \left(\frac{\bar{s}}{2n^2} \right) n \left(\frac{I_{z,n}}{I_H} \right)^2 \exp \left\{ (I_{z,n} - k)/KT \right\} n_e n_{z+1}$$

photons (cm³ sec keV)⁻¹ for $k > I_{z,n}$, (2.3)

= 0 for $k < I_{z,n}$,

where $(\bar{s}/2n^2)$ is the imcompleted fraction of shell, $I_{z, n}$ is the ionization potential of the state n , and the gaunt factor is assumed to be unity. For hydrogenic ions, (e.g. OIX + e \rightarrow OVIII), $(\bar{s}/2n^2)n(I_{z, n}/I_H)^2$ can be replaced by $\bar{s}Z^4/2n^5$, where Z is the atomic number of ion. As $\bar{s}/2n^5 \sim 1/n^3$, the intensity at $k < I_{z, n_0}$ is much smaller than that for $k > I_{z, n_0}$ where n_0 is the principal quantum number of the ground state.

We list the values S/Z^4 in Table 2, where $S = (\bar{s}/2n^2)n(I_{z, n}/I_H)^2$.

The energy generation rate by recombination radiation is

$$U = 1.3 \times 10^{-25} (KT)^{-1/2} z^4 \left\{ \frac{\bar{s}_{n_0}}{2n_0^5} + 1.202 - \sum_{n=1}^{n_0} \frac{1}{n^3} \right\} n_e n_{z+1} \text{ erg (cm}^3 \text{ sec)}^{-1} \quad (2.4)$$

where z is the charge of the ion after recombination.

2.3 Two photon decays

Two photons are emitted with a continuous spectrum from metastable 2S state of hydrogenic and helium-like ions. The spectrum can be written as (Tucker and Koren 1971),

$$\frac{dP}{dk} = \frac{6P(2S-1S)}{E_T} \left(\frac{k}{E_T} \right) \cdot \left(1 - \frac{k}{E_T} \right) \text{ photons (cm}^3 \text{ sec keV)}^{-1} \quad (2.5)$$

where E_T is the energy difference between 2S and 1S states. $P(2S - 1S)$ is the photon emission rate in the two photon processes

$$P(2S - 1S) = n(2S)A(2S - 1S),$$

where $n(2S)$ is the level population of the 2S state. The two-photon transition probabilities are $A(2S - 1S) \approx 8Z^6 \text{ sec}^{-1}$ for hydrogenic ions and $A(2^1S - 1^1S) \approx 16 (Z - 1)^6 \text{ sec}^{-1}$ for helium line ions. In the case of low density plasma, $P(2S - 1S) = C(1S - 2S)n_e n_1$ where $C(1S - 2S)$ is the collisional excitation rate which is discussed in the next section.

3. Rate Coefficients

Empirical and semi-empirical formulae for ionization and excitation by electron impact are reviewed by Kato (1977). Here we describe only formulae we recommend the readers to use.

3.1. Collisional excitation rate coefficient

The collisional rate coefficient for excitation from level i to level j is given by

$$C_{ij} = 2.5 \times 10^{-9} \bar{\Omega} \omega_i^{-1} (KT)^{-1/2} e^{-\frac{E_{ij}}{KT}} \text{ cm}^3 \text{ s}^{-1}, \quad (3.1)$$

where $\bar{\Omega}$ is the mean collision strength, ω_i the statistical

weight of lower level i and E_{ij} the excitation energy in keV.

The rate coefficient C_{ij} can be written with use of the Bethe-approximation as

$$C_{ij} = 5.0 \times 10^{-10} f_{ij} \bar{g} (E_{ij}/KT) E_{ij}^{-1} (KT)^{-1/2} e^{-E_{ij}/KT} \text{ cm}^3 \text{ s}^{-1} \quad (3.2)$$

where f_{ij} is the absorption oscillator strength and \bar{g} is the integrated gaunt factor. Mewe (1972a) gave the following expression for $\bar{g}(y)$ with $y = E_{ij}/KT$,

$$\bar{g}(y) = A + (By - Cy^2 + D) \left[\ln\left(\frac{y+1}{y}\right) - \frac{0.4}{(y+1)^2} \right] + Cy \quad (3.3)$$

The values of A, B, C and D are given in Kato (1977) for H, He, Li and Ne isoelectronic sequences. For all other sequences,

$$A = 0.15, B = C = 0, D = 0.28 \text{ (allowed, } \Delta n \neq 0)$$

$$A = 0.6, B = C = 0, D = 0.28 \text{ (allowed, } \Delta n = 0)$$

$$A = 0.15, B = C = D = 0 \text{ (forbidden monopole and quadrupole transitions)}$$

$$A = B = D = 0, C = 0.1 \text{ (spin exchange transitions)}$$

In the case of forbidden transitions, the value of f_{ij}

may be assumed to be equal to that of the nearest allowed transition. The de-excitation rate C_{ji} is given as

$$C_{ji} = C_{ij} \frac{\omega_i}{\omega_j} e^{E_{ij}/KT} \quad (3.4)$$

3.2. Ionization

(1) Direct collisional ionization

Lotz (1967, 1968) deduced an empirical formula of cross section referring to many experimental results and gave the rate coefficient

$$S_d = 2.1 \times 10^3 \sum_{j=1}^N \frac{a_j \zeta_j}{(KT)^{3/2}} \left\{ \frac{1}{X_j} \text{Ei}(X_j) - \frac{b_j \exp C_j}{X_j + C_j} \text{Ei}(X_j + C_j) \right\} \quad (3.5)$$

where $X_j = I_j/KT$, i_j the binding energy of the j -th subshell ($j=1$ means the outermost subshell), ζ_j the number of equivalent electrons of j -subshell, and $\text{Ei}(X) = \int_x^\infty e^{-t}/t dt$. The number N of subshells to consider is taken to be 1 for H and He, to be 2 for Li through A, and to be 3 for K through Zn. The values of parameters a_j , b_j and c_j are tabulated by Lotz (1967, 68) for ions ionized till three degrees from H to Zn. For ions ionized more than four times, Lotz assumed $a_j = 4.5 \times 10^{-14}$ and $b_j = c_j = 0$.

Inner shell ionization by electron impact can be neglected as far as the ionization equilibrium is concerned,

but it can have a considerable influence on the forbidden line intensity, especially under the non-stationary condition (Mewe and Schrijver, 1977). They considered processes such as $1s^2 2s^2 S_{1/2} + e \rightarrow 1s 2s^1 S_0$ or $3S_1 + 2e$, and $1s^2 2p^2 P + e \rightarrow 1s 2p^1 P$ or $3P + 2e$, respectively.

(2) Autoionization

Goldberg et al (1965) have shown that the rate by autoionization is comparable to or greater than that by direct ionization for certain ions such as Fe XV and Fe XVI, for which the number of electrons in the first inner shell is large compared with that in the outershell. The autoionization rate is given

$$S_a = \sum_j C_{gj} \frac{A_a^j}{A_r^j + A_a^j}$$

where C_{gj} is the excitation rate of an inner shell electron to a state lying above the first continuum, A_a and A_r are the autoionization and radiative transition probabilities, respectively. As $A_a \gg A_r$ for the lowest level, $S_a \approx \sum_j C_{gj}$.

Jordan (1969) gave the following empirical formula

$$S_a = 1.0 \times 10^{-10} f W^{-1} (KT)^{1/2} e^{-W/KT} \text{ cm}^3 \text{ s}^{-1} \quad (3.6)$$

with

$$\begin{aligned}
f &= 0.70s, W = W_1 \quad \text{for } W_1 > I_1, \\
f &= 0.13s, W = I_1 \quad \text{for } W_1 < I_1 < 1.8W_1, \\
f &= 0.049s, W = I_1 \quad \text{for } 1.8W_1 < I_1 < 2.4W_1, \\
f &= 0.023s, W = I_1 \quad \text{for } 2.4W_1 < I_1,
\end{aligned}$$

where $W_1 \simeq I_2 - I_1$, I_1 and I_2 are the energies of the first and second ionization limit, respectively, and s is the number of electrons in the shell from which the excitation takes place.

We show in Fig.1 the calculated rate coefficients of both direct ionization and autoionization for oxygen and iron ions.

3.3. Recombination

(1) Radiative recombination

Jordan (1969) used the following formulae for the radiative recombination rate

i) For $KT > 0.05$ keV

$$\alpha_r(X^{Z+1} \rightarrow X^Z) = 3.5 \times 10^{-15} (z+1)^2 I_z^{1/2} / KT \text{ cm}^3 \text{ s}^{-1}, \quad (3.7)$$

where I_z is the ionization potential of an ion X^Z .

ii) For $KT < 0.05$ keV

$$\alpha_r(X^{Z+1} \rightarrow X^Z) = 2.8 \times 10^{-13} I_z n_o g / \sqrt{KT} \text{ cm}^3 \text{ s}^{-1}, \quad (3.8)$$

where n_0 is the ground state principal quantum number, $g \simeq 4$ for iron and nickel and $g \simeq 3$ for lighter atoms.

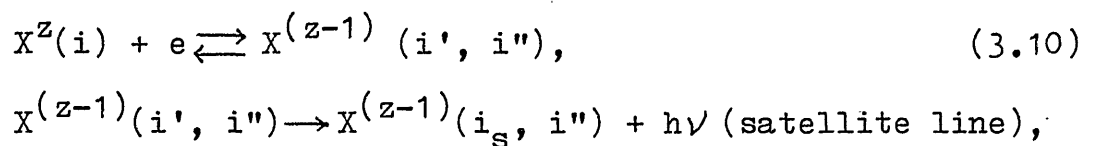
Recently Aldrovandi and Péquignot (1973, 1974) have calculated the recombination rates to the ground level from the photoionization cross section and to excited states with the hydrogenic approximation for the ions C through Ar and Ca. For quantitative use we recommend their formula

$$\alpha_r = A_r (1160 KT)^{-\eta} \text{ cm}^3 \text{ s}^{-1}. \quad (3.9)$$

The numerical values of A_r and η are listed in Table 3. In most cases, eq (3.9) gives the rate coefficients in agreement with the numerically calculated results better than 10% in the range of temperature $T_{\text{max}} \geq T_e \geq T_{\text{max}}/10^3$. For some ions indicated by asterisks, the same accuracy is obtained for $T_{\text{max}} \geq T_e \geq T_{\text{max}}/300$.

(2) Dielectronic recombination

The dielectronic recombination is the process that a free electron is captured and produces a doubly excited state of the ion. The energy level diagram is shown in Fig. 2 for the case of Li-like ion. This process is written as



and this process produces satellite lines, which we shall discuss later. The dielectronic recombination rate r_d and the autoionization rate A_a are related by the principle of detailed balance

$$\frac{r_d(i \rightarrow i', i'')}{A_a(i', i'' \rightarrow i)} = \frac{\omega(i', i'') h^3}{2 \omega(i) (2\pi m k T)^{3/2}} \exp(-E_s / k T), \quad (3.11)$$

where $\omega(i', i'')$ and $\omega(i)$ are the statistical weights of the satellite level of ion $(z - 1)$ and of the ground state of ion z , respectively. Then the total rate α_d is

$$\alpha_d = \frac{h^3}{2(2\pi m k T)^{3/2}} \sum_{i', i''} \frac{\omega(i', i'')}{\omega(i)} e^{-E_s / k T} \frac{\sum_{i_s} A_r(i', i'' \rightarrow i_s, i'') A_a(i', i'' \rightarrow i)}{i_s \sum_{i_s} A_r(i', i'' \rightarrow i_s, i'') + \sum_{i'''} A_a(i', i'' \rightarrow i''')}. \quad (3.12)$$

Burgess (1965) gave a simplified general expression for α_d

$$\alpha_d(X^z \rightarrow X^{z-1}) = 7.6 \times 10^{-14} (k T)^{-3/2} B(z) \sum_j f(i, j) A(x) e^{-\bar{E} / k T} \text{cm}^3 \text{s}^{-1}, \quad (3.13)$$

where $A(x) = x^{1/2} / (1 + 0.105x + 0.015x^2)$ for $x > 0.05$,

$$B(z) = z^{1/2} (z+1)^{5/2} (z^2 + 13.4)^{-1/2} \quad z \leq 20,$$

and $\bar{E} / k T = 0.0136 (z+1)^2 \epsilon_{ij} a^{-1} (k T)^{-1}$,

with $a = 1 + 0.015 z^3 (z+1)^{-2}$

$$\epsilon_{ij} = \nu_i^{-2} - \nu_j^{-2}$$

$$x = (z+1) \epsilon_{ij},$$

z is the charge number, $f(i, j)$ is the $i \rightarrow j$ oscillator strength, ν_i and ν_j are effective principal quantum numbers of the state i and j of the recombining ion X^z , respectively. Aldrovandi and Péquignot (1973, 1974) gave a four-term parametric expression

$$\alpha_d = A_d (KT)^{-3/2} \exp(-W_1/KT) (1 + B_d \exp(-W_2/KT)) \quad (3.14)$$

from the expression (3, 12). The values of parameters A_d , B_d , W_1 and W_2 are given in Table 3. The numerical results are fitted to better than 10% in the range $T_{\text{crit}} - T_{\text{max}}$ for all ions, except for NIII, OIII, NeV and SX and for MgVI, MgVII, SiVIII, SiIX and SiXI for which the accuracies are not worse than 15% and 25%, respectively.

Several authors have calculated the rate coefficients for typical ions; Ansari et al (1970) gave the results based on eq. (3, 12) for C, N, O, Ne, Mg, Si, S and Fe ions. Nakamura et al (1977) also calculated them for C, O and Fe ions from eq. (3, 12) but taking into account only one transition in the summation. Mattioli (1975) showed the results calculated with the formula by Beigman et al (1968) about O and Fe ions.

We compare their results about O ions in Fig.3(a). For OVII and OVIII ions, agreement between Ansari et al (1970) and Mattioli (1975) is very good but the results by Nakamura et al (1977) is larger by a factor of 2 than

others. But for ions other than OVII and OVIII, the results by Aldrovandi and Péquignot (1973) are greater than others (e.g. 2.5 times Mattioli (1975) for OVI and OV). This indicates that the one transition approximation is not too bad for H and He-like ions, but not acceptable for other ions whose resonance transition is $\Delta n = 0$.

We also compare the calculated results for Fe ions in Fig. 3(b). Ansari et al (1970) calculated the rate coefficients for FeXI-FeXVII ions, Jordan (1970) tabulated the rate coefficients ($\alpha_r + \alpha_d$) for FeXVII ~ FeXXVI ions, and Nakamura et al (1977) showed their results for FeVIII-FeXXVI ions. Ansari et al (1970) took into account several transitions, so that their rate coefficients are always larger than others. One transition approximation is not enough especially in the high temperature region (e.g. smaller by a factor of 4 at 1 keV for FeXVI). We have found large differences between the result by Nakamura et al (1977) and others. Differences are caused by small values of the radiative recombination rates as well as the values of dielectronic recombination for FeXX-FeXXIV ions.

Allen (1965) gave a simple approximation formula derived from Burgess (1965), and Landini and Fossi (1971) modified Allen's formula.

Recently Jacobs et al (1977) have calculated the

dielectronic recombination of Fe ions and showed that the inclusion of autoionization into excited states reduces the values of α_d . For FeXVII, the dominant 3d-2p contribution is reduced by almost an order of magnitude as a result of the inclusion of autoionization into the 3p excited state of the recombining ion. The values ($\alpha_r + \alpha_d$) for Fe ions by Jacobs et al are shown in Fig.3(c). Jacobs et al (1977) calculated the ionization equilibrium and compared their results with those of Jordan (1969) and Summers (1974). The temperatures of maximum equilibrium abundances obtained by Jacobs et al (1977) are lower than those by Jordan (1969) because of the inclusion of autoionization into excited states of the recombining ions. The comparison between Jacobs et al. (1977) and Jordan (1969) is shown in Fig.4.

When the electron density is high, states of $n > n_t$ (= thermal limit) should not be included in the summation in eq (3.12), since the further excitation and ionization rates from all levels above n_t are greater than those for radiative decay (Jordan 1969). For Fe ions, this density effect is not important for $n_e \sim 10^{12} \text{ cm}^{-3}$ (Jordan 1970). Dielectronic recombination is a dominant recombination process for many ions at low densities and high temperatures.

(3) Two-electron recombination (Three-body recombination)

The two electron recombination becomes efficient

at very high densities and low temperatures. This process is the inverse process of electron impact ionization. The rate coefficient is given by Wilson (1967) as

$$\alpha_2(X^z \rightarrow X^{z-1}) = 4.6 \times 10^{-35} n_e^{-1} z^{-2} (KT)^{-2} \text{ cm}^3 \text{ s}^{-1}, \quad (3.15)$$

and the recombination rate by collisional de-excitation of levels above the thermal limit n_t is given (Wilson 1967) by

$$\alpha_b = 1.5 \times 10^{-34} n_e z^{-2} n_t^{-2} (KT)^{-2} \exp(I_t/KT) \text{ cm}^3 \text{ s}^{-1}. \quad (3.16)$$

4. Line Intensities from a Thin, Hot Plasma

Since the intensity of line emission is proportional to the ion density, we first consider the populations of ionization states.

4.1. Ionization equilibrium

The ion density of ionic stage z is obtained by solving a set of equations

$$\frac{dn_z}{dt} = S_{z-1} n_e n_{z-1} - S_z n_e n_z - \sigma_z n_e n_z + \alpha_{z+1} n_e n_{z+1} \quad (4.1)$$

where S_z is the total ionization coefficient from stage z to stage $z + 1$ and α_z is the total recombination coefficient from stage z to stage $z - 1$. When the ionization state is steady ($dn_z/dt = 0$), the relative population of two successive stages of ionization is given by

$$\frac{n_{z+1}}{n_z} = \frac{S_z}{\alpha_{z+1}} . \quad (4.2)$$

The equilibrium density of an ion, $n_z/n(Z)$, where $n(Z)$ is the total number density of the element, was calculated by Jordan (1969, 1970) for C, N, O, Ne, Mg, Si, S, Fe and Ni for the solar corona condition and for low density plasmas. We use her results for low density plasmas (including collisional ionization, autoionization, direct radiative recombination and full dielectronic recombination) in order to calculate the line intensity in the steady state. Jordan (1969) employed Seaton's (1964) formula for ionization which gives an overestimate for $KT > I_z$. As the ionization equilibrium is attained for $KT < I_z$, the result should be essentially the same as that obtained with eq. (3.5). Summers (1974) calculated the density dependent ionization equilibrium of hydrogen-like through Ar-like ions. He included the dependence on the highly-excited state population with use of z -dependence simplification to calculate α_z and S_z .

a) Ionizing plasma

When a plasma is rapidly heated to a high temperature with a time scale t_H , ionization takes place with a time scale of $t_I \sim 1/S_Z n_e$ till getting the ionization equilibrium for $t_H > t_I$, since $S_Z > \alpha_Z$ for a high temperature plasma. The degree of ionization is smaller than that of the steady state value if $t_I > t_H$. In this case the spectrum is softer than that in the steady state. Generally the maximum abundance of each ion is proportional to $1/S_Z$. Numerical examples of ion abundances for an ionizing plasma at a constant temperature as a function of time is shown in Fig. 5 (a). Itoh (1977) calculated the emission spectrum of a young supernova remnant in the ionizing phase.

b) Recombining plasma

When a highly ionized plasma is cooled rapidly with the time constant t_c , degree of ionization is greater than that in the steady state model for $t_c < t_R$, where $t_R = 1/\alpha_Z n_e$ is the time scale for recombination, and consequently the spectrum is harder than that in the steady state. Numerical examples of ion abundances for recombining plasma is given in Fig. 5(b) for a constant temperature.

Shapiro and Moore (1976) calculated a time dependent equilibrium as a function of temperature for the gas which

is initially in the steady state at 10^6 °K and cools by radiative cooling. In this case, highly ionized ions survive, and the spectrum therefrom is harder than for a steady state gas at the same temperature. Non-steady cooling has been studied also by Kafatos (1973) and by Kafatos and Tucker (1972).

4.2. Level population density

The population density $n_z(p)$ of level p for an optically thin plasma is expressed for the collisional radiative model by

$$\begin{aligned} \frac{dn_z(p)}{dt} = & \sum_{q=1}^{p-1} C_{qp} n_z(q) n_e - \left[\left\{ \sum_{q=1}^{p-1} C_{pq} n_e + \sum_{q=p+1}^{\infty} C_{pq} n_e + S_p n_e \right\} \right. \\ & \left. + \sum_{q=1}^{p-1} A_{pq} \right] n_z(p) + \sum_{q=p+1}^{\infty} \left\{ C_{qp} n_e + A_{qp} \right\} n_z(q) + \alpha_p n_{z+1} n_e, \end{aligned} \quad (4.3)$$

where

C_{qp} : collisional excitation or de-excitation rate coefficient from level q to p

A_{pq} : radiative transition probability from level p to q

α_p : total recombination rate coefficient to level p
 n_{z+1} : ion density of charge $z+1$.

The population density for the steady state is determined by solving the set of equations for $dn_z(p)/dt = 0$. Generally the population of the ground state is much larger than that of other states for low density plasmas of steady state, such as for the solar corona. The population density of level p is written, neglecting the cascade effects from levels higher than level p , as

$$n(p) = C_{1p} n(1) n_e / \sum_{q=1}^{p-1} A_{pq}, \quad (4.4)$$

which is sometimes called the coronal condition or the ionizing phase. When $n_{z+1} \gg n_z$ for a low density plasma of steady state, the cascade effect and the recombination cannot be neglected and

$$n_z(p) \sum_{q=1}^{p-1} A_{pq} = \sum_{q=p+1}^{\infty} A_{qp} n(q) + \alpha_p n_{z+1} n_e, \quad (4.5)$$

which is called the recombining phase. We show examples of the level population of OVII for the ionizing phase ($n_{z+1} = 0$) and for the recombining phase ($n_z = 0$), respectively, in Fig. 6 (Fujimoto and Kato 1978). For high electron densities (eq. (5.1)), the collisional processes are dominant and $n(p)$ reaches to local thermodynamic equilibrium.

4.3. Line intensity

The line intensity from level p to q is given as

$$J_{pq} = n(p) A_{pq}, \quad (4.6)$$

where $n(p)$ is calculated from eq. (4.3).

For the case of thin hot plasmas for which electron collisional excitation from the ground state is dominant, the line intensity is given from (4.4) and (4.6) as

$$J_{pq} = C_{1p} n(1) n_e B_{pq} \text{ photons cm}^{-3} \text{ sec}^{-1}, \quad (4.7)$$

where B_{pq} is the branching ratio of radiative decay from p to q.

4.4 Satellite line

Satellite lines from an ion of charge z are located in the long wavelength side of the resonance lines of ion $z + 1$. They are observed from some plasmas, such as laser plasmas, vacuum sparks, and solar flares. Satellite lines of ion z are produced by two mechanisms; (1) dielectronic recombination from $z + 1$ ion to z ion, and (2) inner shell excitation of z ion. Examples of the observed satellite lines from a laser plasma are shown in Fig. 7.

(1) Satellite lines from dielectronic recombination

Satellite lines are emitted by dielectronic recombination as shown in eq. (3.10) and in Fig.2.

The intensity of satellite line in photons per unit volume is given from eq. (3.11) by

$$\begin{aligned}
 J_S(z-1) &= r_d \frac{A_r}{(A_a + \sum A_r)} n_z n_e \\
 &= \frac{\omega(i', i'')}{2\omega_z(i)} \frac{h^3}{(2\pi mKT)^{3/2}} \frac{A_a A_r (r', r'' \rightarrow r_s, i'')}{(A_a + \sum A_r)} \\
 &\quad \exp(-E_s/KT) n_e n_z \\
 &= \frac{5.24 \times 10^{-27}}{(KT)^{3/2}} \frac{\omega(i', i'')}{\omega(i)} \frac{A_a A_r}{(A_a + \sum A_r)} \exp(-E_s/KT) n_e n_z \\
 &\quad \text{photons cm}^{-3} \text{ sec}^{-1} \tag{4.8}
 \end{aligned}$$

The intensity ratio of the satellite to the resonance lines gives informations on the electron temperature and ion abundances. When the plasma is hot and thin, so that a resonance line is produced by collisional excitation from the ground state, the intensity of a resonance line is obtained from eqs. (4.7) and (3.2) as

$$\begin{aligned}
 J_R^i(z) &= 5.0 \times 10^{-10} f_{ij} \bar{g}(y) E_{pq}^{-1} (KT)^{-1/2} \exp \\
 &\quad (-E_{pq}/KT) B_{pq} n_z n_e. \tag{4.9}
 \end{aligned}$$

From eqs. (4.8) and (4.9), we get the ratio

$$\frac{J_S(z-1)}{J_R^i(z)} = 1.05 \times 10^{-17} \frac{\omega(i', i'')}{\omega(i)} \frac{E_{pg}}{KT} \frac{A_a A_r \exp((E_{pg} - E_s)/KT)}{(A_a + \sum A_r) f \bar{g}(y)} \quad (4.10)$$

which has no density dependence but only the temperature dependence. For the recombining phase plasma, the resonance line is produced by recombination as given by (Fujimoto and Kato 1978)

$$J_R^r(z-1) = \frac{\omega(p)}{2\omega_z(i)} \left(\frac{h^2}{2\pi m k T} \right)^{3/2} \exp(I(p)/KT) r_0(p, z-1) A_r(p) n_z n_e \quad (4.11)$$

where $r_0(p, z-1)$ is the population coefficient which coincides with the Saha decrement in the case of the recombining phase and is a function of temperature and density. The ratio

$$\frac{J_S(z-1)}{J_R^r(z-1)} = \frac{(r', r'') A_r(r', r'' \rightarrow r_s, r'')}{(p) A_r(p \rightarrow 1)} \frac{A_a}{(A_a + \sum A_r)} \frac{\exp(-(E_s + I)/KT)}{r_0(p, z-1)} \quad (4.12)$$

has no density dependence either, except in the factor r_0 . If we know the electron density by other means, the value

of r_0 is obtainable. Then, we can know the temperature from the ratio $J_S(z-1)/J_p^r(z-1)$. When the final state (r_s, r'') of a satellite line coincides with the initial state (p) of the resonance line, $E_S + I$ is equal to $E(r', r'' \rightarrow p)$ which is the transition energy of a satellite line.

Generally for the lowest levels, $A_a \gg A_r$ and then $A_a / (A_a + A_r) \approx 1$. The calculated ratios of the satellite to the resonance line intensities for the ionizing phase and for the recombining phase are shown in Fig.8, respectively.

(2) Satellite lines from inner-shell excitation

The satellite line intensity produced by inner-shell excitation of ion z is written

$$J_S' = n_z(p)n_e C' \frac{A_r}{(A_a + \sum A_r)} \quad (4.13)$$

where C' is the collisional rate of inner-shell excitation and $n_z(p)$ is the population density of states from which the excitation takes place. The inner-shell excitation rate C' can be calculated by eq. (3.1) or eq. (3.2) with use of the effective oscillator strength \bar{F} (Gabriel 1972, Bhalla et al 1975). The excitation from an excited level is negligible in the low density plasma. Generally the satellite line intensity J_S by dielectronic recombination is larger than that by inner shell excitation J_S' , but

the latter is not always negligible.

5. Calculated Results

We present here the emission spectrum calculated for thin hot plasmas under ionization equilibria

5.1. Assumptions and applicability

Plasmas considered here are so thin that all the density effects are negligible, as shown in what follows.

When the electron density is high, excitation to all levels above a certain level n_t can be regarded as ionization, since the excitation and ionization rates from these levels are larger than the radiative decay rate. The electron density and the value of n_t are related to one another as (Griem 1964)

$$n_e = 7 \times 10^{17} (z+1)^7 \left[\frac{KT}{(z+1)^2 I_H} \right]^{1/2} \exp\left(\frac{4(z+1)^2 I_H}{17 n_t^3 KT} \right)^{17/2} n_t^{-17/2}. \quad (5.1)$$

The density effect is found important if $n_e \gtrsim 10^8 \text{ cm}^{-3}$ for neutral atoms and $n_e \gtrsim 5 \times 10^{14}$ for ions of charge 10. The excitation energy of the level n_t is given by

$$E_t \simeq 1.3 \times 10^{-4} (I_z/KT)^{1/7} n_e^{2/7} \text{ eV}. \quad (5.2)$$

The collisional ionization rate via such bound levels is given by Wilson (1964, 1967) as

$$S_t = 1.4 \times 10^{-8} z^{-2} (KT)^{-1/2} n_t^{-2} \exp [-(I_z + E_t)/KT]$$

$$\text{cm}^3 \text{ s}^{-1}. \quad (5.3)$$

Recombination processes are also modified at high electron densities. Levels with $n > n_t$ should not be included in the summation over levels in calculating the dielectronic recombination rate. On the other hand, radiative decay from bound levels above n_t to lower levels is equivalent to recombination. The recombination rate for this process is given by (Wilson 1967) as

$$\alpha_t(X^Z \rightarrow X^{Z-1}) = 3.0 \times 10^{-17} z^4 (KT)^{-3/2} n_t^{-1} \exp (E_t/KT)$$

$$\text{cm}^3 \text{ s}^{-1}. \quad (5.4)$$

Three body recombination becomes important for $n_e \gg 10^{17} z^7 (KT/I_z) \text{ cm}^{-3}$, and the rate coefficient is given in eq. (3.15).

In order to calculate the line intensity, we use the ionization equilibrium calculated by Jordan (1969, 1970) for C - Ni ion and by Jacobs et al (1977) for Fe ions. They considered collisional direct ionization, autoionization, radiative recombination and full dielectronic recombination. The rate coefficients of these processes are discussed in §3. Three-body recombination and the density-dependence of

direct radiative and dielectronic recombination are neglected.

Atomic data for line emission are based on Kato (1976). Satellite lines and K X-ray emission associated with K-electron ionization for ions which have outer shells are neglected, whereas K X-rays associated with K-electron excitation are taken into account.

We neglect the excitation from levels other than the ground level. In most cases the cascade processes are also negligible, but we take into account cascade effects for He-like and Ne-like ions (Kato 1976).

We use the cosmic abundances by Allen (1973) ((a) in Table 4) in this article, although slightly different abundances ((b) in Table 4) were used by Tucker and Koren (1971) and also adopted by Kato (1976). The value $n(Z)/n_H$ for each element is shown in Table 4.

5.2. Prominent lines

The line intensity in a thin, hot plasma is given from eq. (4.7) as,

$$J_{pq} = n_e n_H \frac{n(Z)}{n_H} \frac{n(Z, z)}{n(Z)} C_{1p} B_{pq}, \quad (5.5)$$

and the line emission power is written as

$$U_{pq} = n_e n_H \frac{n(Z)}{n_H} \frac{n(Z, z)}{n(Z)} C_{1p} B_{pq} k_{pq}, \quad (5.6)$$

where k_{pq} is the energy of an emitted photon. As hydrogen and helium are far more abundant than other elements and are fully ionized in X-ray emitting celestial objects, there holds $n_e = n_H (1 + 2 n(\text{He})/n_H)$.

Hence eq. (5.5) is expressed as

$$J_{pq} = \frac{n_e^2}{\{1 + 2n(\text{He})/n_H\}} \frac{n(Z, z)}{n(Z)} \frac{n(Z)}{n_H} C_{1p} B_{pq}. \quad (5.7)$$

We show in Fig.9 the intensities $J_{pq}/n_e n_H$ of representative lines as functions of temperature for ions of O ($Z = 8$), S ($Z = 16$) and Fe ($Z = 26$) in the energy range 0.06 - 1.0 keV. In the energy range 0.5 - 1.0 keV strong lines are emitted from OVIII (H-like), OVII (He-like) and FeXVII (Ne-like). The emission from SVII - SX and from FeIX and FeX is strong in the range 0.1 - 0.5 keV. Ions OVI, OV, FeVIII, FeIX and FeX emit strong lines in the energy range 0.06 - 0.1 keV. We use the ion abundances calculated by Jacobs et al (1977) for Fe ions which are ionized more than the ninth degrees and for the temperature range higher than $\log T = 6.2$. For comparison we also give the intensities obtained from the ion abundances by Jordan (1969, 1970) by dotted lines in Fig.9. The temperatures at the maximum intensities by Jordan are higher than those obtained with

the results by Jacobs et al.

In Fig. 10, the values of C_{1p} B_{pq} , which are equal to the photon emission rates per ion and per electron, $J_{pq}/n_e n_z$, are given for the lines shown in Fig. 9, and the transitions and wavelengths of these lines are listed in Table 5.

5.3. Comparison with other results

About 40 lines from 1 to 100 Å were taken into account by Landini and Fossi (1970, hereafter referred to as LF), 230 lines in the wavelength range of 1 - 60 Å and 90 lines of 60 - 220 Å respectively by Mewe (1972b, 1975), 459 lines from 1 to 70 Å by Tucker and Koren (1971, hereafter referred to as TK), and 795 lines from 1 to 250 Å by Kato (1976) to calculate the emissions for solar coronal conditions. Raymond and Smith (1977) and Stern et al (1978) have calculated the line intensities from 1 to 200 Å and from 100 to 1000 Å, respectively, for interstellar plasma conditions. As they all gave the emission powers in units of ($\text{erg cm}^3 \text{s}^{-1}$), wavelength in Å and temperature in °K, we use the same units in this section. Mewe (1972b, 1975), TK, Kato (1976) Stern et al (1978) used the ion abundances calculated by Jordan, whereas LF and Raymond and Smith (1977) evaluated them by themselves.

We have compared the spectra at $\log T = 6.2$ calculated by LF, TK and Kato (1976) in Fig. 11. In comparison with the results by Kato, TK gives larger powers, whereas LF

gives smaller ones. The reason for the smaller values by LF is considered as due to the fact that a small number of lines are taken into account. The intensities for the lines from Si and S ions by TK are generally larger than those by Kato (1976). The difference arises from the difference in the values of collision strength, as discussed in Appendix of Kato (1976). A good agreement is obtained between the results by Kato (1976) and those by Mewe (1972b, 1975) for strong lines.

We recalculate the line intensities for a tenuous plasma in this article. The ion abundances of Kato (1976) are changed from those with the density effect of the solar corona condition to those without the density effect, and the element abundances from the TK abundances to the Allen abundances. We compare the results with those by Stern et al (1978), by Mewe (1972b, 1975) and by Raymond and Smith (1977). Some examples of the comparison for iron lines are given in Fig. 12. Generally our values are larger by a factor of 2 to 3 than those by Stern et al (1978) even for the transitions for which the same values of the oscillator strength and branching ratio are used.* We guess that the difference comes from the values of the temperature

* The numerical results given in Stern et al (1977) are subject to errors in their computer code. The revised results are in good agreement with ours within 30% for two lines in Fig. 12.

averaged gaunt factor $\bar{g}(y)$ in eq. (3.2). Stern et al (1978) mentioned that the values of the branching ratios assumed to be the same for a given transition for all members of an isoelectronic sequence may lead to a substantial error. However, this argument does not hold, since generally the values of branching ratio for a given allowed transition do not vary so much, at most within a factor of 2. The main reason for the difference of the intensities is considered to be due to different values of $\bar{g}(y)$. We also compare our results with Mewe's under the same conditions and get good agreement with each other as seen in Fig. 12. We have to take into account the difference of the ion abundances for the comparison with Raymond and Smith (1977), because they used the ion abundances calculated by them. Generally the temperature at the maximum intensity by Raymond and Smith (1977) is higher than others. This difference is probably due to the difference in the ionization rate coefficients, since they used those of Summers which give smaller values than those used by Jordan (1969, 1970) and also by Lotz (1967).

5.4. Radiation losses

We calculate the radiation loss rates for twelve elements, H, He, C, N, O, Ne, Mg, Si, S, Ca, Fe and Ni in the temperature range $10^4 - 10^7$ °K under ionization equilibrium. For the lines of wavelengths from 1 to 250 \AA

the atomic data employed by Kato (1976) are used. We add 139 lines of wavelengths longer than 250 \AA , so that their contributions account for practically the total radiation loss by line emission for all the wavelength range. The radiation loss rate calculated for each element is presented in Fig. 13. Fig. 13 (a) shows the radiation loss rate $U/n_e n(Z)$ of each element, whereas Fig. 13 (b) presents the cooling rate $U/n_e n_H$ for the interstellar plasma of the Allen abundances. The total emission rates by bremsstrahlung (B) and by direct recombination (R) are also shown. The ions of degree of ionization lower than CaIV, FeVIII and NiX are not considered in this calculation. The total cooling rate in Fig. 13(b) is in good agreement with that by Raymond et al (1976). One can see that bremsstrahlung is of negligible importance for $T < 5 \times 10^6 \text{ K}$. Recombination radiation is also negligible except for $T < 2 \times 10^4 \text{ K}$. Dielectronic recombination contributes more than radiative recombination for ions with shells other than the K-shell, yet is unimportant compared with line emission. However, dielectronic recombination affects the ionization equilibrium and accordingly influences the loss rate by line emission, as discussed below.

Contributions of representative lines to the total line emission are given for each of three important elements, O, S and Fe in Fig. 14. For O and S the contributions of strong lines are shown in Fig. 14(a) and (b), respectively,

whereby the ion abundances are adopted from Jordan (1969). For Fe the ion abundances calculated by Jacobs et al. (1977) are adopted, and the emission power of the total Fe ions thus obtained is compared with that based on Jordan's ion abundances in Fig. 14(c). The emission rate based on the ion abundances of Jacobs et al shows a minimum at about $\log T = 6.5$, whereas that on Jordan's abundances shows a monotonic decrease at temperatures of $\log T > 6.1$. This is because the dielectronic recombination rate is reduced in comparison with the rate which does not include the autoionization into excited states. This results in that the ion abundance reaches a maximum at a lower temperature, and consequently in that the rate of line emission is reduced for ions with a closed L-shell plus a few electrons and a few holes. Although the ion abundances of O and S with revised dielectronic recombination rates are not available yet, this effect is considered to be of little practical importance: As the L-shell is not filled up, for O this effect is small; for S this effect can be important, but its contribution to the total radiation is of minor importance in the temperature range of interest, $5.3 \leq \log T \leq 5.8$.

6. Observed X-Ray Spectrum

6.1. Proportional counter

Proportional counters are commonly used to observe the

X-ray spectra of celestial objects, because of their applicability over a wide energy range of interest, of high efficiency, of large area and of low cost. We consider here proportional counters as detectors of practical use.

The efficiency of a proportional counter is determined by the transmission probability through the counter window and by the absorption probability of the counter gas, both depending on the photon energy. We show in Fig. 15 the energy dependences of the transmission probability for three typical thicknesses 0.8, 1.5 and 3.9 μ of the polypropylene window which is of current use for cosmic soft X-ray experiments (Hayakawa et al 1972, Kato et al 1974). The transmission probability has a sharp minimum associated with the K-absorption edge of Carbon at 284 eV and decreases rapidly as energy decreases below 150 eV.

The absorption probability by gas can be made practically 100 % at low energies by using appropriate gas at a considerable pressure. It decreases as energy increases and peaks at the absorption edge. A significant fraction of energy absorbed by K-electron ionization is released as a K X-ray photon if the K-fluorescence yield is large, and K X-rays escape out of the gas. In this case the energy absorbed in the gas forms the so-called escape peak, which appears at an energy equal to the incident energy minus the K X-ray energy.

When X-rays are absorbed by gas, they produce the primary electrons whose average number is nearly equal to the absorbed energy divided by a constant energy which is characteristic of the counter gas and is about 30 eV for Ar. The number of primary electrons obeys a Poisson distribution, and its dispersion relative to the average number gives the energy resolution $\Delta k/k$.

This is expressed as

$$\Delta k / k = R/\sqrt{k}, \quad (6.1)$$

where $R = 0.48$ is a typical value. This gives the value of 20 % at 5.9 keV, the K X-ray energy of a radioactive source ^{55}Fe commonly used for calibration. Since $\Delta k/k \gtrsim 1$ for $k < 0.2$ keV, the line energy can be hardly determined by pulse height measurements in the very low energy region.

The pulse height distribution measured with a counter is expressed as $P(k_x, k)dk$, where k_x is the X-ray energy and k the pulse height in energy units. The function $P(k_x, k)$ has the main peak centered at k_x and the escape peak at about $k_x - k_0$, where k_0 is the energy of the K_0 photons. For the incident X-ray spectrum $f(k_x)dk_x$, the pulse height spectrum is given as

$$g(k) = \int f(k_x)\epsilon(k_x)P(k_x, k)dk_x \quad (6.2)$$

where $\epsilon(k_x)$ is the counter efficiency. Generally $F(k_x, k)$ can be expressed as a Gaussian distribution.

The incident spectrum $f(k_x)$ can be obtained by solving the integral equation (6.2). In practice we assume a spectrum which depends on several parameters and find a best fit by varying the values of the parameters. Spectra for the thermal emission from thin plasmas are often adopted as the assumed spectra, and the emission measure, the temperature and the element abundances are regarded as variable parameters. Since the contribution of several strong lines dominate over others, it may be useful to show relative contributions of these lines at different temperatures.

Fig. 16(a) - (f) show the photon emission coefficient times the counter efficiency against temperature for each strong lines. If two lines are very close to each other, such as two closely spaced lines of OVII, they are combined to form one line. The value of $f(k)\epsilon(k)$ can be obtained from Fig. 16 as

$$f(k)\epsilon(k) = J(k)\epsilon(k) \int \delta(k - k_i) EM / 4\pi \quad (6.3)$$

where k_i is the photon energy for a given line and EM is the emission measure, the integral of $n_e n_H$ over the X-ray source along the line of sight. The element abundances compiled by Allen (1973) are assumed. The calculated results

for three window thicknesses, 0.5, 1.3 and 3.9 μm hydrocarbon film, are presented for the L (0.1 ~ 0.4 keV)- and M (0.4 ~ 1.0 keV)-bands separately. Some strong lines, such as the CVI Ly α , are omitted, since they are strongly absorbed by the window film because of the K-absorption edge of carbon. These figures may be useful for understanding how one can obtain the relative contributions of strong lines.

An example for spectral fitting is given in Fig. 17. The spectra of the Lupus Loop region observed with 1 μ and 4 μ proportional counters are fitted by a mixture of four lines, OVII (0.56 keV), OVIII (0.65 keV), FeXVII (0.83 keV) and NeIX (1.016 keV). The flux of each line is thus obtained with a reasonably small χ^2 value.

6.2. Pulse height spectrum

We show examples of the pulse height spectrum $g(k)$ in eq. (6.2) which is folded with the counter efficiency and energy resolution. As a standard proportional counter, we take the value 0.48 for R . The calculated pulse height spectra from a hot plasma of Allen's abundances for several temperatures and for three thicknesses of polypropylene window are given in Fig. 18. The contributions of respective elements to the pulse height spectrum are also shown. Dominant contributions come from Fe, Si and S in the energy region below 0.5 keV at low temperatures, whereas at high temperatures Fe, C and Ne are dominant in the energy range 0.5 - 1 keV.

Continuous emission becomes important below 0.5 keV, as shown by dotted lines.

The pulse height spectra obtained from the calculated spectra by LF, by TK and by Kato (1976) at $\text{Log } T = 6.2$ (which are shown in Fig. 11) are compared in Fig. 19. They are normalized by the intensity at 1 keV. The slope by TK is the steepest and that by LF is the least steep. The reason for this difference is discussed in §5.3. As TK overestimates line emissions in the energy range 0.18 - 0.4 keV from Si and S ions, the temperature derived from an observed spectrum with use of the results by TK gives a higher value than that by Kato (1976). The pulse height spectrum below 0.2 keV by TK declines more rapidly towards low energy than those by others since TK discarded the lines below 0.18 keV.

The proportional scintillation counter has a better resolution than proportional counters, since scintillation light emitted from the counter gas is measured. The resolution is better by a factor of two than the ordinary proportional counter at present. The pulse height spectra with $R = 0.24$ and $R = 0.12$ are shown in Fig. 20.

Since cosmic soft X-rays are subject to absorption by neutral interstellar matter, the pulse height spectra with $R = 0.48$ modified by interstellar absorption are shown in Fig. 21. The absorption cross section per hydrogen atom is taken from Brown and Gould (1970).

The author would like to express her thanks to Professor S. Hayakawa for his suggestions and helpful discussions. Cooperation of the staff of FACOM 190 computer at Institute of Plasma Physics is also acknowledged.

References

- Aldrovandi, S.M.V., and Pequignot, D. 1973, *Astron. & Astrophys.* 25, 137.
- Aldrovandi, S.M.V., and Pequignot, D. 1974, *Revista Brasileira de Fisica.* 4, 491.
- Allen, C.W. 1965, *Space Sci. Rev.* 4, 91.
- Allen, C.W. 1973, *Astrophysical Quantities* (3rd Ed.), University of London.
- Ansari, S.M.R., Elwert, G., and Mücklich, P. 1970, *Z. Naturforsch.* 25a, 1781.
- Bhalla, C.P., Gabriel, A.H., and Presnyakov, L.P. 1975, *Mon. Not. R. Astr. Soc.* 172, 359.
- Brown, R.L., and Gould, R.J. 1970, *Phys. Rev. D.* 1, 2252.
- Burgess, A. 1965, *Ap. J.* 141, 1588.
- Fujimoto, T., and Kato, T. 1968, private communication.
- Gabriel, A.H., 1972, *Mon. Not. R. Astr. Soc.* 160, 99.
- Gaffet, B. 1978, preprint.
- Goldberg, L., Dupree, A.K., and Allen, J.W. 1965, *Ann. d'Astr.* 28, 589.
- Griem, H.R. 1964, *Plasma Spectroscopy*, McGraw-Hill, New York.
- Hayakawa, S., Kato, T., Makino, F., Ogawa, H., Tanaka, Y., and Yamashita, K. 1970, *Japanese Journal of Applied Physics* 9, 542.

- Itoh, H. 1977, Publ. Astron. Soc. Japan 20, 313.
- Jacobs, V.L., Davis, F., Kepple, P.C., and W. Blaha. 1977,
Ap. J. 211, 605.
- Jordan, C. 1969, Mon. Not. R. Astr. Soc. 142, 501.
- Jordan, C. 1970, *ibid.*, 148, 17.
- Kafatos, M. 1973, Ap. J. 182, 433.
- Kafatos, M.C., and Tucker, W.H. 1972, Ap. J. 175, 837.
- Kato, T. 1976, Ap. J. Suppl. 30, 397.
- Kato, T. 1977, IPPJ-AM-2.
- Kato, T. 1978, to be published in IPPJ-AM-5.
- Kato, T., Kohno, T., Nagase, F., Nishimura, K., Tanaka, Y.
and Yamashita, K. 1972, Japanese Journal of Applied
Physics 11, 1351.
- Karzas, W.J., and Latter, R. 1961, Ap. J. Supple., 6, 167.
- Landini, M., and Monsignori Fossi, B.C. 1970, Astr. and Ap.
6, 468.
- Landini, M., and Monsignori Fossi, B.C. 1971, Solar Physics
20, 322.
- Lotz, W. 1967, Report Institute Für Plasma Physics IPP 1/62.
- Lotz, W. 1968, *ibid.* IPP 1/76.
- Mattioli, M. 1975, EUR-CEA-FC-761.
- Mewe, R. 1972a, Astr. and Ap. 20, 215.
- Mewe, R. 1972b, Solar Phys. 22, 459.
- Mewe, R. 1975, Solar Phys. 44, 383.
- Mewe, R., and Schrijver, J. 1977, Astr. and Ap.
- Nakamura, K., Kawanishi, B., and Tajima, T. 1977, FAERI-W,
7010.

- Raymond, J.C. and Smith, B. 1977, *Astrophys. J. Suppl.*
35, 419.
- Raymond, J.C., Cox, D.P., and Smith, B. 1976b, *Ap. J.*
204, 290.
- Seaton, M.J., 1964, *Planet Space Sci.* 12, 55.
- Shapiro, P., and Moore, R. 1976, *Ap. J.* 207, 460.
- Spitzer, Jr., L. 1962, *Physics of Fully Ionized Gases*,
(Second Edi.) Interscience Publishers, New York.
- Stern, R., Wang, E., and Bowyer, S. 1978, *Ap. J. Suppl.* June.
- Summers, H.P. 1974, *Mon. Not. R. Astr. Soc.* 169, 663.
- Tucker, W.H., and Koren, M. 1971, *Ap. J.* 168, 283.
- Wilson, R. 1964, *Atomic Collision Processes in Plasmas*
AERE-R 4818,
- Wilson, R. 1967, *Plasmas in Space and in the Laboratory*,
ESRO SP-20.
- Yamaguchi, N., Shiho, R., and Mizui, J. 1978, private
communication.

Table 1.

Gaunt factor $\bar{g}_{ff}(k, KT)$ for bremsstrahlung

$\frac{KT}{z^2}$ (keV)	$u = k/KT$	$\bar{g}_{ff}(u)$
0.0014 ~ 0.0136	<0.1 >0.1	$1.12u^{-1/6}$ ~1
0.0136 ~ 0.136	<0.1 >0.1	$u^{-0.19}$ $1.2u^{-0.1}$
0.136 ~ 1.36	<0.1 >0.1	$\pi/\sqrt{3}K_0 (\frac{u}{2})e^{u/2}$ $u^{-0.3}$
1.36 ~ 13.6	all range	$\pi/\sqrt{3} K_0 (\frac{u}{2})e^{u/2}$

Table 2

The values of S/Z^4 for recombination radiation

	Z	n=1	n=2	n=3
HI-like	all	1	0.125	0.037
HeI-like				
CVIII→OVII	8	0.36	0.073	0.022
SiXV→SiXIV	14	0.42	0.093	0.028
FeXXVI→FeXXV	26	0.46	0.107	0.032
LiI-like				
OVI	8	-	0.044	0.012
SiXIII	14	-	0.067	0.020
FeXXIV	26	-	0.087	0.027

Table 3

Parameters for recombination coefficients of eq. (3.9) and eq. (3.14)

Ion	A_r ($\text{cm}^3 \text{s}^{-1}$)	η	T_{max} (keV)	T_{crit} (keV)	A_d ($\text{cm}^3 \text{s}^{-1} \text{keV}^{3/2}$)	W_1 (keV)	B_d	W_2 (keV)
HeI	4.3(-13)	.672	.0086	.0043	4.8(-14)	.041	0.3	.0081
CI	4.7(-13)	.624	.0026	.0010	1.7(-14)	.0095	3.0	.0042
CII	2.3(-12)	.645	.0086	.0010	1.8(-13)	.013	0.5	.020
CIII	3.2(-12)	.770	.026	.0009	9.6(-14)	.0078	2.0	.032
CIV	7.5(-12)	.817	.086	.038	1.2(-12)	.29	0.2	.044
CV	1.7(-11)	.721	.026	.060	1.2(-12)	.35	0.2	.066
NI	4.1(-13)	.608	.0086	.0016	1.3(-14)	.011	3.8	.0041
NII	2.2(-12)	.639	.0086	.0016	4.3(-14)	.012	4.1	.0059
NIII	5.0(-12)	.676	.026	.0021	3.0(-13)	.016	1.4	.033
NIV	6.5(-12)	.743	.026	.0013	1.4(-13)	.0095	3.0	.051
NV*	1.5(-11)	.850	.26	.059	1.9(-12)	.41	0.2	.062
NVI	2.9(-11)	.750	.86	.068	1.7(-12)	.47	0.2	.084
OI	3.1(-13)	.678	.0043	.0023	3.5(-14)	.015	2.5	.011
OII	2.0(-12)	.646	.0086	.0019	3.5(-14)	.015	3.3	.0050
OIII	5.1(-12)	.666	.026	.0021	7.1(-14)	.016	6.0	.0078
OIV	9.6(-12)	.670	.026	.0022	4.3(-13)	.019	2.0	.051
OV*	1.2(-11)	.779	.052	.0014	1.8(-13)	.011	3.2	.069
OVI*	2.3(-11)	.802	.26	.086	2.8(-12)	.53	0.2	.082
CVII	4.1(-11)	.742	.86	.13	2.2(-12)	.60	0.2	.11
NeI	2.2(-13)	.759	.0086	.0026	3.3(-14)	.027	1.3	.013
NeII	1.5(-12)	.693	.0086	.0028	7.8(-14)	.025	0.6	.015
NeIII	4.4(-12)	.675	.017	.0028	1.9(-13)	.022	0.7	.039
NeIV	9.1(-12)	.668	.026	.0030	1.4(-13)	.021	4.3	.015
NeV	1.5(-11)	.684	.052	.0031	2.5(-13)	.021	4.8	.030
NeVI	2.3(-11)	.704	.086	.0031	1.0(-12)	.025	1.6	.095
NeVII*	2.8(-11)	.771	.086	.0025	2.8(-13)	.015	5.0	.11
NeVIII*	5.0(-11)	.832	.52	.13	4.6(-12)	.84	0.2	.12
NeIX	8.6(-11)	.769	2.6	.33	3.3(-12)	.95	0.2	.22

- Table 3-1 -

Note: Table 3-2 and Table 3-3 are to be found after Tables 4 and 5 due to a printer's error.

Table 4

Element abundances

Element Abundance	H	He	C	N	O	Ne	Mg	Si	S	Ca	Fe	Ni
a) Allen	1.0	8.5(-2)	3.3(-4)	9.1(-5)	6.6(-4)	8.3(-5)	2.6(-5)	3.3(-5)	1.6(-5)	2.6(-6)	4.0(-5)	2.0(-6)
b) Tucker and Koren	1.0	2.0(-1)	5.3(-4)	6.2(-5)	3.1(-4)	3.9(-5)	3.1(-5)	5.0(-5)	2.0(-5)	2.0(-6)	5.0(-5)	5.0(-6)

Table 5

Transitions of Prominant Lines in Fig. 9 and Fig. 10.

Ion	k(KeV)	$\lambda(\text{\AA})$	Isoel. Seq.	Tran. No.	Transition
OVIII	0.653	19.0	H	1	1s - 2p
OVIII	0.775	16.0	H	2	1s - 3p
OVII	0.574	21.6	He	4	1s ² (¹ S) - 1s2p(¹ P)
OVII	0.561	22.09	He	6	1s ² (¹ S) - 1s2s(³ S)
OVII	0.569	21.80	He	5	1s ² (¹ S) - 1s2p(³ P)
OVII	0.666	18.63	He	3	1s ² (¹ S) - 1s3p(¹ P)
OVI	0.083	150.10	Li	5	2s - 3p
OVI	0.107	115.80	Li	2	2s - 4p
OVI	0.118	104.81	Li	1	2s - 5p
OV	0.064	192.85	Be	6	2s2p(³ P) - 2s3d(³ D)
SXII	0.340	36.50	B	6	2p(² P) - 3d(² D)
SX	0.292	42.50	N	1	2p ³ (⁴ S) - 2p ² 3d(⁴ P)
SX	0.238	52.0	N	4	2s2p ⁴ (⁴ P) - 2s2p ³ 3s(⁴ P)
SIX	0.252	49.20	O	1	2p ⁴ (³ P) - 2p ³ 3d(³ D)
SVIII	0.234	53.0	F	2	2p ⁵ (² P) - 2p ⁴ 3d(² S, ² P, ² D)
SVII	0.204	60.8	Ne	5	2p ⁶ (¹ S) - 2p ⁵ 3d(¹ P)
SVII	0.172	72.03	Ne	7	2p ⁶ (¹ S) - 2p ⁵ 3s(¹ P)
FeXXII	0.10	124.0	B	10	2s ² 2p(² P) - 2s2p ² (² P)
FeXX	0.102	121.0	N	6	2s ² 2p ³ (⁴ S) - 2s2p ⁴ (⁴ P)
FeXIX	0.115	108.0	O	6	2s ² 2p ⁴ (³ P) - 2s2p ⁵ (³ P)
FeXIX	0.919	13.50	O	1	2p ⁴ (³ P) - 2p ³ 3d(³ D)
FeXVII	0.739	16.77	Ne	7	2p ⁶ (¹ S) - 2p ⁵ 3s(¹ P)
FeXVII	0.802	15.46	Ne	6	2p ⁶ (¹ S) - 2p ⁵ 3d(³ D)
FeXVII	0.827	15.0	Ne	5	2p ⁶ (¹ S) - 2p ⁵ 3d(¹ P)
FeXIV	0.221	56.20	Al	14	3s ² 3p(² P) - 3s3p4p(² D)
FeXIII	0.061	202.0	Si	3	3p ² (³ P) - 3p3d(³ D)
FeXII	0.064	195.14	P	4	3p ³ (⁴ S) - 3p ² 3d(⁴ P)
FeXII	0.188	66.10	P	1	3p ³ (⁴ S) - 3p ² 4d(⁴ P)
FeXI	0.139	89.20	S	3	3p ⁴ (³ P) - 3p ³ 4s(³ S)
FeX	0.073	170.90	Cl	4	3p ⁵ (² P) - 3p ⁴ 3d(² D)
FeX	0.128	97.0	Cl	2	3p ⁵ (² P) - 3p ⁴ 4s(² P, ² D)
FeX	0.161	77.0	Cl	1	3p ⁵ (² P) - 3p ⁴ 4d(² D, ² P)
FeIX	0.072	171.06	A	4	3p ⁶ (¹ S) - 3p ⁵ 3d(¹ P)
FeIX	0.120	103.58	A	2	3p ⁶ (¹ S) - 3p ⁵ 4s(¹ P)
FeIX	0.149	83.0	A	1	3p ⁶ (¹ S) - 3p ⁵ 4d[3/2], [5/2]
FeVIII	0.067	185.20	K	7	3p ⁶ 3d(² D) - 3p ⁵ 3d ² (² F)
FeVIII	0.074	167.50	K	5	3p ⁶ 3d(² D) - 3p ⁵ 3d ² (² D)

Ion	A_r ($\text{cm}^3 \text{s}^{-1}$)	η	T_{max} (keV)	T_{crit} (keV)	A_d ($\text{cm}^3 \text{s}^{-1} \text{keV}^{3/2}$)	W_1 (keV)	B_d	W_2 (keV)
MgI*	1.4(-13)	.855	.0026	.00034	4.3(-14)	.0044	0.0	-
MgII*	8.8(-13)	.838	.0086	.0064	8.6(-14)	.053	0.0	-
MgIII	3.5(-12)	.734	.026	.0057	9.9(-14)	.038	3.0	.035
MgIV	7.7(-12)	.718	.043	.0047	2.4(-13)	.034	3.2	.075
MgV	1.4(-11)	.716	.086	.0038	3.8(-13)	.029	3.2	.086
MgVI	2.3(-11)	.695	.086	.0039	3.0(-13)	.027	6.7	.046
MgVII	3.2(-11)	.691	.086	.0039	3.5(-13)	.027	4.4	.031
MgVIII	4.6(-11)	.771	.17	.0043	9.6(-13)	.031	3.5	.14
MgIX*	5.8(-11)	.804	.26	.0029	3.5(-13)	.018	10.0	.18
MgX*	9.1(-11)	.830	.86	.21	6.6(-12)	1.2	0.2	.21
MgXI	1.5(-10)	.779	.43	.34	4.3(-12)	1.3	0.2	.30
SiI	5.9(-13)	.601	.0026	.00095	1.6(-13)	.0095	0.0	-
SiII*	1.0(-12)	.786	.0052	.00095	3.5(-13)	.010	0.0	-
SiIII	3.7(-12)	.693	.0086	.00095	2.8(-13)	.0086	0.0	-
SiIV	5.5(-12)	.821	.026	.015	3.5(-13)	.010	0.0	-
SiV	1.2(-11)	.735	.052	.0082	2.0(-13)	.047	10.0	.086
SiVI	2.1(-11)	.716	.086	.0069	4.0(-13)	.042	4.0	.11
SiVII	3.0(-11)	.702	.086	.0064	5.8(-13)	.036	8.0	.15
SiVIII	4.3(-11)	.688	.086	.0059	2.8(-13)	.033	6.3	.052
SiIX	5.8(-11)	.703	.17	.0057	2.8(-13)	.032	6.0	.095
SiX	7.7(-11)	.714	.27	.0056	1.2(-12)	.036	5.0	.22
SiXI*	1.2(-10)	.855	.86	.0039	4.6(-13)	.022	10.5	.24
SiXII	1.5(-10)	.831	2.6	.32	8.6(-12)	1.6	0.2	.27
SiXIII	2.1(-10)	.765	4.3	.54	5.3(-12)	1.7	0.2	.38
SI	4.1(-13)	.630	.0026	.0019	1.8(-15)	.0095	0.0	-
SII	1.8(-12)	.686	.0052	.0010	1.2(-13)	.010	2.5	.0076
SIII	2.7(-12)	.745	.0086	.0012	2.3(-13)	.011	6.0	.013
SIV	5.7(-12)	.755	.026	.0013	1.1(-12)	.016	0.0	-
SV	1.2(-11)	.701	.026	.0012	6.3(-13)	.013	0.0	-
SVI*	1.7(-11)	.849	.086	.025	7.8(-13)	.16	0.0	-
SVII	2.7(-11)	.733	.086	.011	3.3(-13)	.056	22.0	.16

- Table 3-2 -

Ion	A_r ($\text{cm}^3 \text{ s}^{-1}$)	η	T_{max} (keV)	T_{crit} (keV)	A_d ($\text{cm}^3 \text{ s}^{-1} \text{ keV}^{3/2}$)	W_1 (keV)	B_d	W_2 (keV)
SVIII	4.0(-11)	.696	.086	.0095	5.3(-13)	.051	6.4	.17
SIX	5.5(-11)	.711	.13	.0076	8.6(-13)	.047	13.0	.20
SX	7.4(-11)	.716	.13	.0076	7.6(-13)	.041	6.8	.10
SXI	9.2(-11)	.714	.22	.0076	7.8(-13)	.036	6.3	.11
SXII*	1.4(-10)	.755	.52	.0072	1.6(-12)	.043	4.1	.29
SXIII*	1.7(-10)	.832	.86	.0052	5.8(-13)	.026	12.0	.31
SXIV	2.5(-10)	.852	8.6	.43	1.1(-11)	2.1	0.2	.40
SXV	3.3(-10)	.783	8.6	.77	6.3(-12)	2.2	0.2	.47

Figure Captions

- Fig.1. Ionization rate coefficients (a) for oxygen ions and (b) for iron ions. The solid line represents the rate by autoionization, and the dashed line by direct collisional ionization.
- Fig.2. Energy level diagram of dielectronic recombination from He-like to Li-like ions.
- Fig.3. Comparison between the rate coefficients of dielectronic recombination σ_d calculated by several authors. The dashed line represents the radiative recombination coefficient σ_r . (a) For O ions; the solid curves indicate the results (σ_d) by Aldrovandi and Pequignot (1973), the dotted curves (σ_d) by Ansari et al (1970), and the dot-dashed curves ($\sigma_d + \sigma_r$) by Nakamura et al (1977). (b) For Fe ions; the solid curves (σ_d) by Ansari et al (1970), the dotted curves ($\sigma_r + \sigma_d$) by Jordan (1970) and the dot-dashed curves ($\sigma_r + \sigma_d$) by Nakamura et al (1977). (c) $\sigma_r + \sigma_d$ by Jacobs et al (1977) for Fe ions.

Fig.4. The ionization equilibrium for Fe ions calculated by Jacobs et al (1977) (solid lines). The results by Jordan (1969, 1970) are shown by dashed lines for the sake of comparison. Adopted from Jacobs et al (1977).

Fig.5. Time history of ionization of O ions. (a) Ionizing plasma for a constant temperature $KT = 0.3$ keV. The initial ion abundances are taken to be $n(\text{OVII})/n(\text{O}) = 1.0$. Solid curves: with dielectronic recombination and autoionization. Dashed curves: without dielectronic recombination and autoionization. (b) Recombining plasma for a constant temperature $KT = 0.1$ keV. $n(\text{OIX})/n(\text{O}) = 1.0$ for the initial ion abundances.

Fig.6. The population density of OVII for $T_e = 10^6$ °K and $n_e = 10^{18}$ cm⁻³. (a) Ionizing phase; $n(\text{OVIII}) \approx 0.0$. (b) Recombining phase; $n(\text{OVII}) \approx 0.0$.

Fig.7. Observed satellite lines from a laser plasma. (Yamaguchi et al 1978).

Fig.8. The calculated ratios of the satellite to resonance line intensities for O ions as a function of temperature. (a) Ionizing phase, (b) Recombining phase. The dashed line represents the results for $r_0(P, z - 1) = 1.0$.

Fig.9. Line intensities $J_{pq} / n_e n_H$ of strong lines as functions of temperature for plasmas of ionization equilibrium with Allen's abundances. The numbers in the parantheses indicate the energies of lines in keV.

- (a) O ions. The energy range of the lines is 0.5-1.0keV.
- (b) O ions, 0.06-0.1 keV,
- (c) S ions, 0.1-0.5 keV,
- (d) Fe ions, 0.5-1.0 keV,
- (e) Fe ions, 0.1-0.5 keV,
- (f) Fe ions, 0.06-0.1 keV.

Fig.10. Photon emission rate per ion per electron $J_{pq} / n_e n_z$ for the lines shown in Fig.9.

- (a) O ions, 0.5-1.0 keV,
- (b) O ions, 0.06-0.1 keV,
- (c) S ions, 0.1-0.5 keV,
- (d) Fe ions, 0.5-1.0 keV,
- (e) Fe ions, 0.1-0.5 keV,
- (f) Fe ions, 0.06-0.1 keV.

Fig.11. Comparison of spectra at $\log T = 6.2$ ($KT = 0.14$ keV) calculated by Landini and Fossi (1970), by Tucker and Koren (1971) and by Kato (1976).

Fig.12. Comparison between the line intensities of iron ions against temperature calculated by Kato (1976) (solid curves), by Stern et al (1976) (dashed curves), by Raymond and Smith (1977) (dot-dashed curves) by Mewe (1972b, 1975) (dotted curves). The numbers indicate the wavelengths of the lines in \AA .

Fig.13. (a) Radiation loss rate per electron and per atom of atomic number Z , $U/n_e n_Z$ ($\text{erg cm}^3 \text{sec}^{-1}$) for H, He, C, N, O, Ne, Mg, Si, S, Ca, Fe and Ni ions. (b) Radiation loss rate $U/n_e n_H$ for the interstellar plasma of Allen's abundances.

Fig.14. Contribution of each line to the total line emission. (a) O ions, (b) S ions, (c) Fe ions. The dashed line shows the total emission rate obtained with the ion abundances by Jordan (1969, 1970), whereas the solid lines by Jacobs et al (197.). The numbers represent the wavelengths of the lines in \AA .

Fig.15. The energy dependences of the transmission probabilities for 0.8, 1.5 and 3.9 μ polypropylene windows.

Fig.16. Photon emission rate times the counter efficiency as a function of temperature for each strong line. The number in the parentheses gives the energy of the line in keV. The element abundances by Allen are used. (a) 0.5 μ polypropylene window, the energy range of the lines is 0.4 - 1.0 keV. (b) 1.3 μ , 0.4 - 1.0 keV. (c) 3.9 μ , 0.4 ~ 1.0 keV. (d) 0.5 μ , 0.1 - 0.4 keV. (e) 1.3 μ , 0.1 ~ 0.4 keV (f) 3.9 μ , 0.1 - 0.4 keV.

Fig.17. An example for spectral fitting of the spectra of Lupus Loop observed with 1 μ and 4 μ proportional counters. Four strong lines OVII (0.56 keV), OVIII (0.65 keV), FeXVII (0.83 keV) and NeIX (1.016 keV) are used to fit the spectra. The sum of their contributions is shown by a step-wise solid line.

Fig.18. The pulse height spectra $g(k) / n_e^2$ obtained by proportional counters from a hot plasma of Allen's abundances for several temperatures and three thickness of polypropylene window. The counter resolution $R = 0.48$ is assumed. The contributions of the line emissions of respective elements and the continuous emission are also shown. (a) 1.5 μ , $\log T = 6.1$, (b) = 1.5 μ , $\log T = 6.3$, (c) 1.5 μ , $\log T = 6.5$, (d) 0.8 μ ,

$\log T = 6.1$. (e) 0.8μ , $\log T = 6.5$, (f) 3.9μ , $\log T = 6.1$, and (g) 3.9μ , $\log T = 6.5$.

Fig.19. Comparison between the pulse height spectra calculated by LF, by TK and by Kato (1976) for $\log T = 6.2$ and the window thickness 1.5μ .

Fig.20. The pulse height spectra for the resolutions $k = R\sqrt{k}$ with $R = 0.24$ and $R = 0.12$.

Fig.21. The pulse height spectra modified by interstellar absorption. The dashed lines indicate the contributions of continuous emission. The numbers represent the hydrogen column densities N_H in H atoms cm^{-2} .

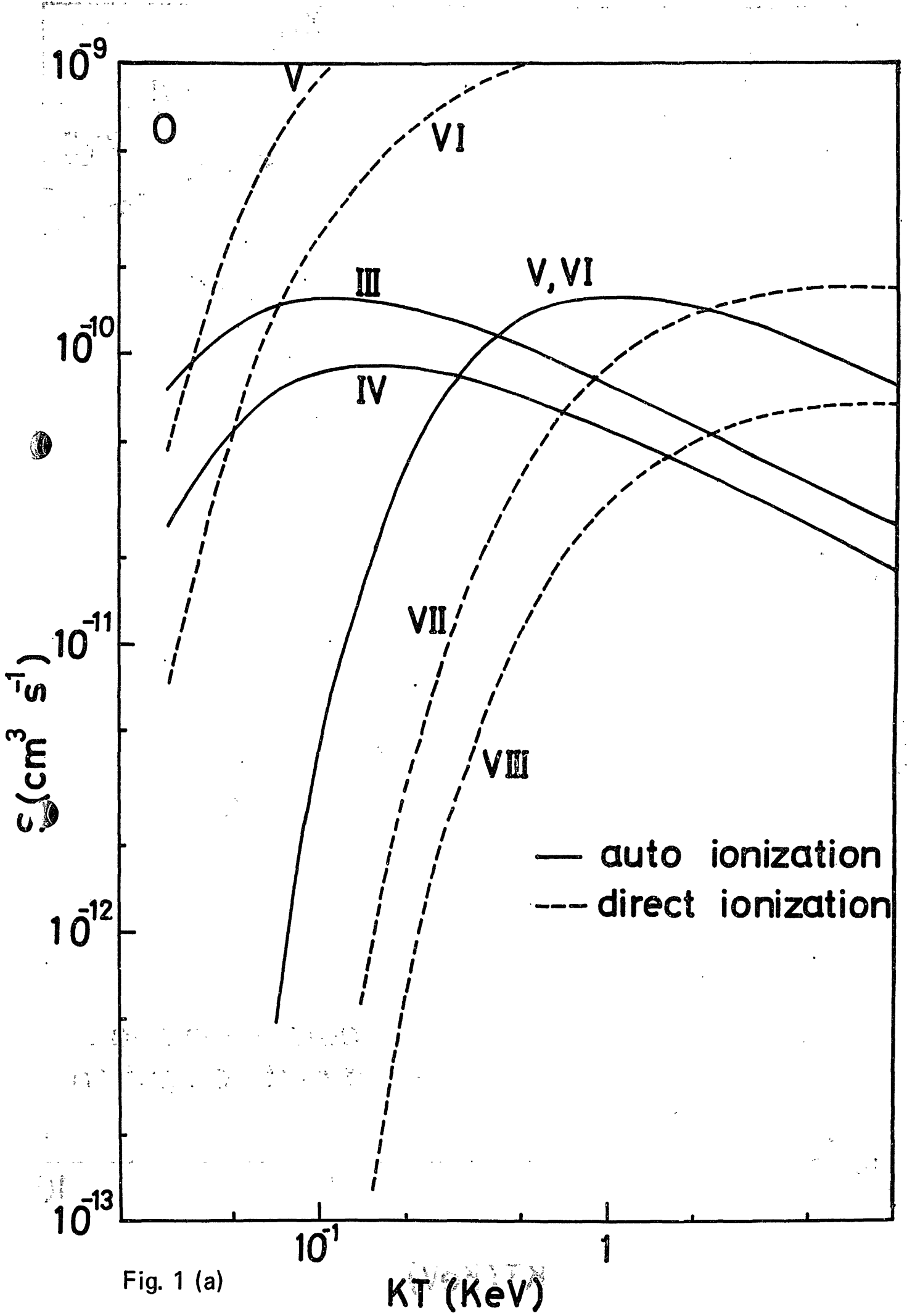


Fig. 1 (a)

KT (KeV)

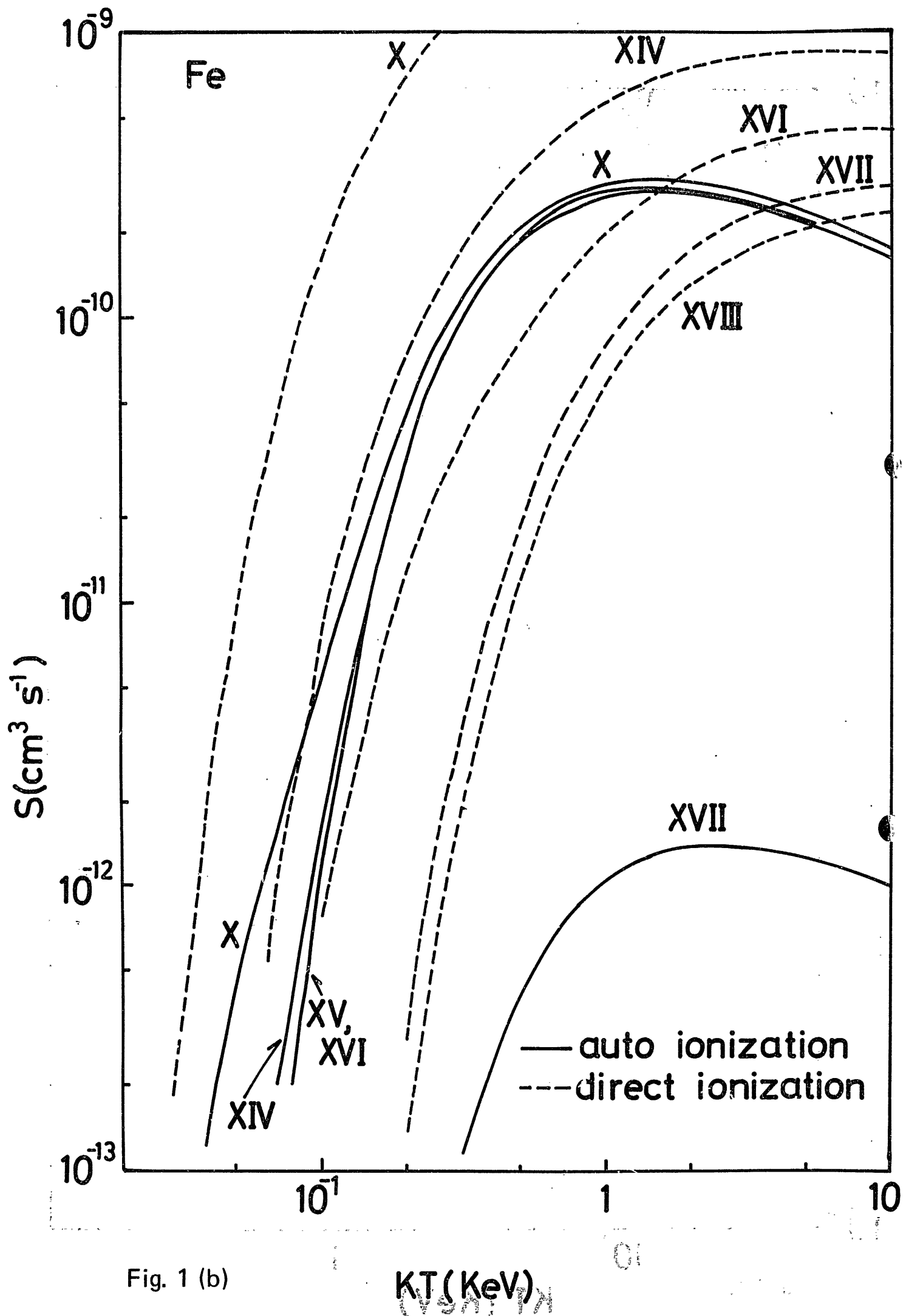
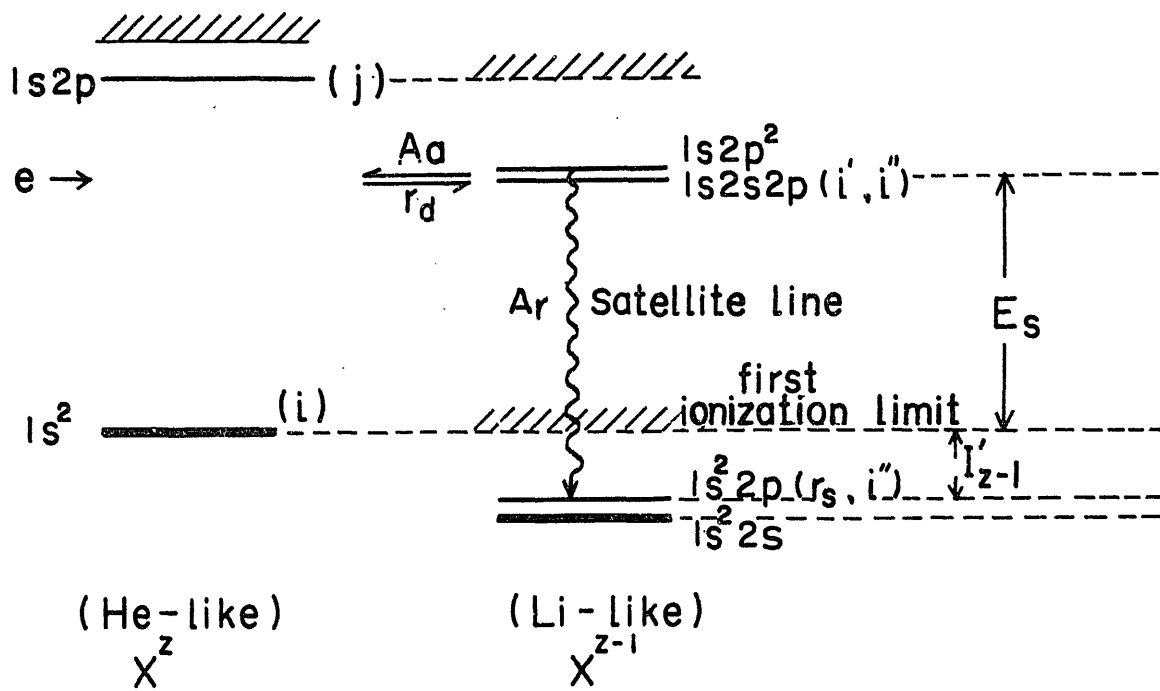


Fig. 1 (b)

KT (KeV)

Fig. 2



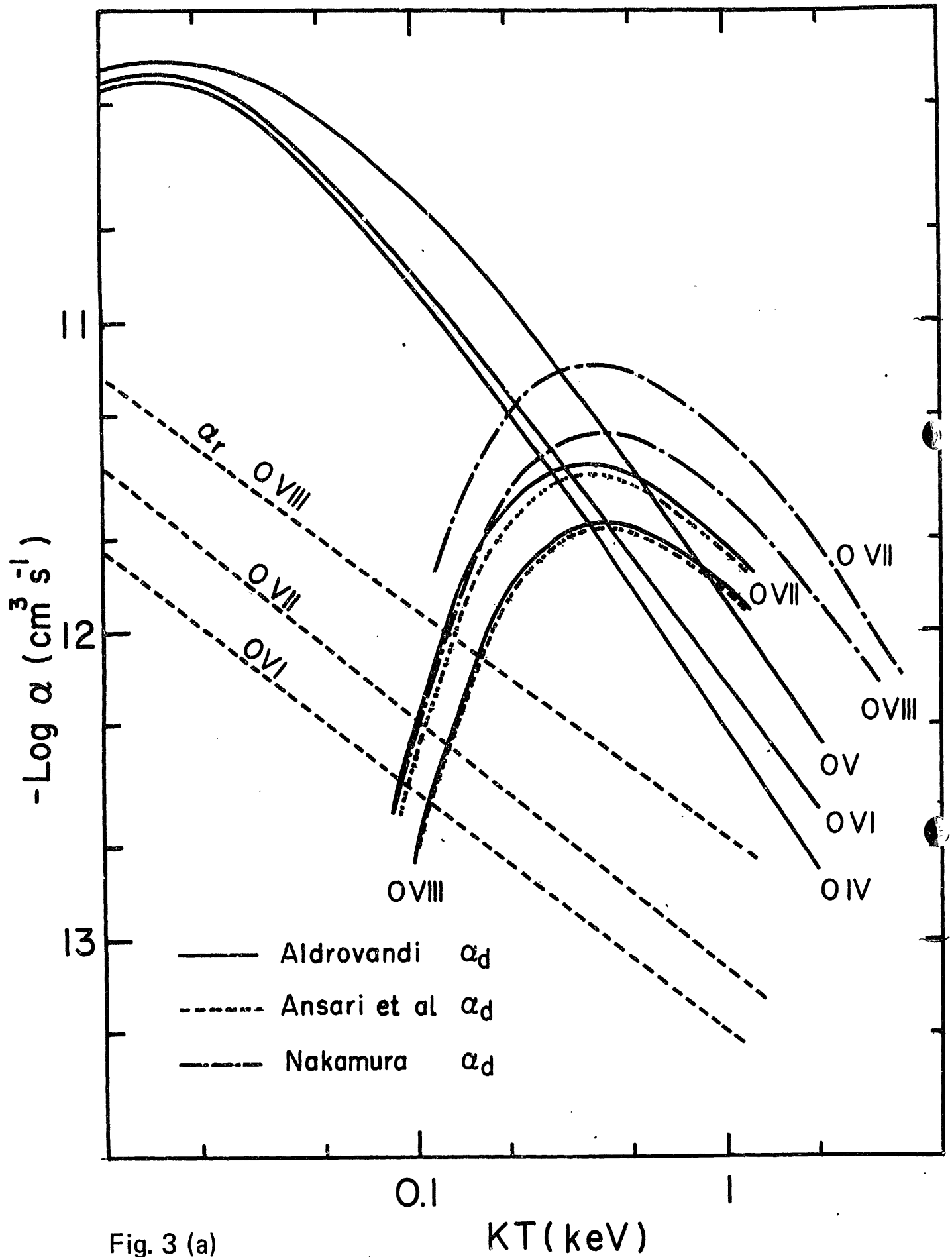


Fig. 3 (a)

Fe

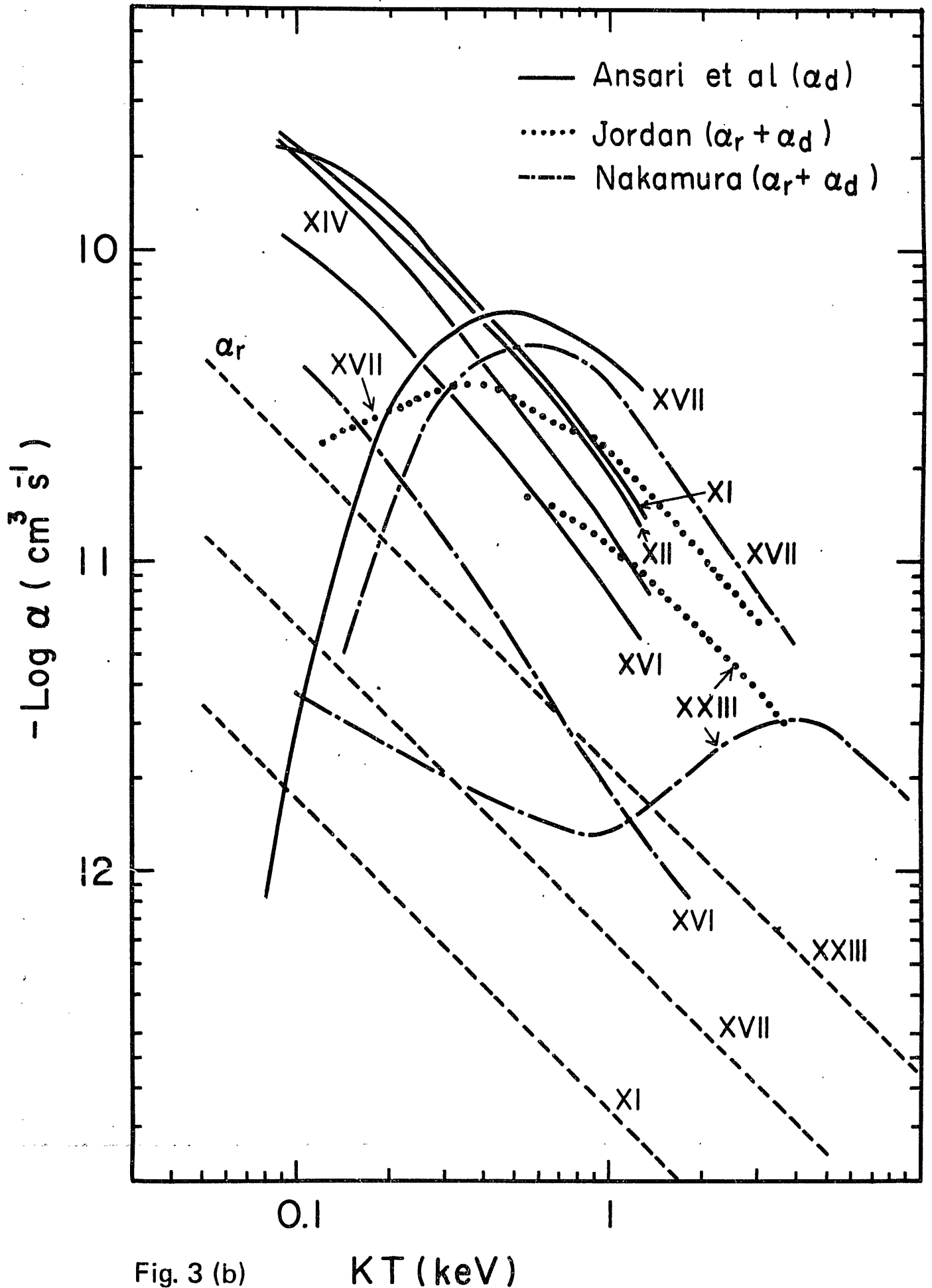


Fig. 3 (b)

KT (keV)

Fe

Jacobs et al (1977)

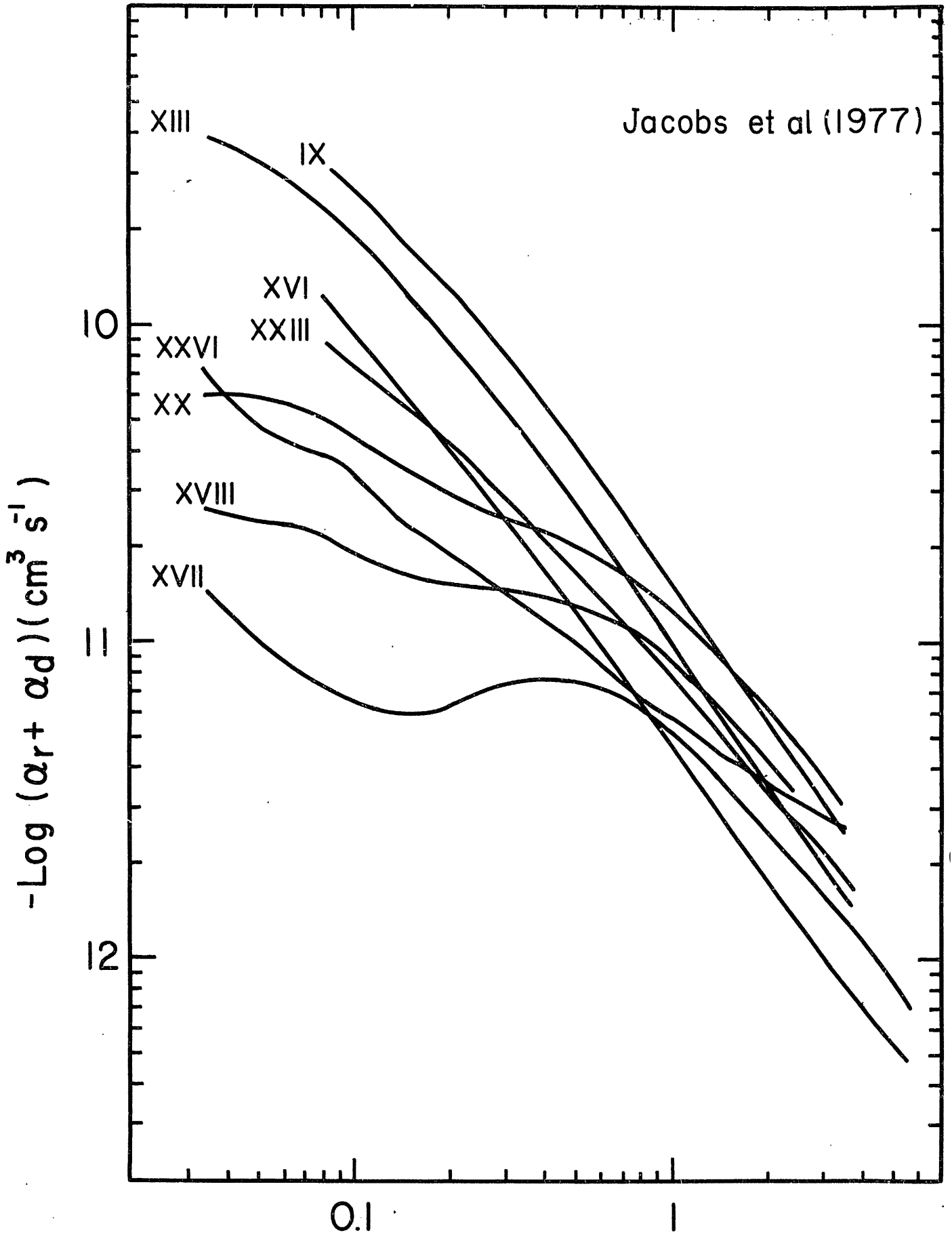


Fig. 3 (c)

KT (keV)

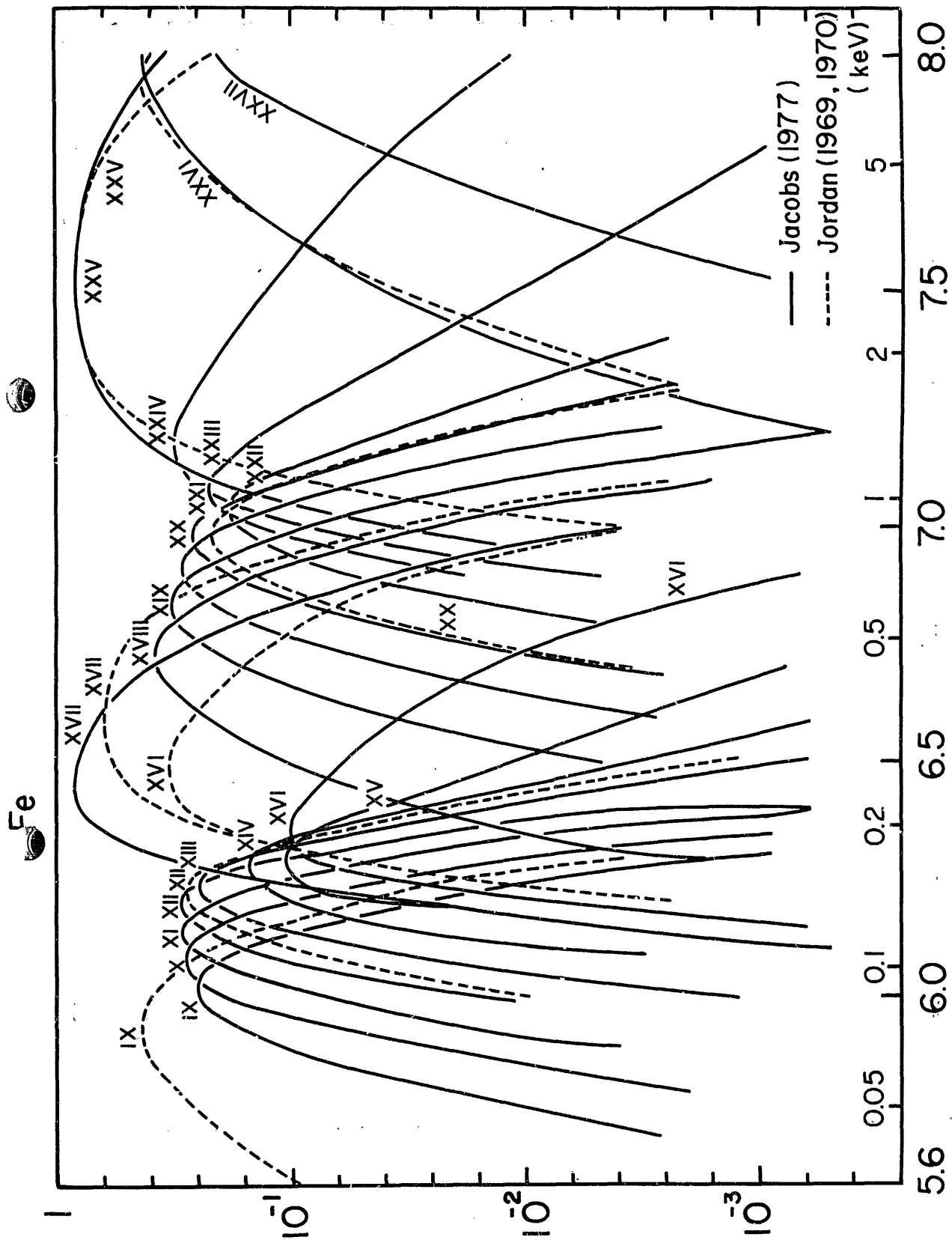


Fig. 4 $\text{Log } T (^{\circ}\text{K})$

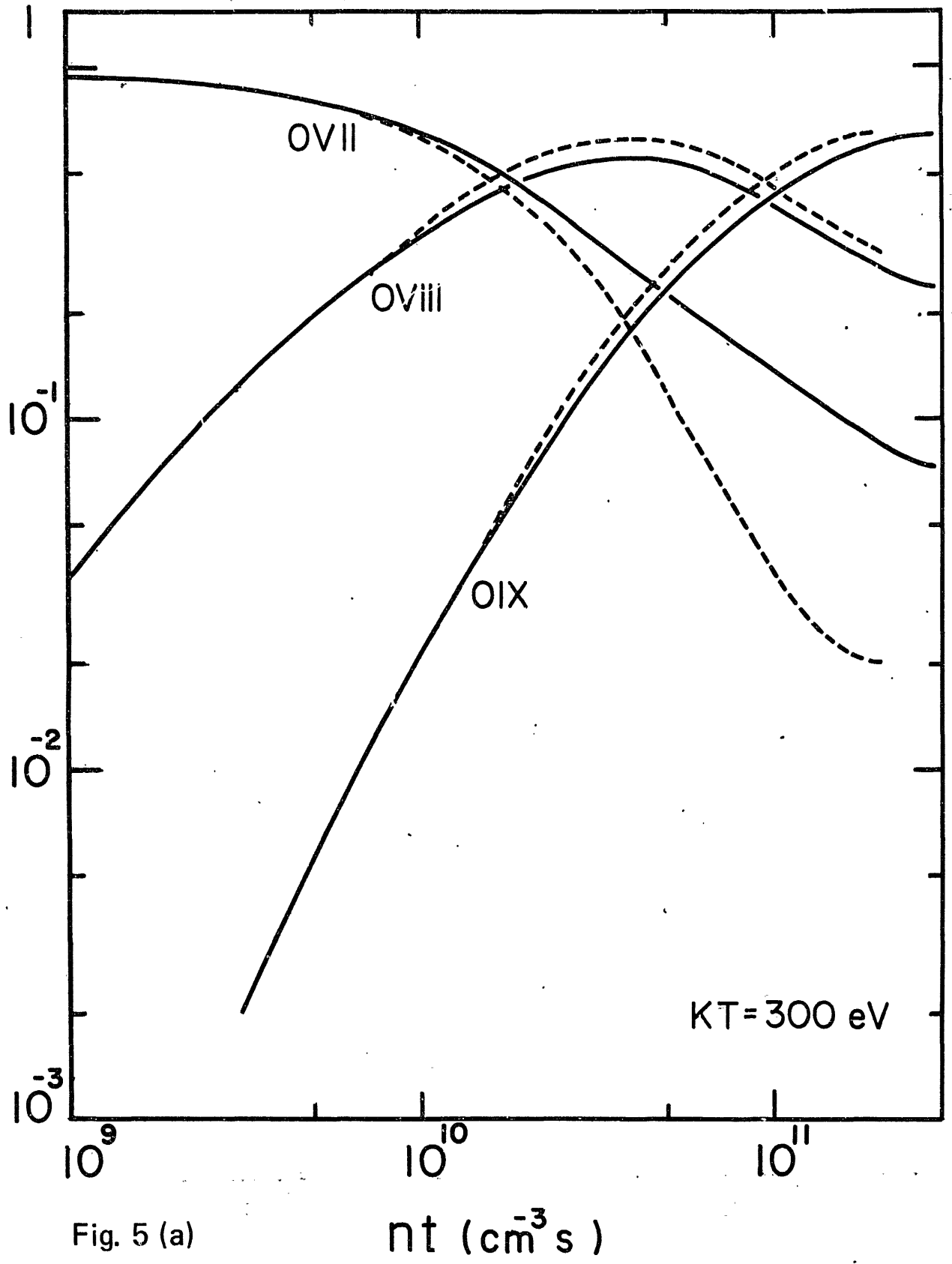


Fig. 5 (a)

nt ($\text{cm}^{-3} \text{s}$)

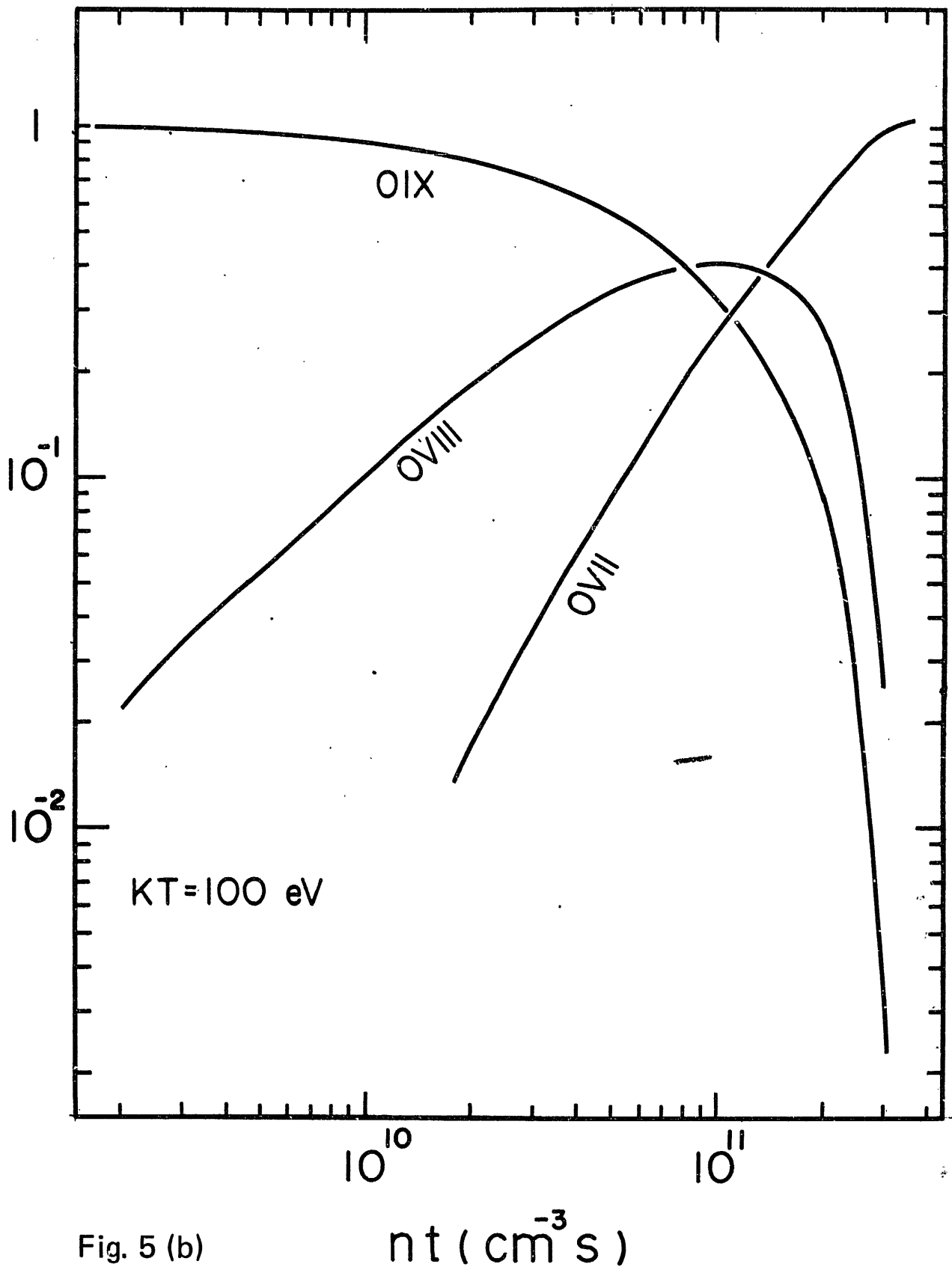


Fig. 5 (b)

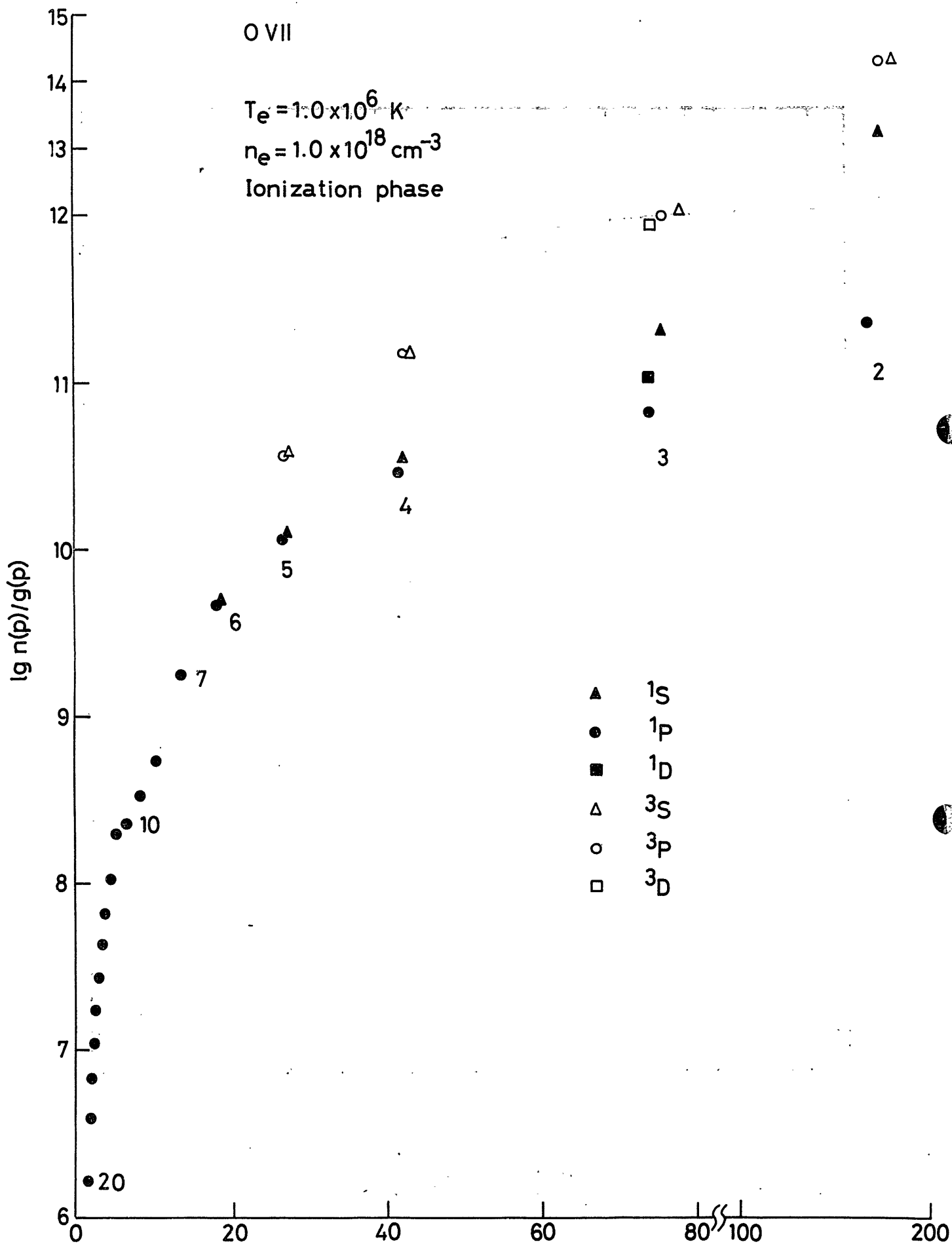


Fig. 6 (a) E (eV)

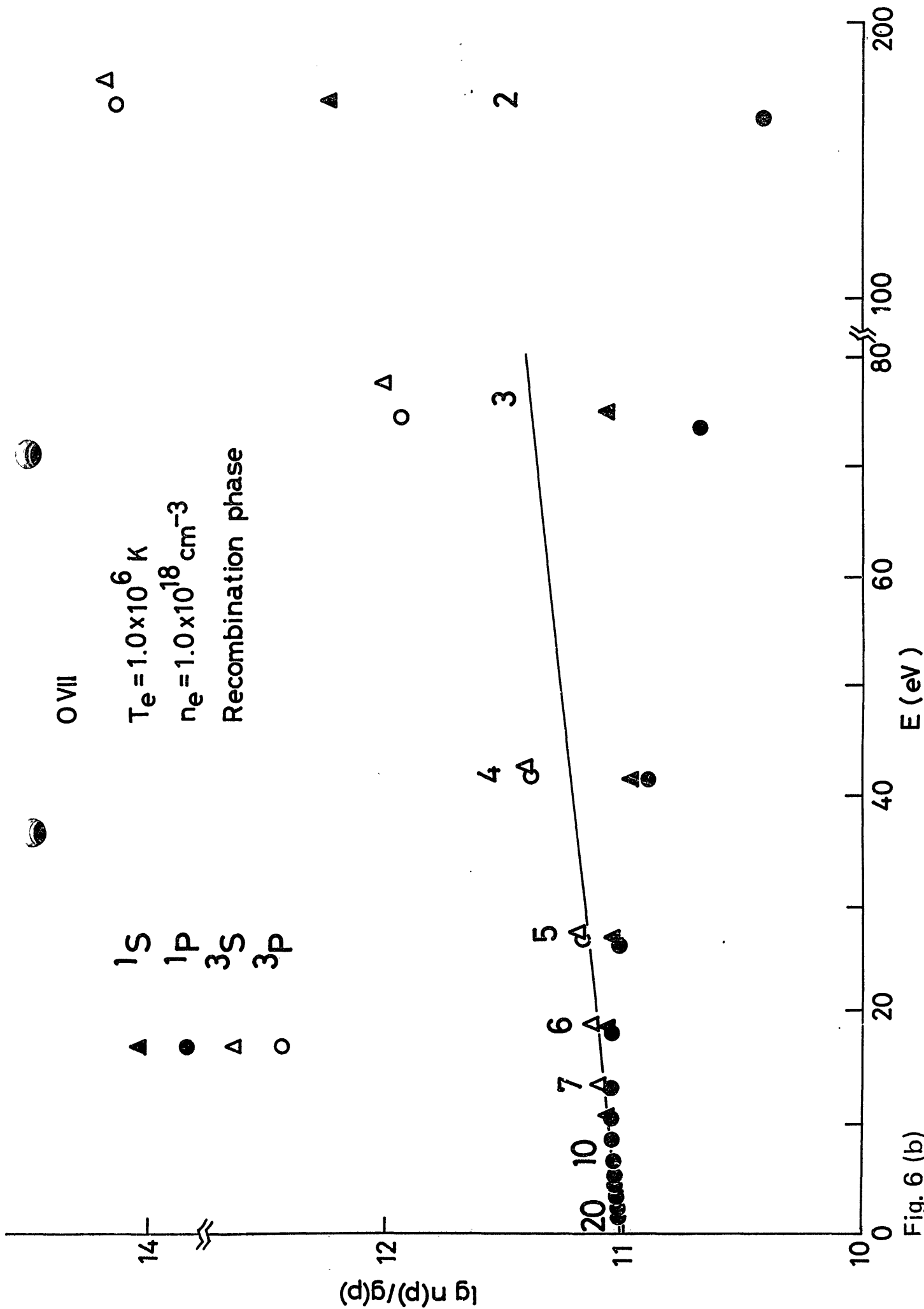


Fig. 6 (b)

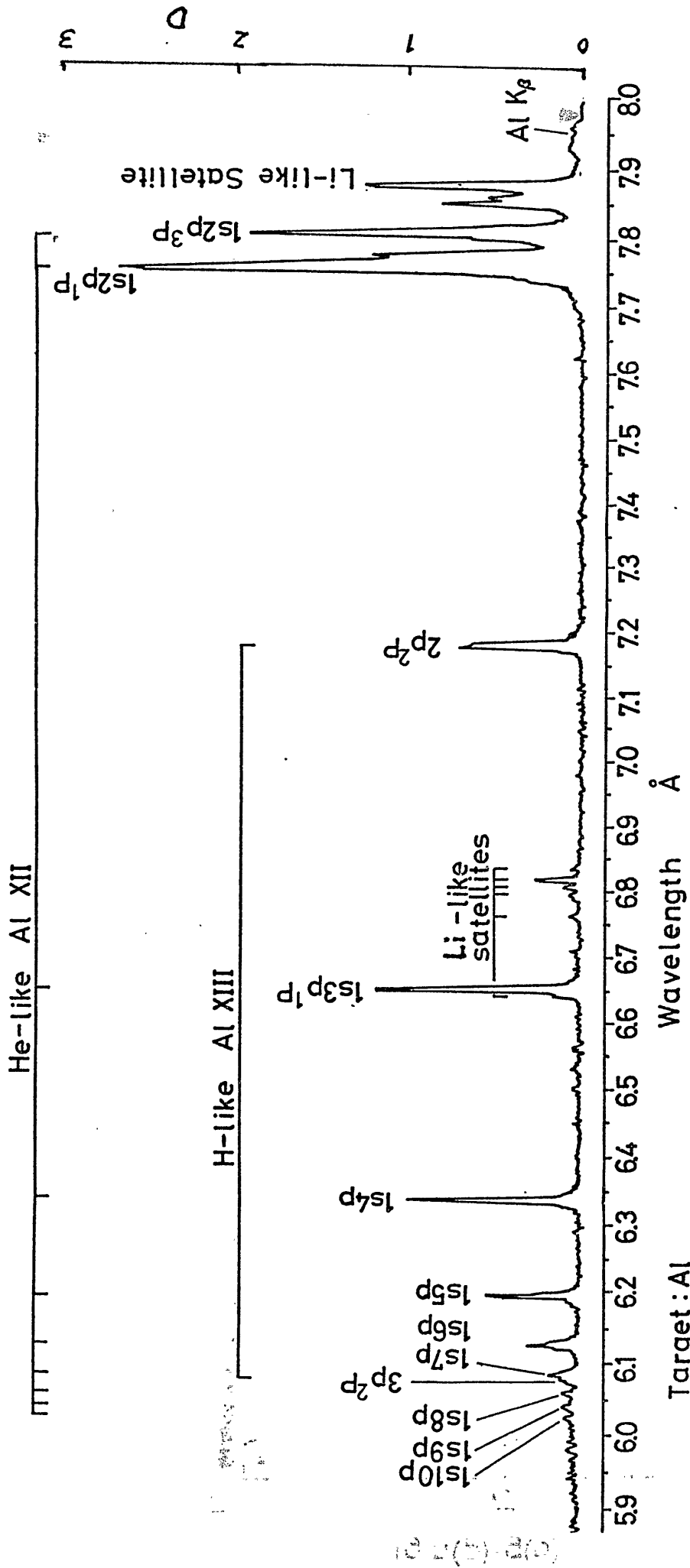


Fig. 7

$I_s(\text{Li-like satellite}) / I_r(\text{He-like resonance})$

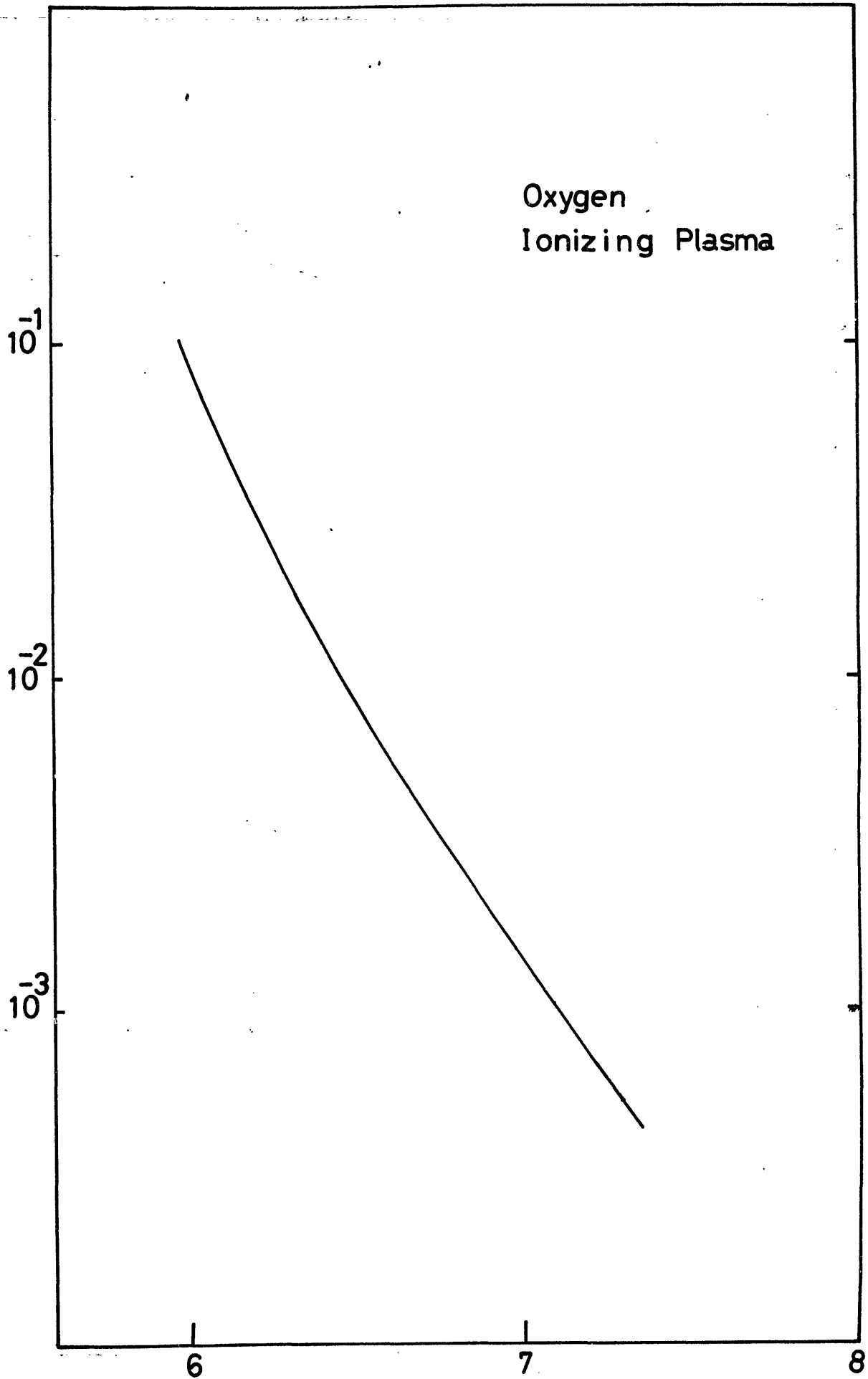


Fig. 8 (a)

Log T (K°)

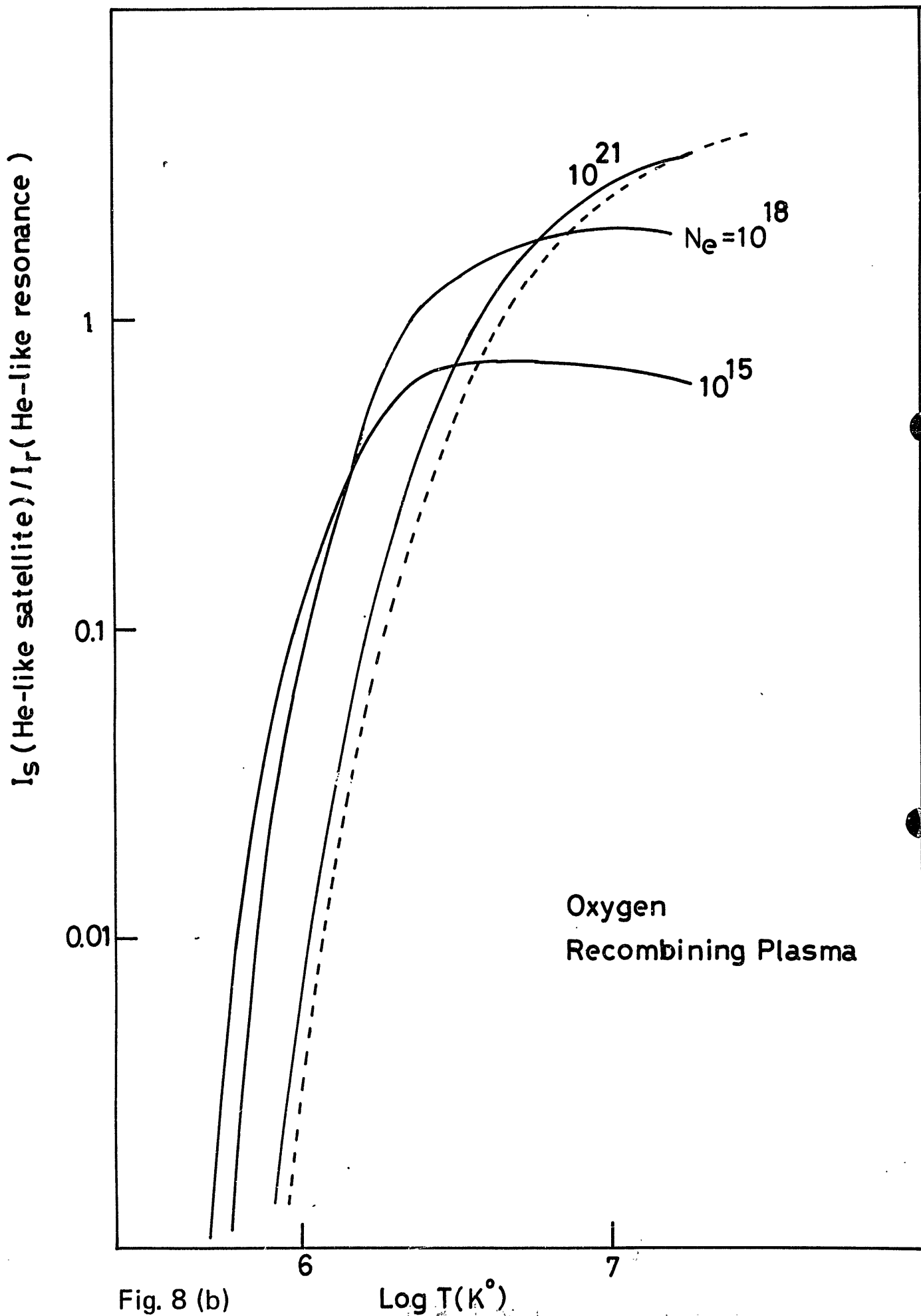


Fig. 8 (b)

$\text{Log } T(\text{K}^\circ)$

Oxygen
Recombining Plasma

KT (keV)

0

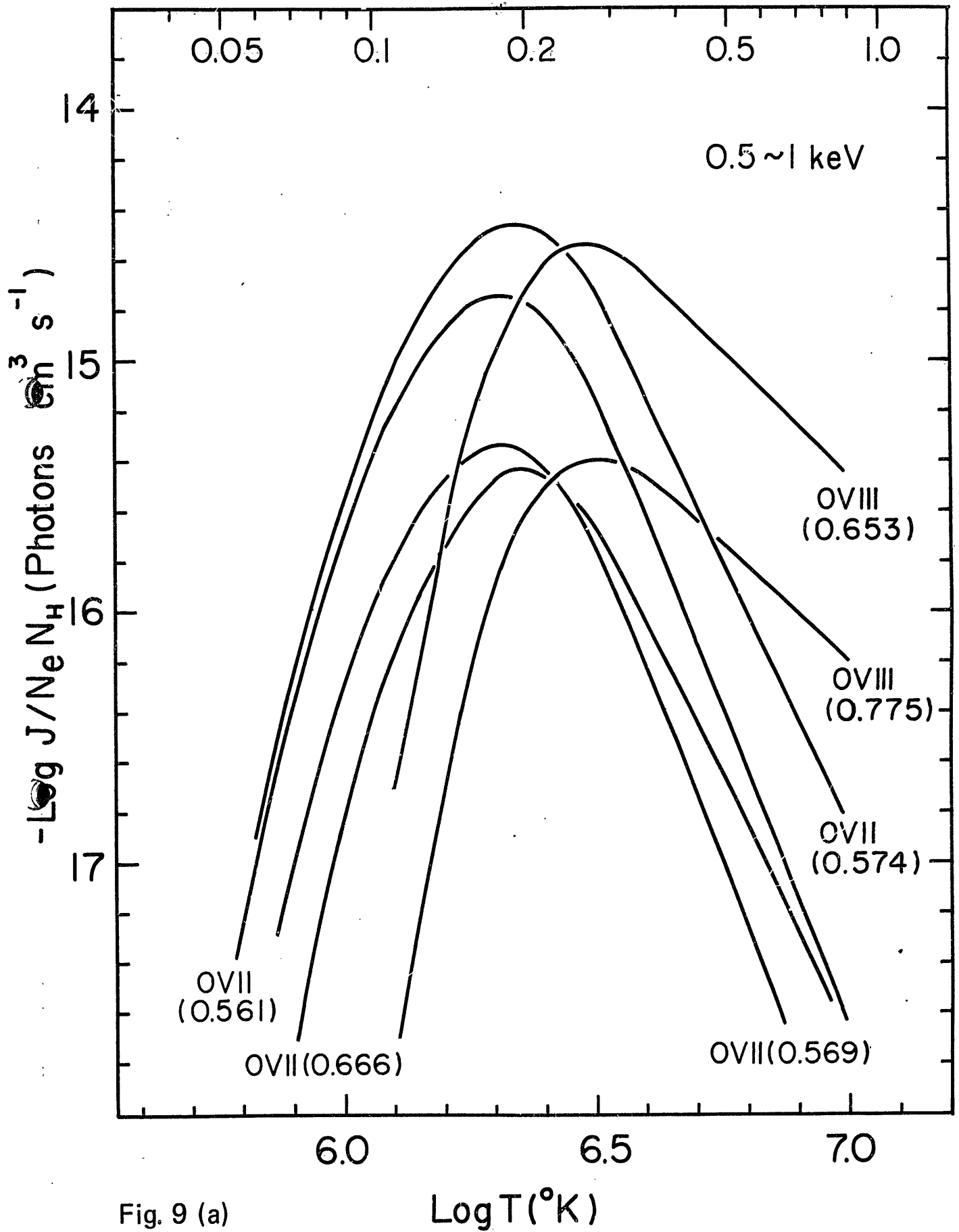


Fig. 9 (a)

Log T (°K)

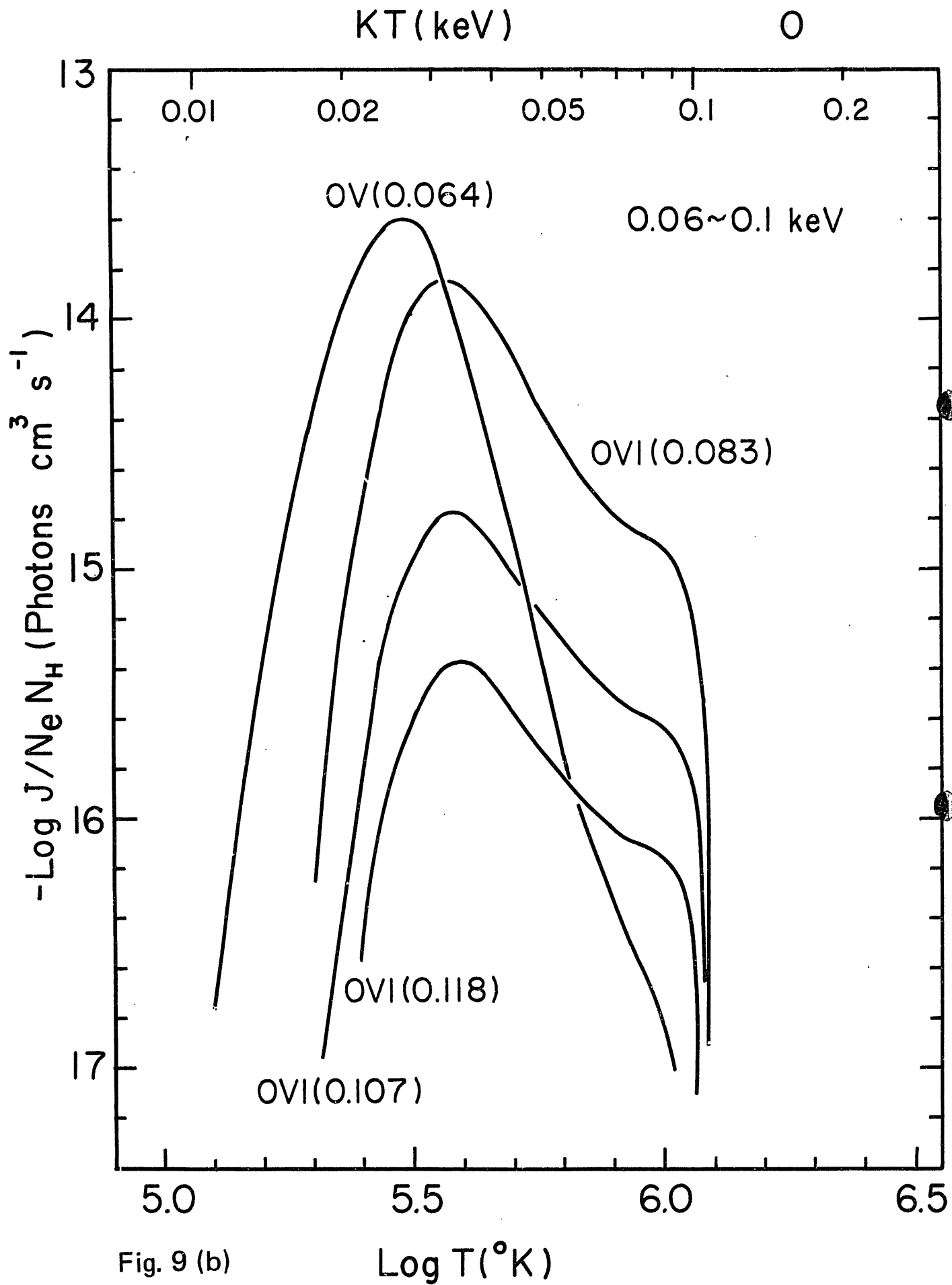


Fig. 9 (b)

$\text{Log } T (^{\circ}\text{K})$

KT (keV)

S

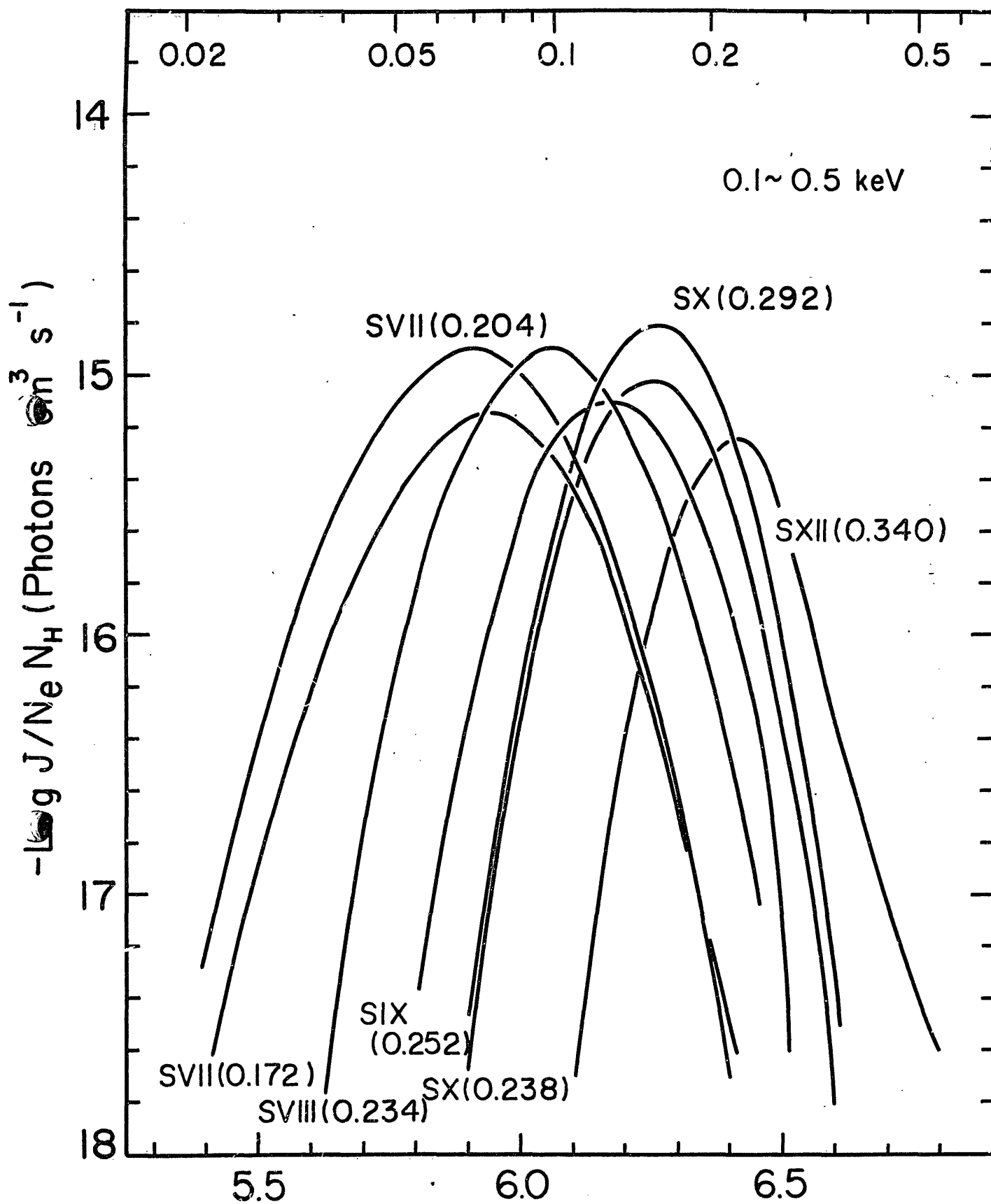


Fig. 9 (c)

Log T ($^{\circ}\text{K}$)

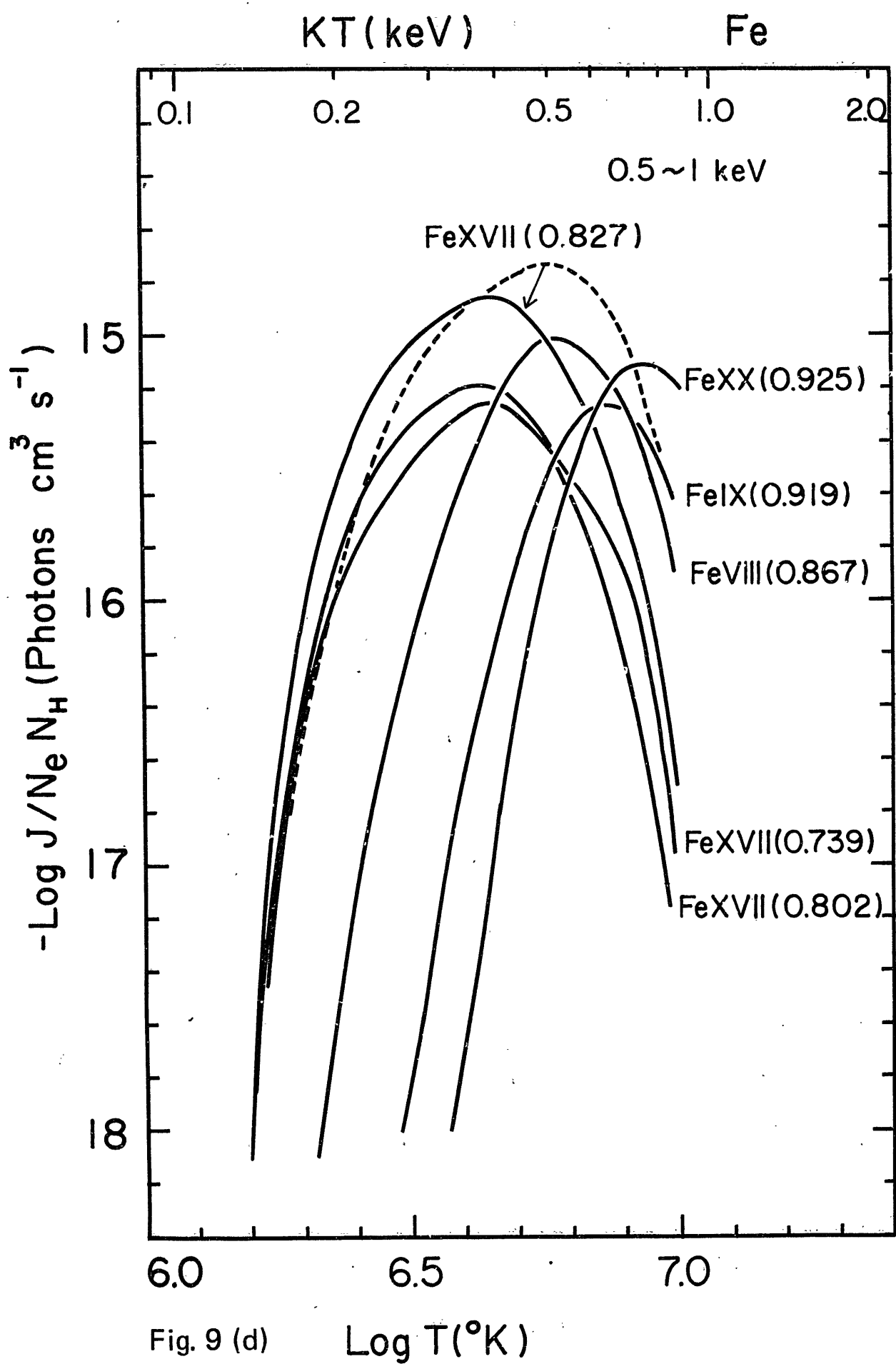


Fig. 9 (d)

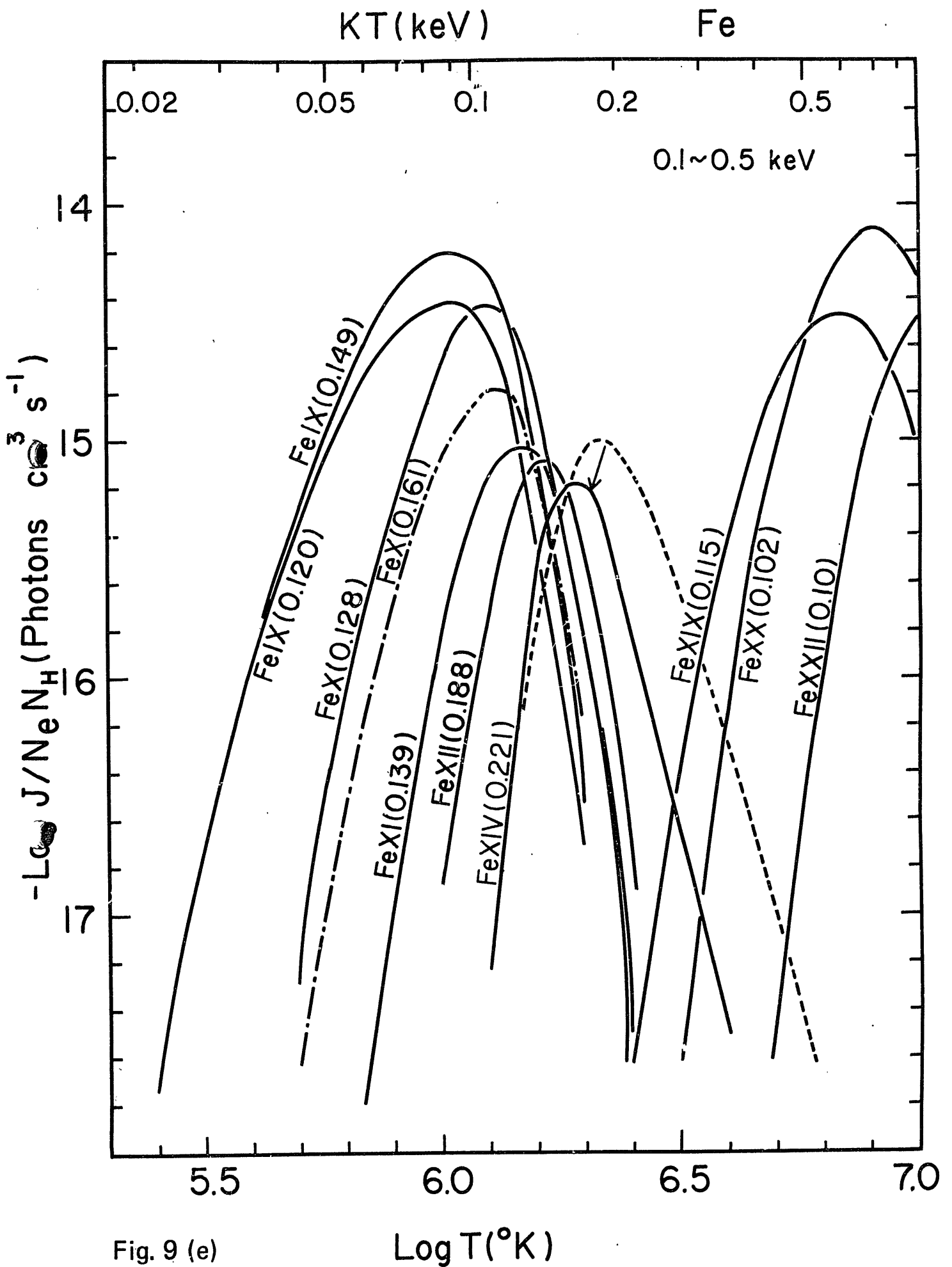


Fig. 9 (e)

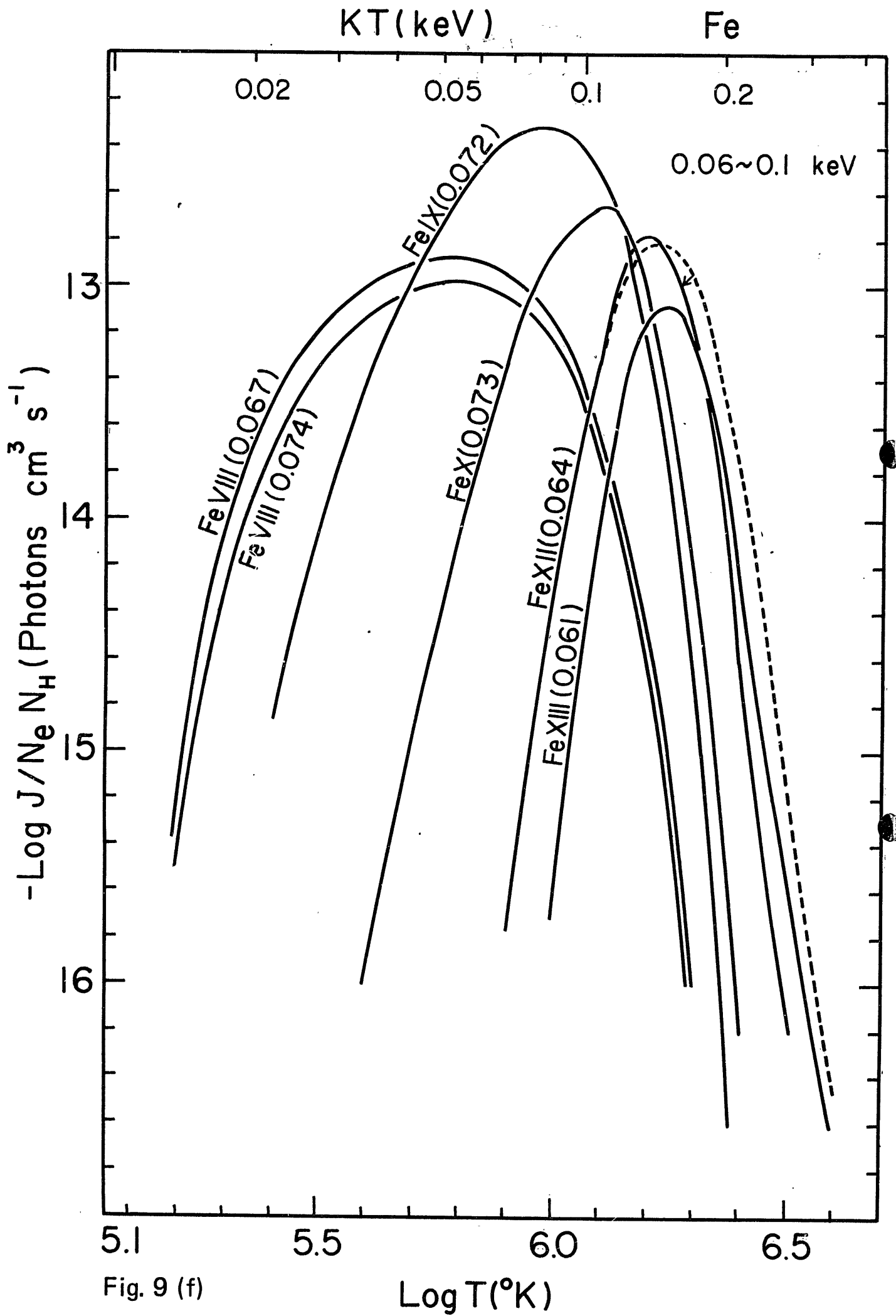


Fig. 9 (f)

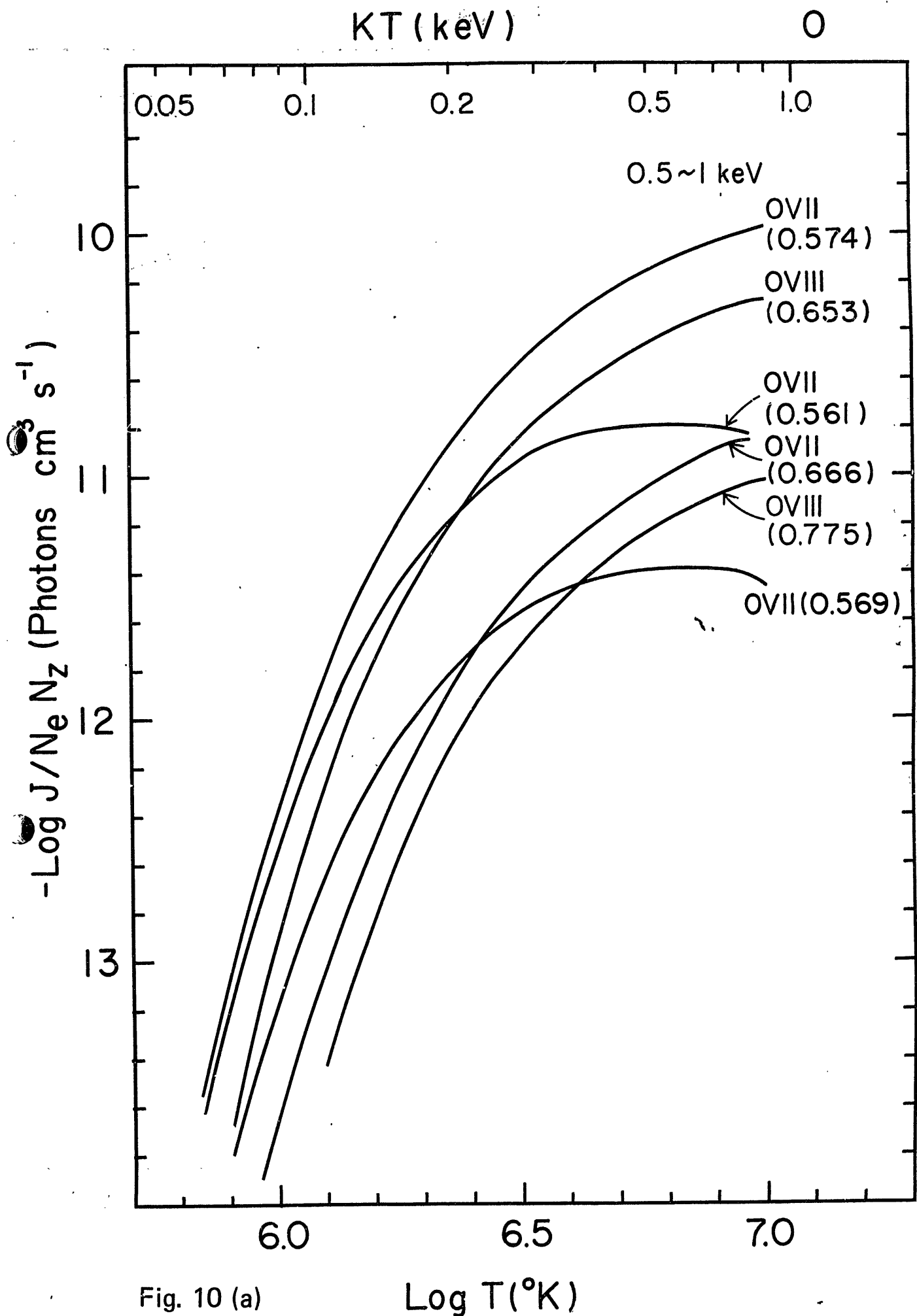


Fig. 10 (a)

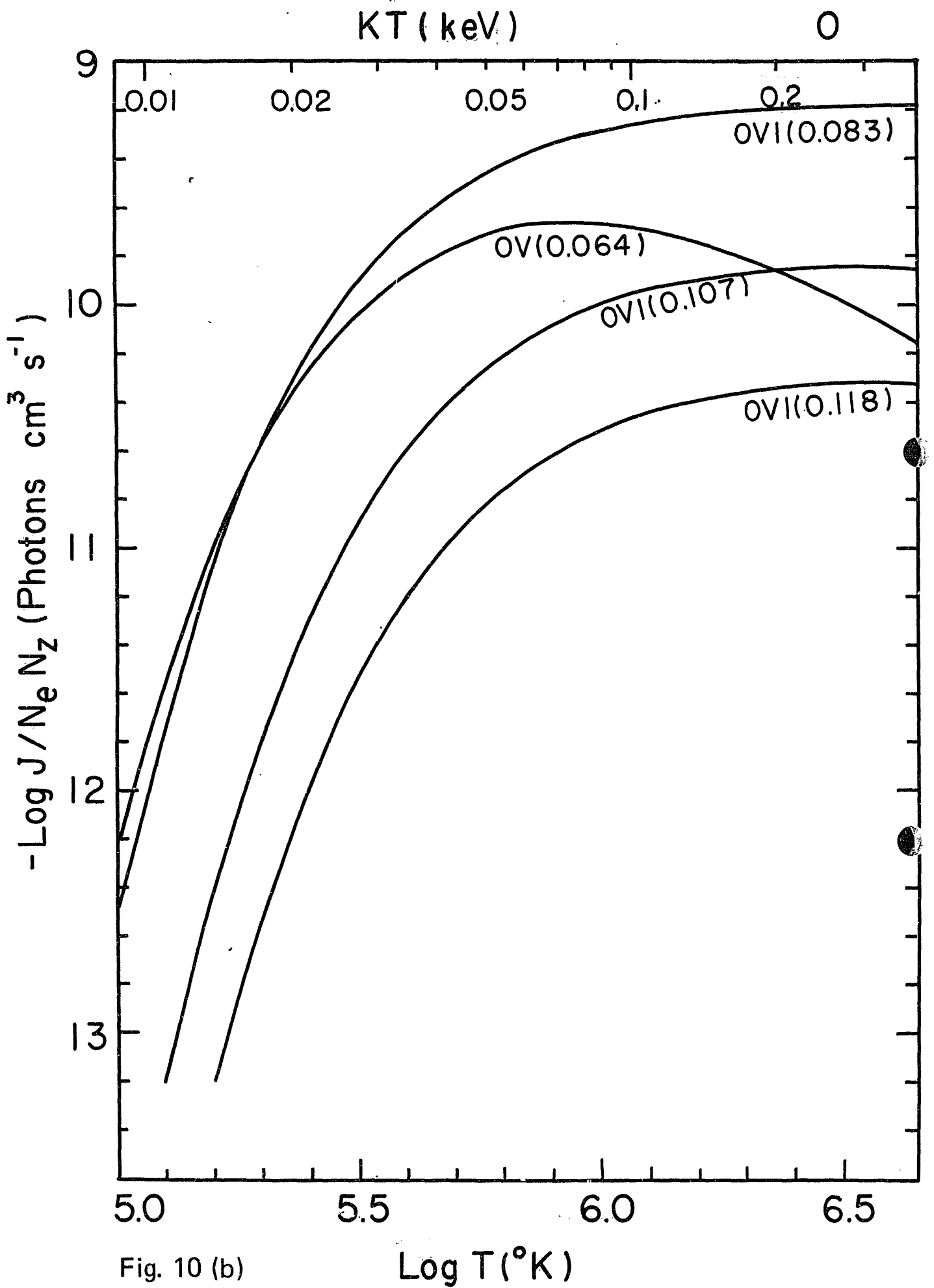


Fig. 10 (b)

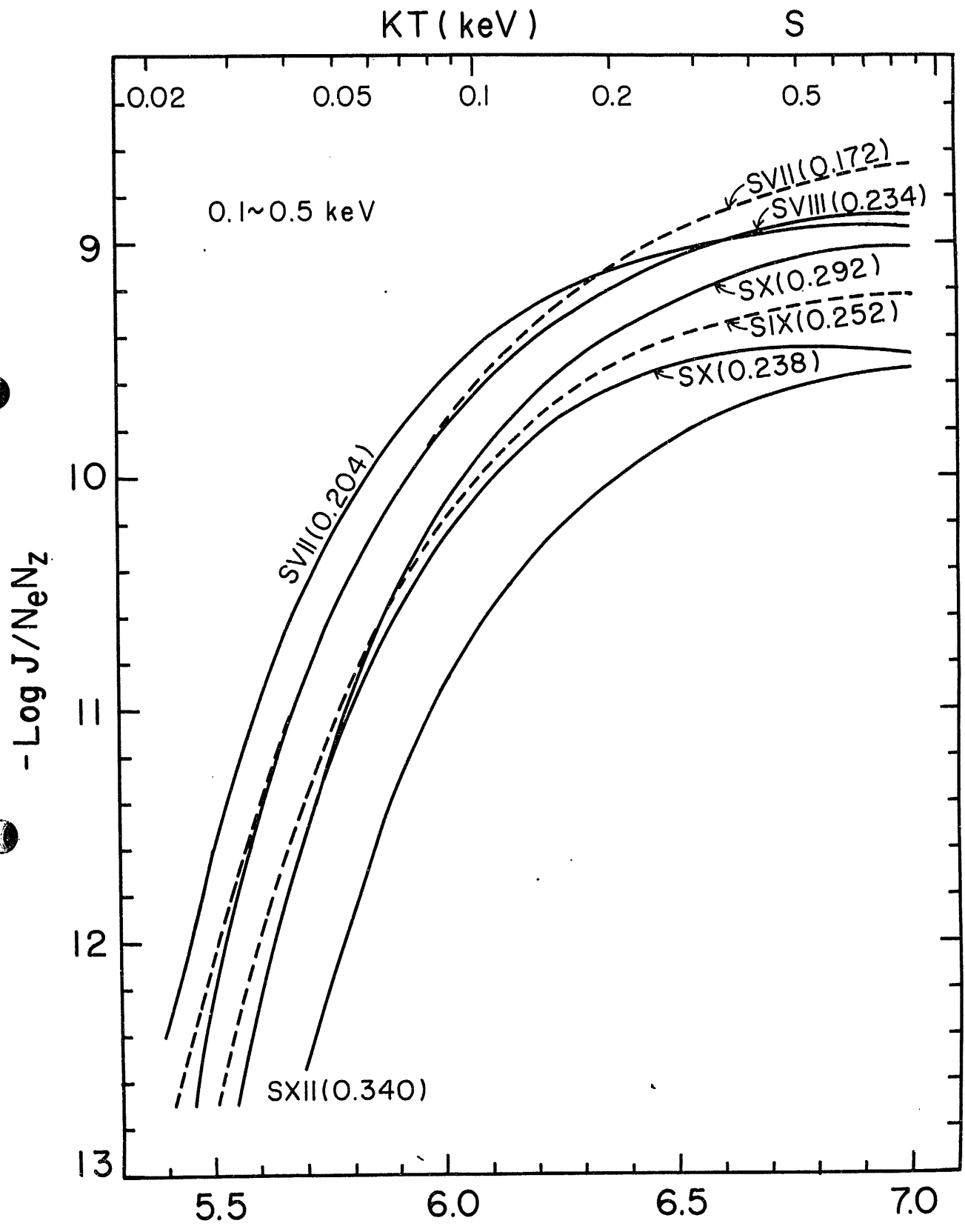


Fig. 10 (c)

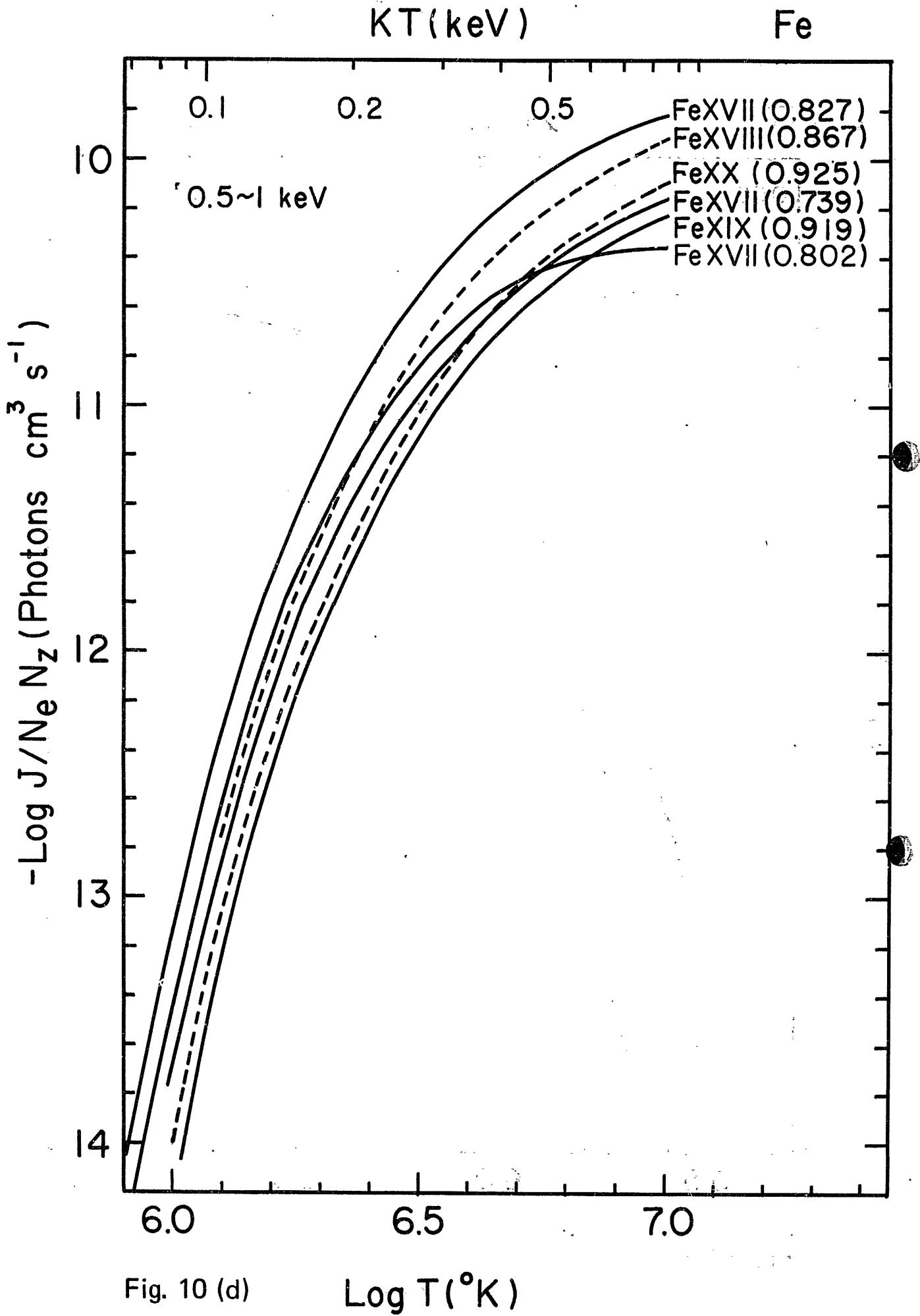


Fig. 10 (d)

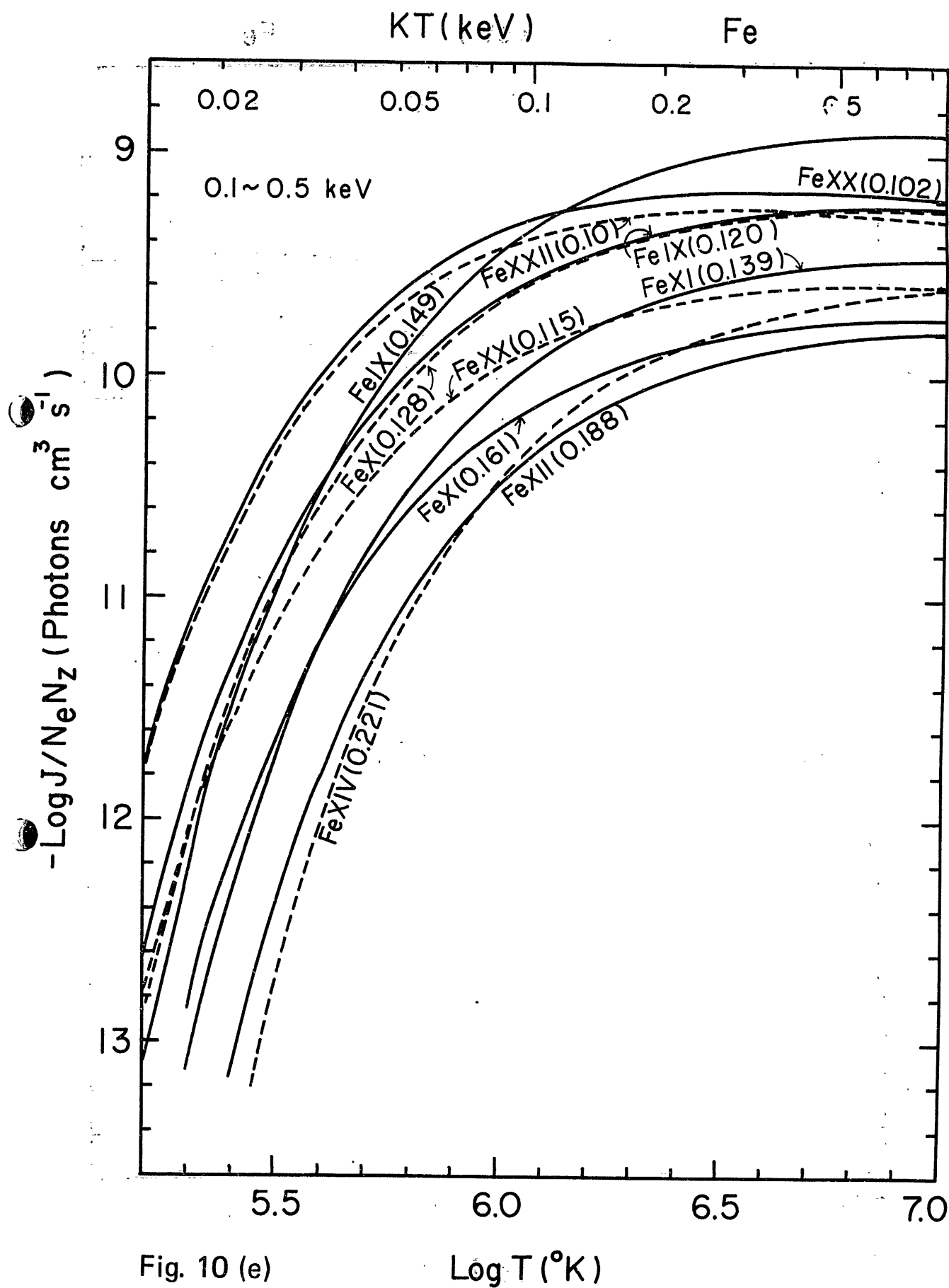


Fig. 10 (e)

$\text{Log } T$ ($^{\circ}\text{K}$)

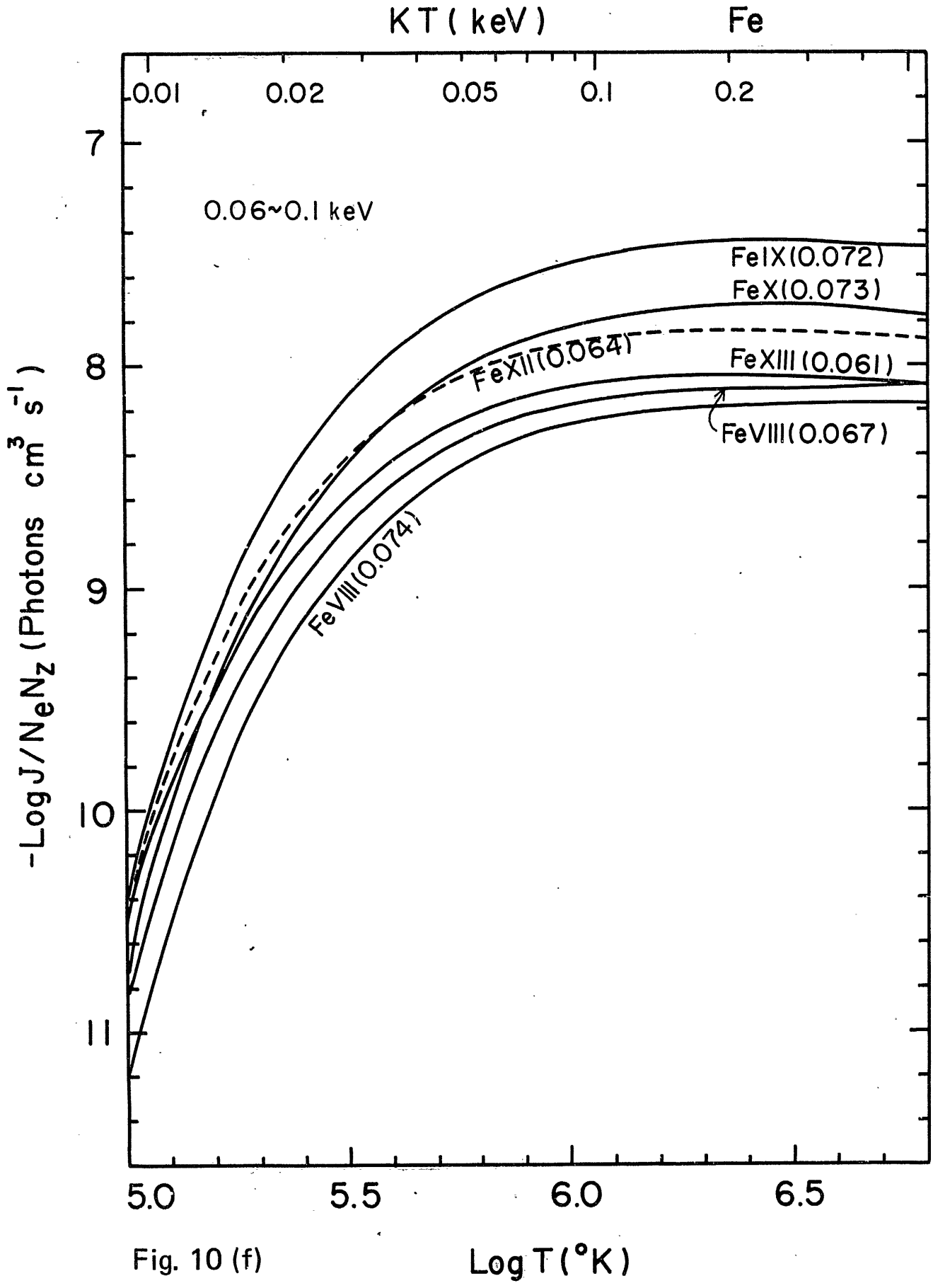


Fig. 10 (f)

Log T = 6.2
(KT = 0.14 KeV)

Kato
TK
LF

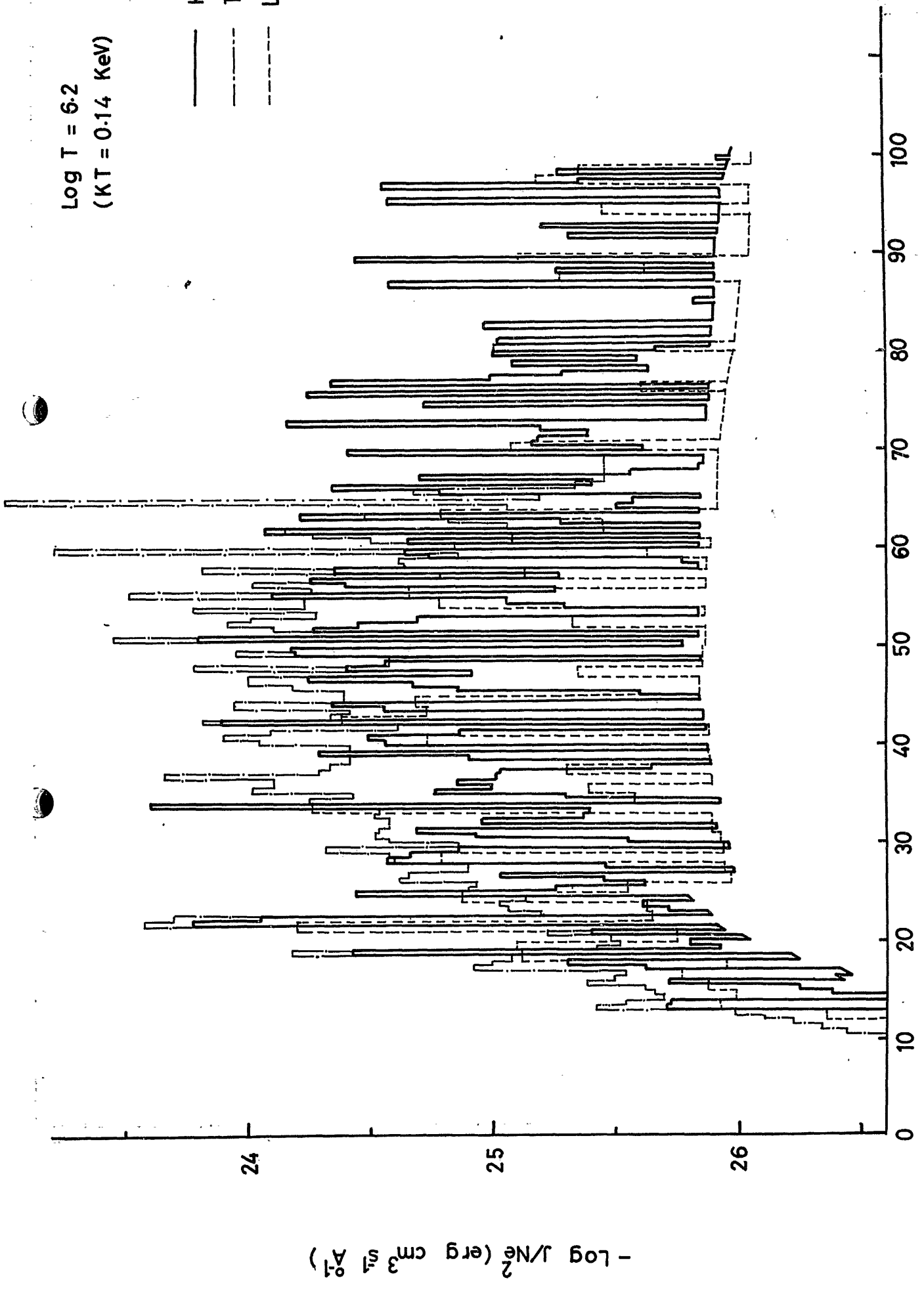


Fig. 11

λ (Å)

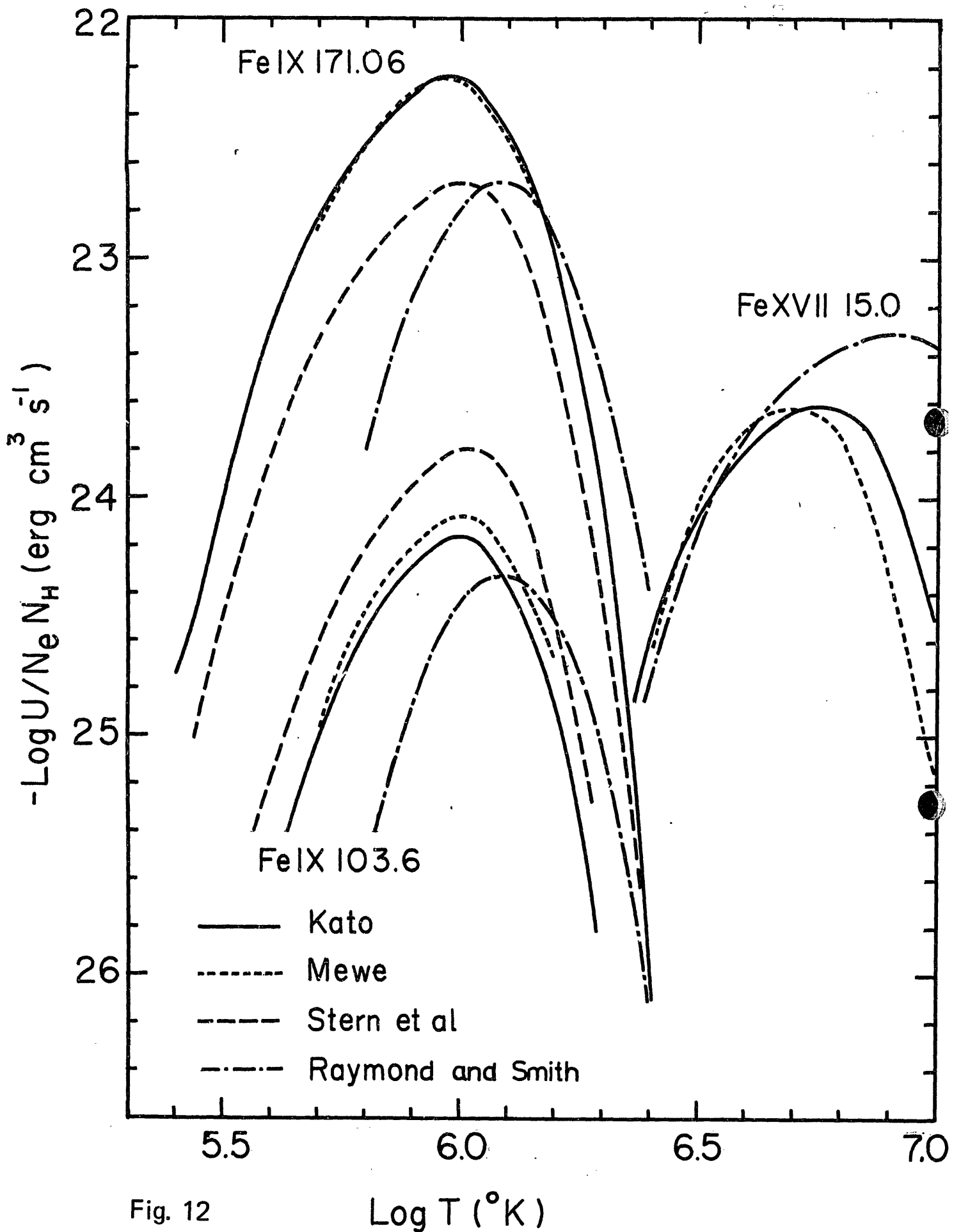


Fig. 12

$\text{Log } T \text{ (}^\circ\text{K)}$

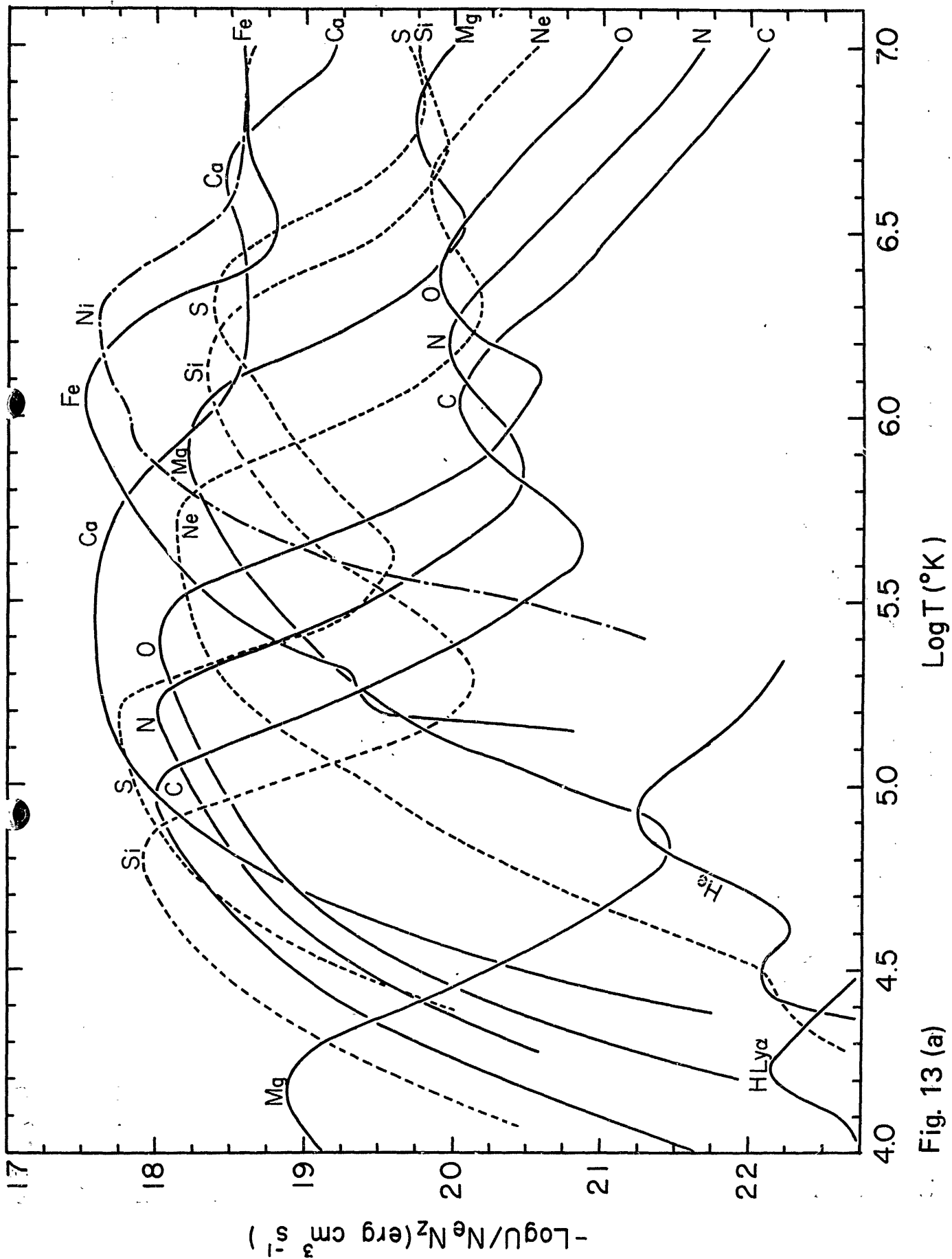


Fig. 13 (a)

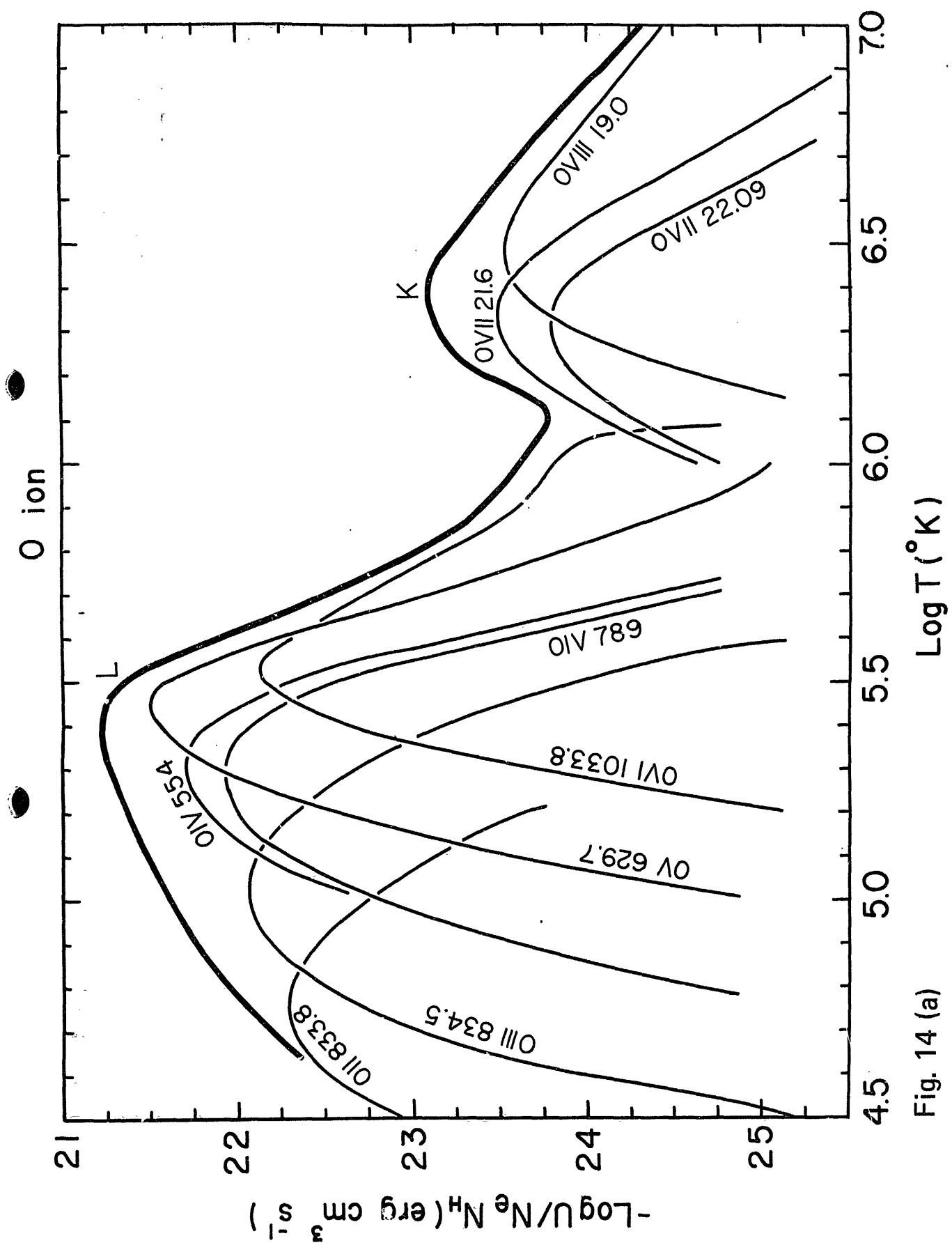


Fig. 14 (a)

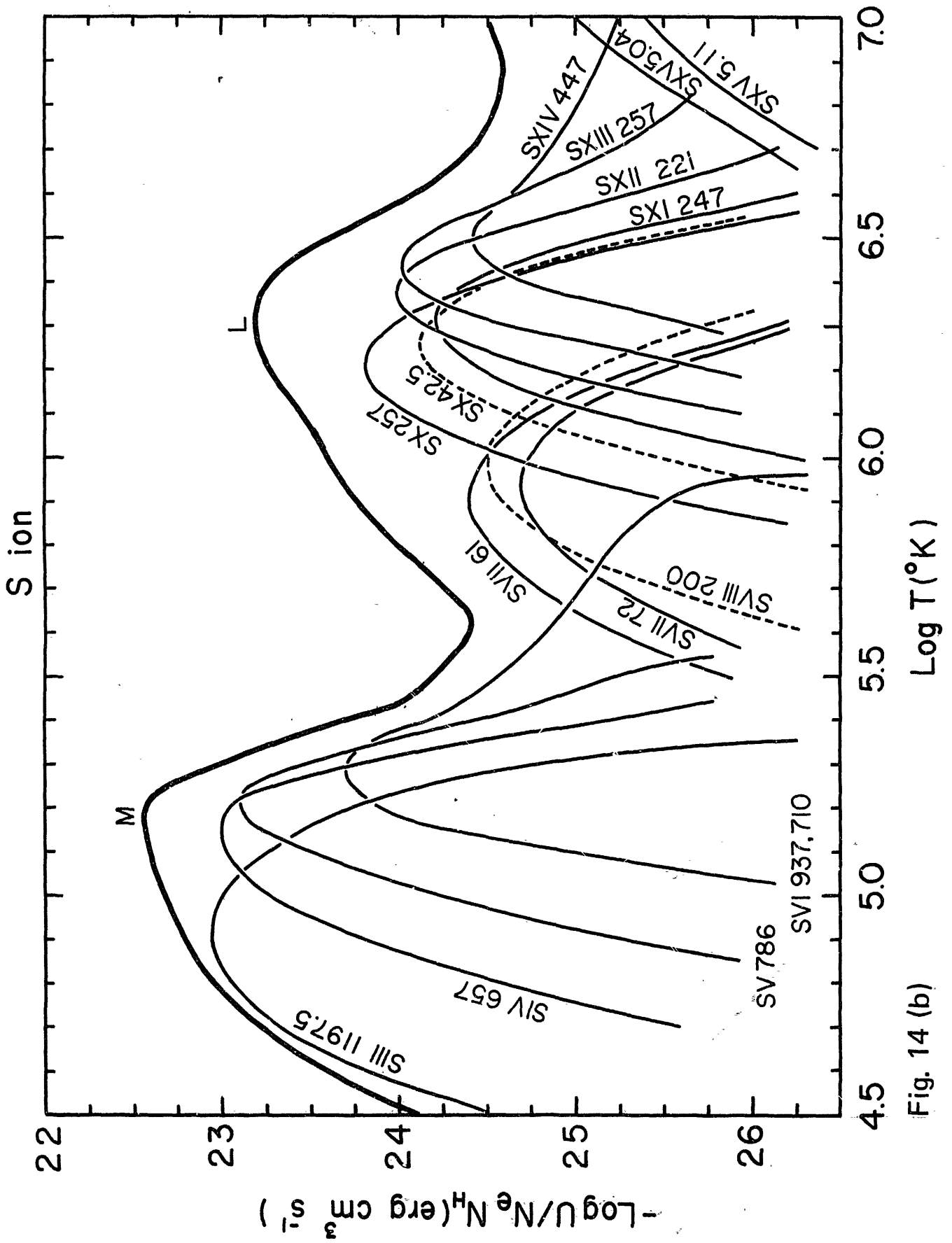


Fig. 14 (b)

Fe ion

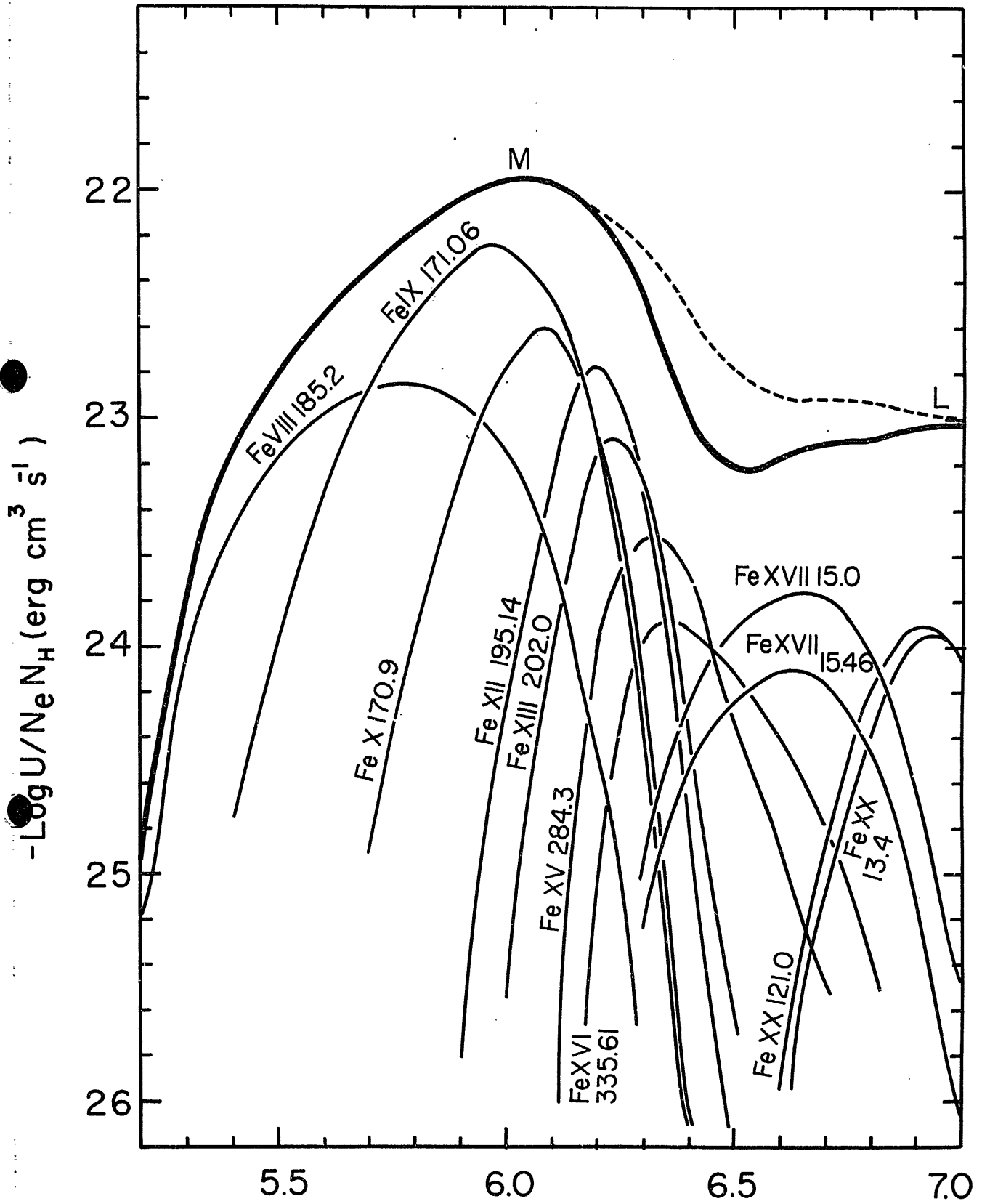


Fig. 14 (c)

$\text{Log } T (^{\circ}\text{K})$

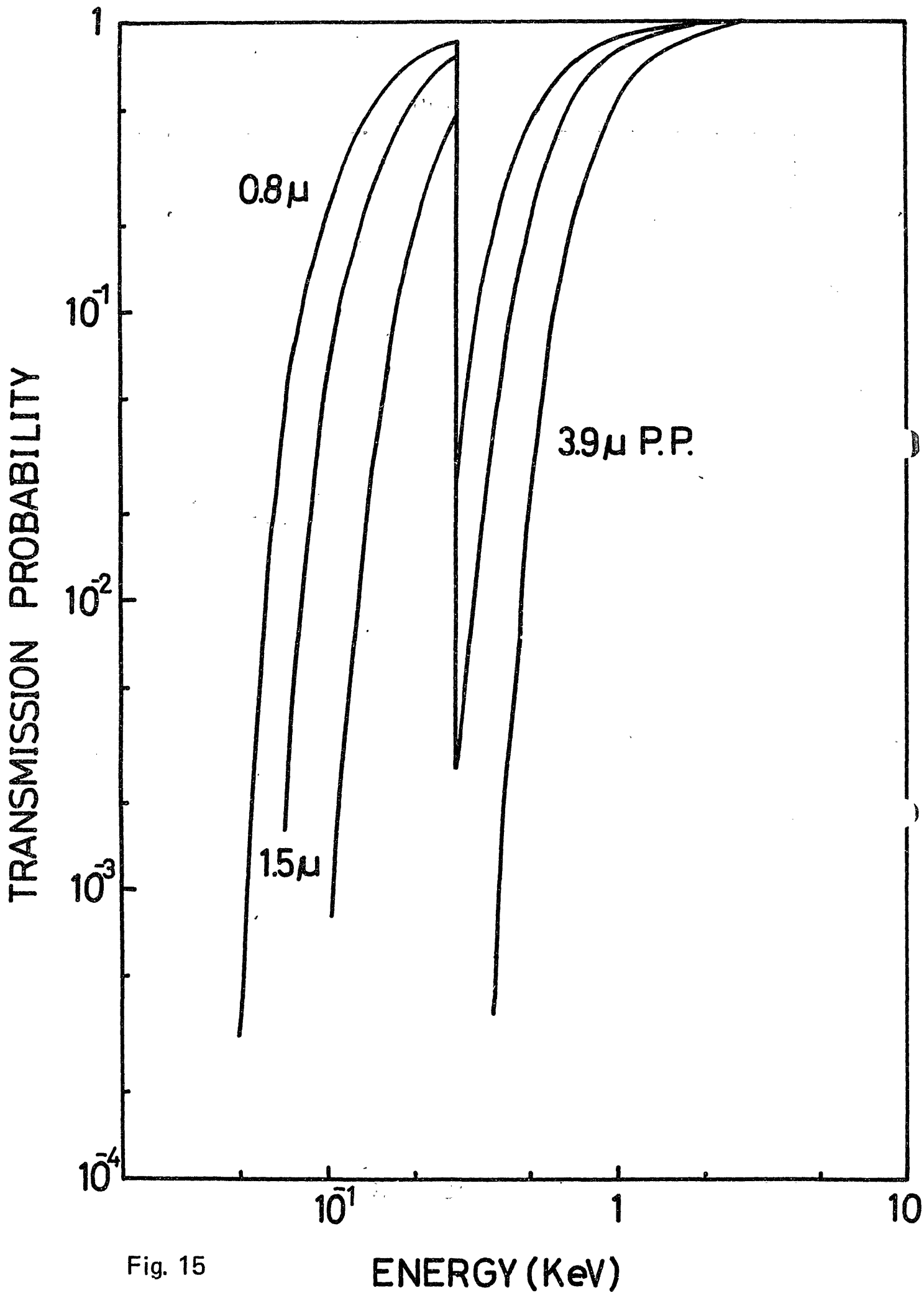


Fig. 15

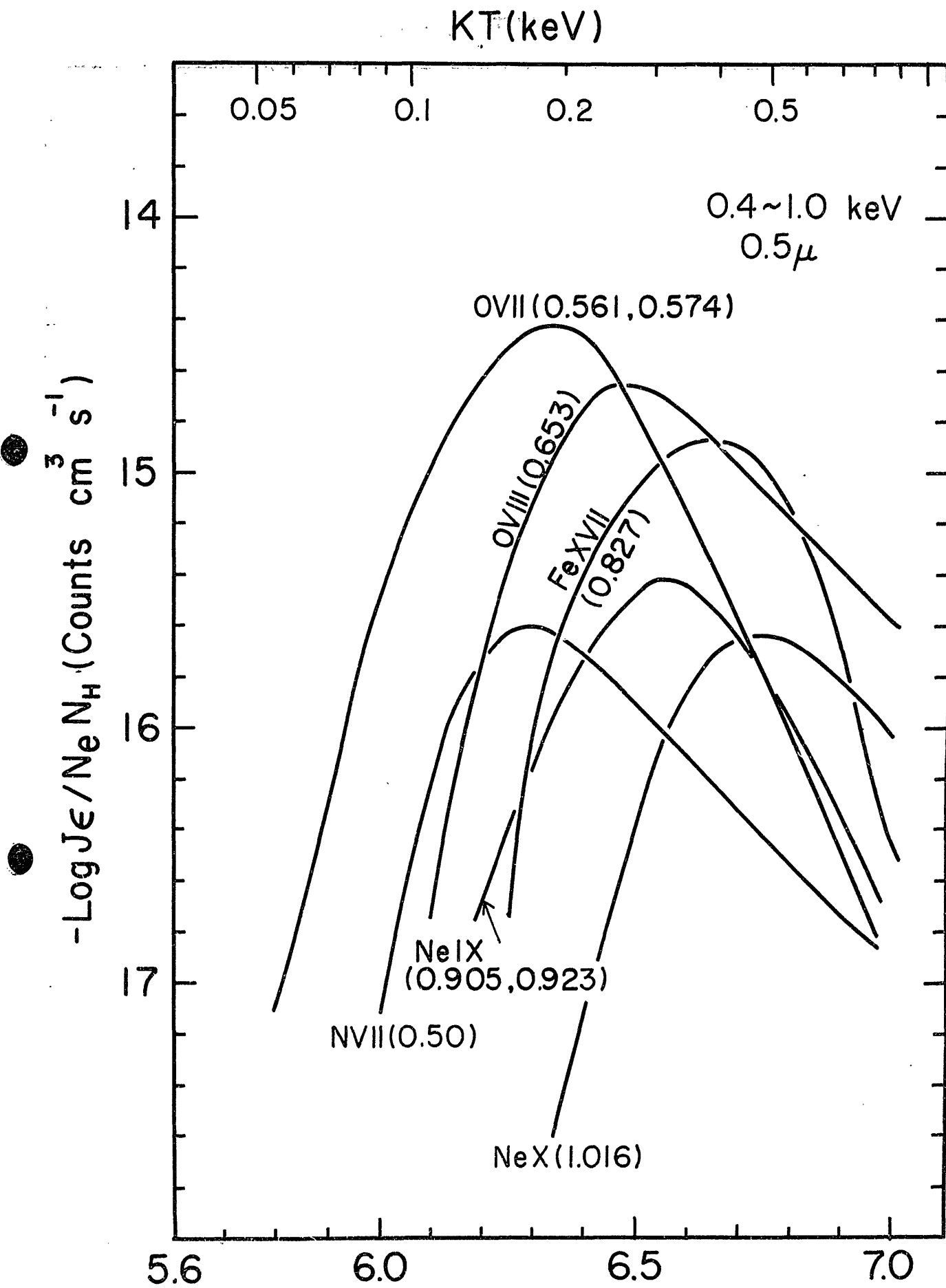


Fig. 16 (a)

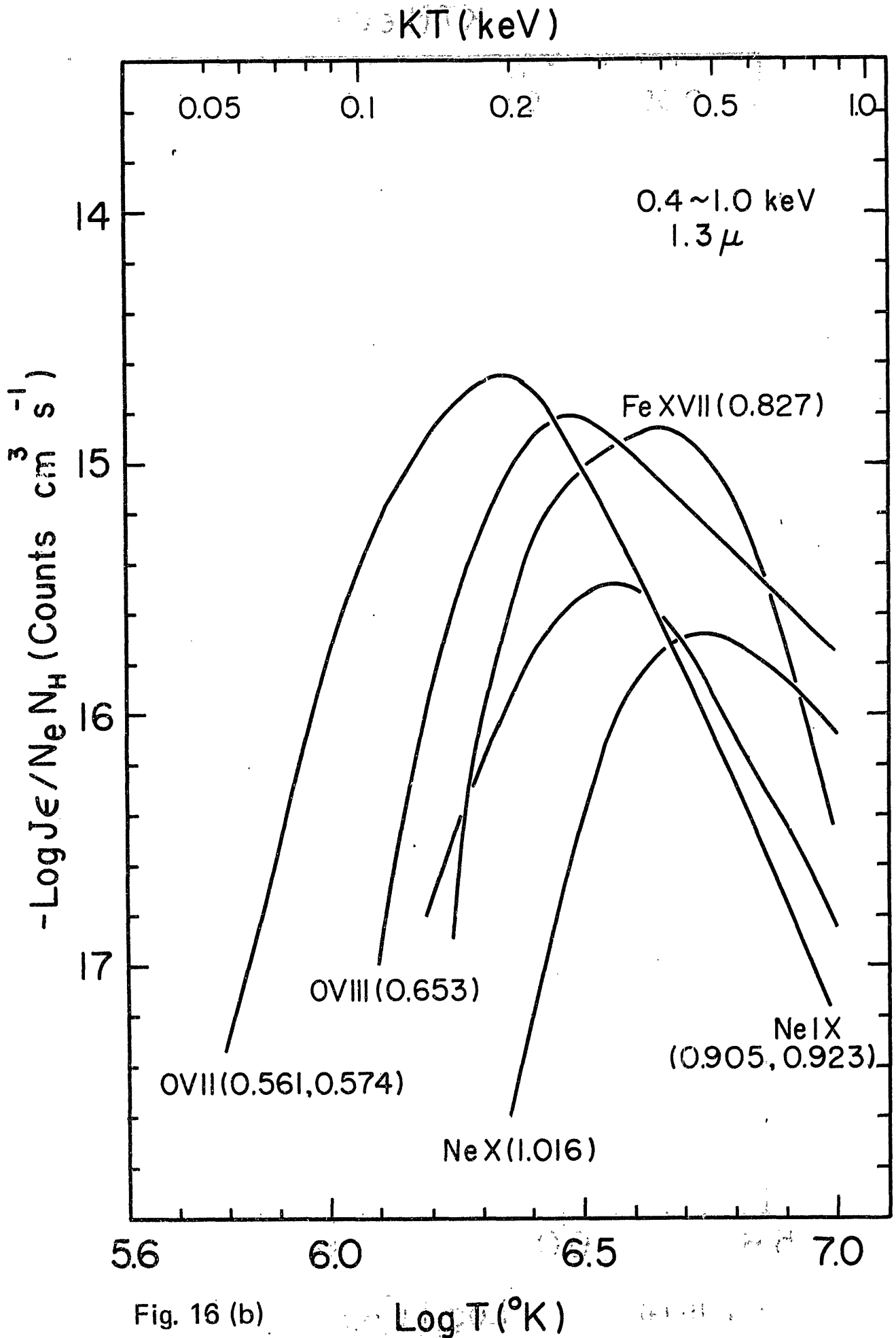


Fig. 16 (b)

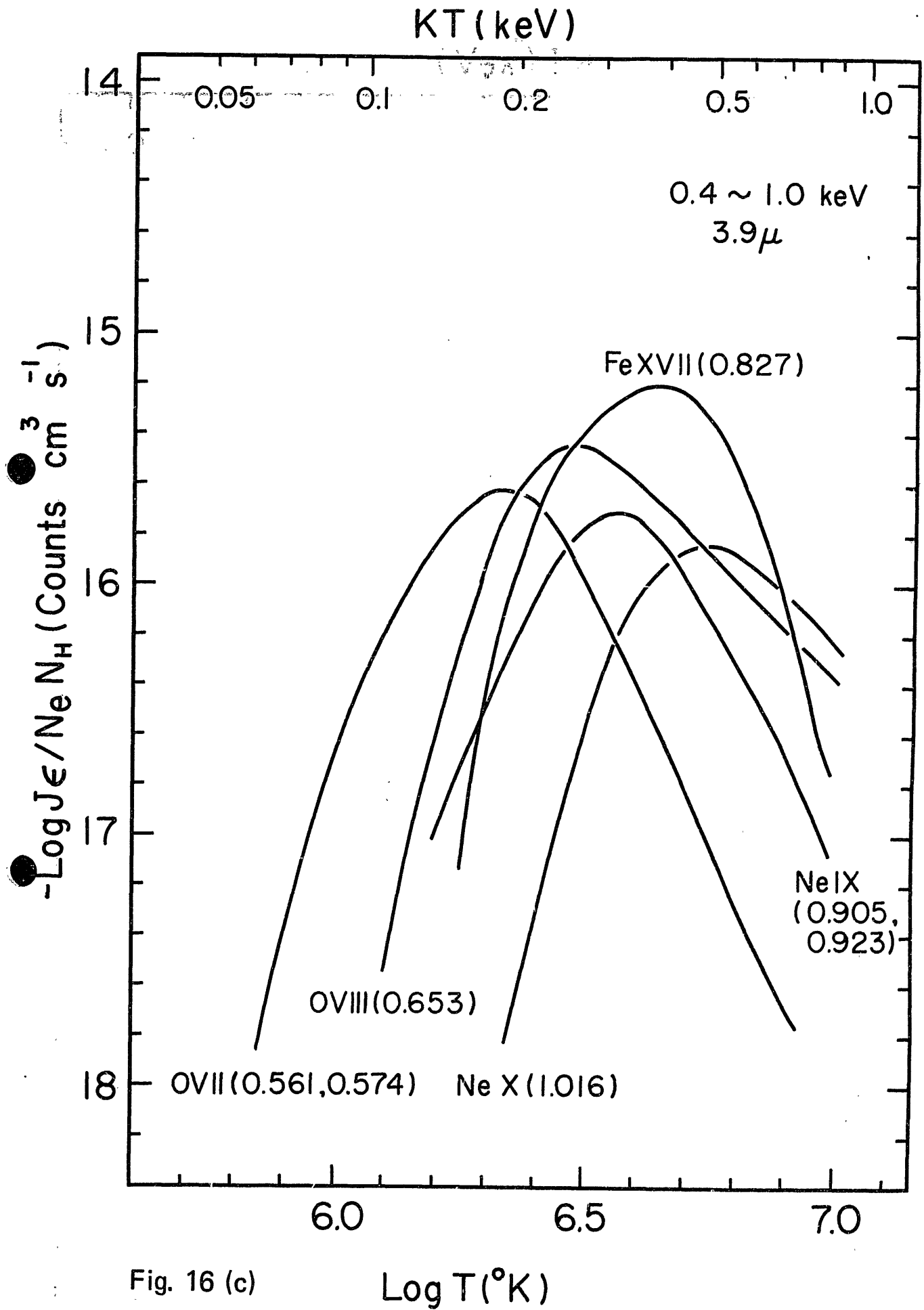


Fig. 16 (c)

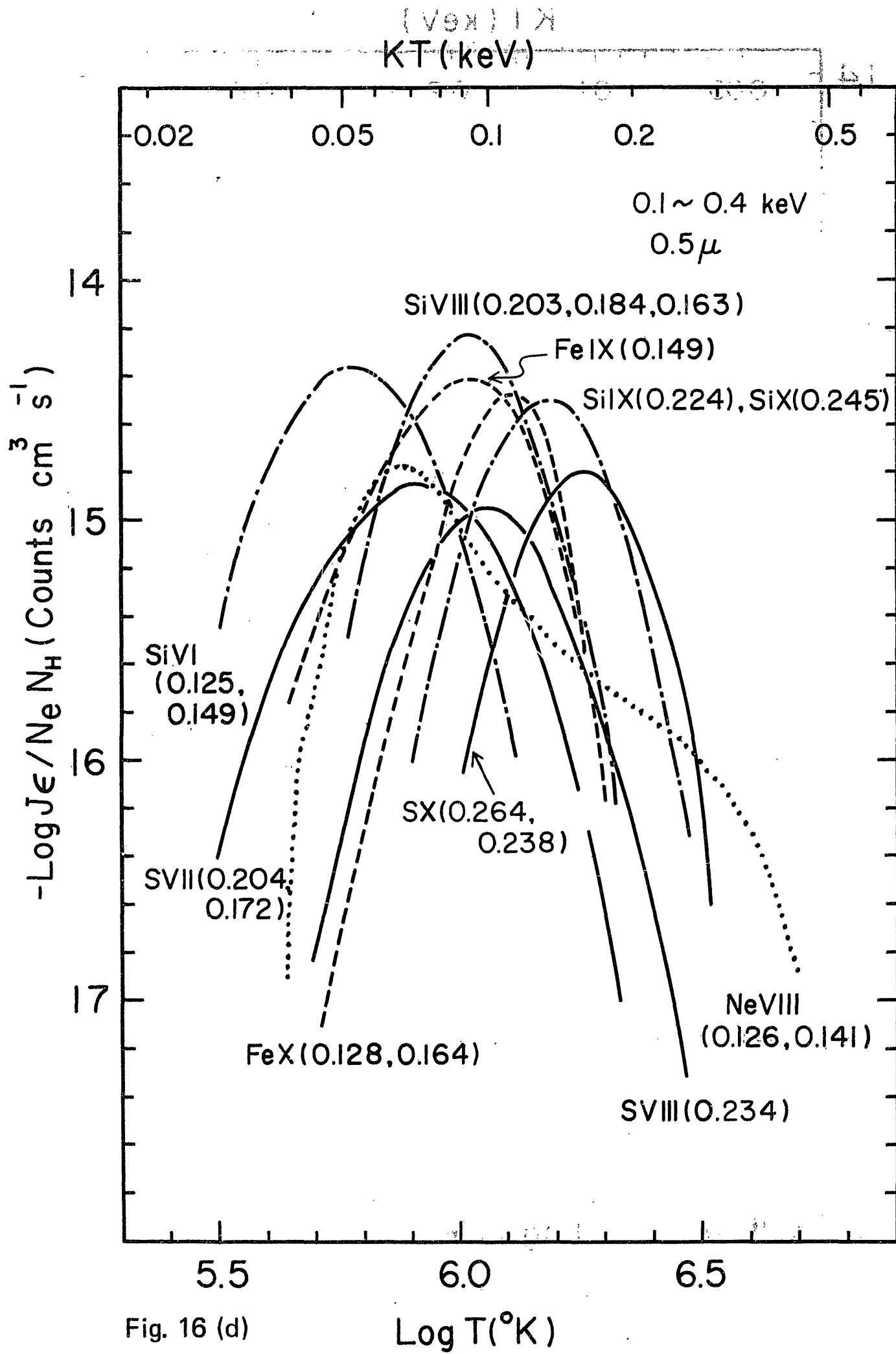


Fig. 16 (d)

Log T (°K)

KT (keV)

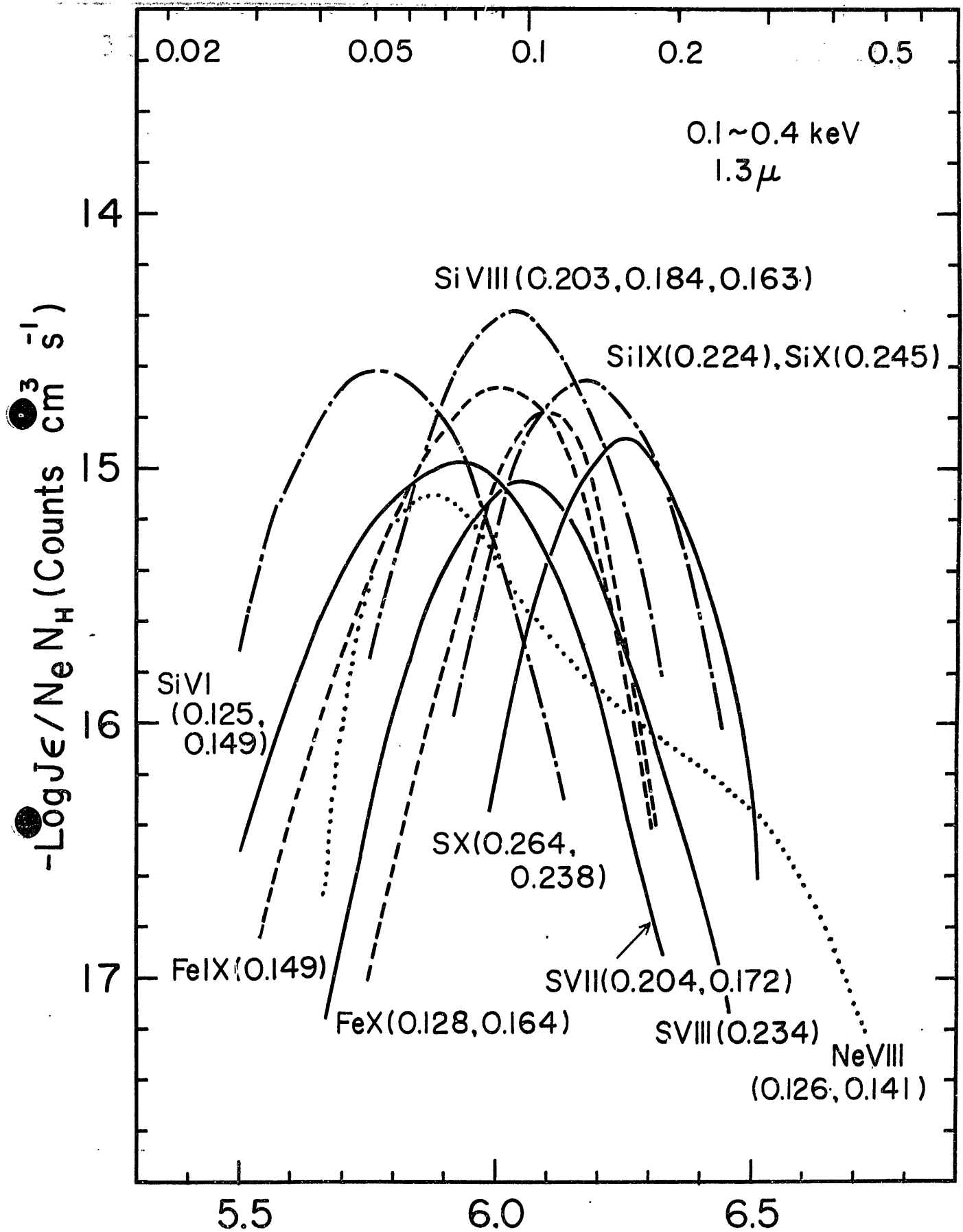


Fig. 16 (e)

$\text{Log } T (^{\circ}\text{K})$

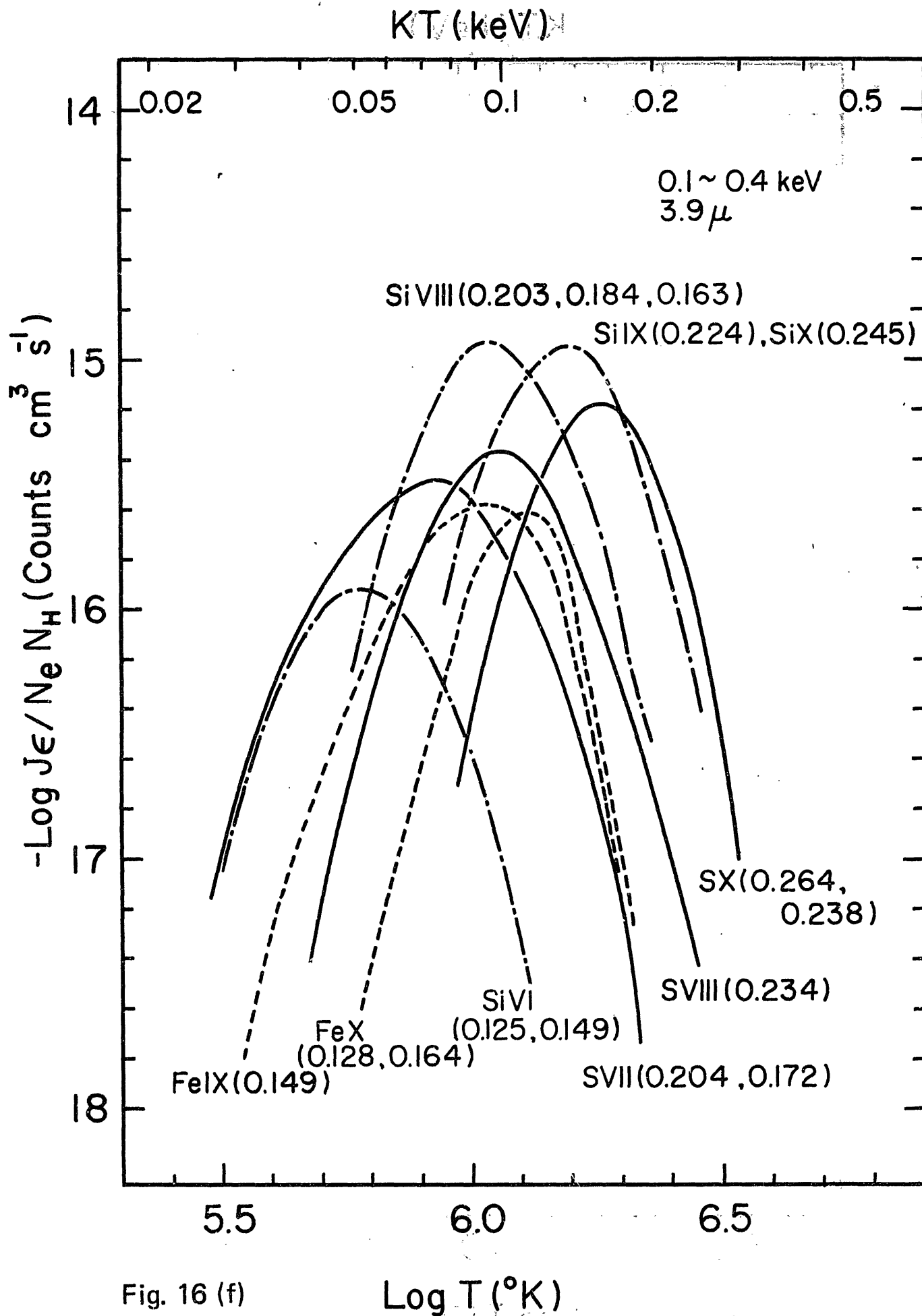


Fig. 16 (f)

Lupus Loop

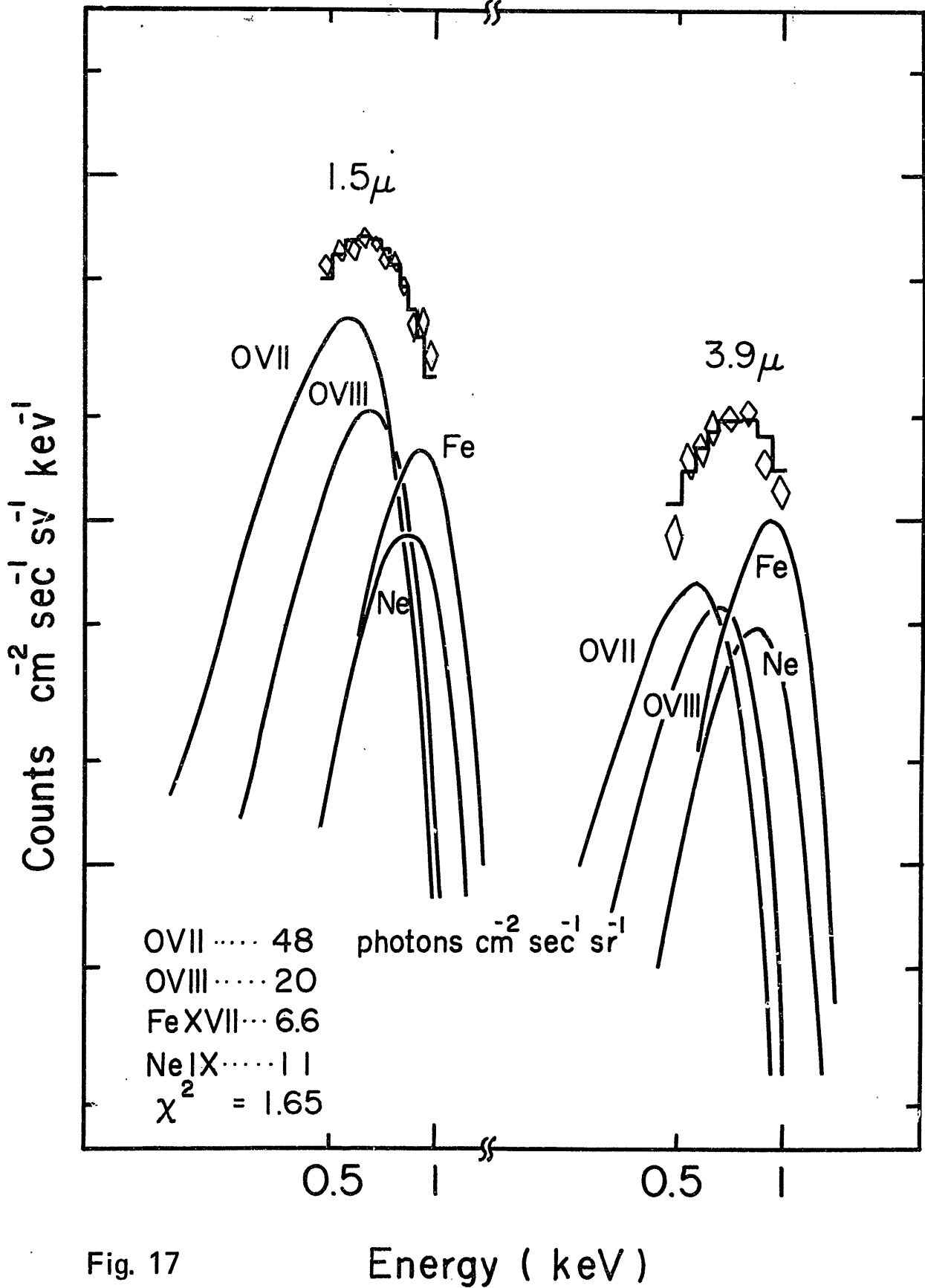


Fig. 17

Energy (keV)

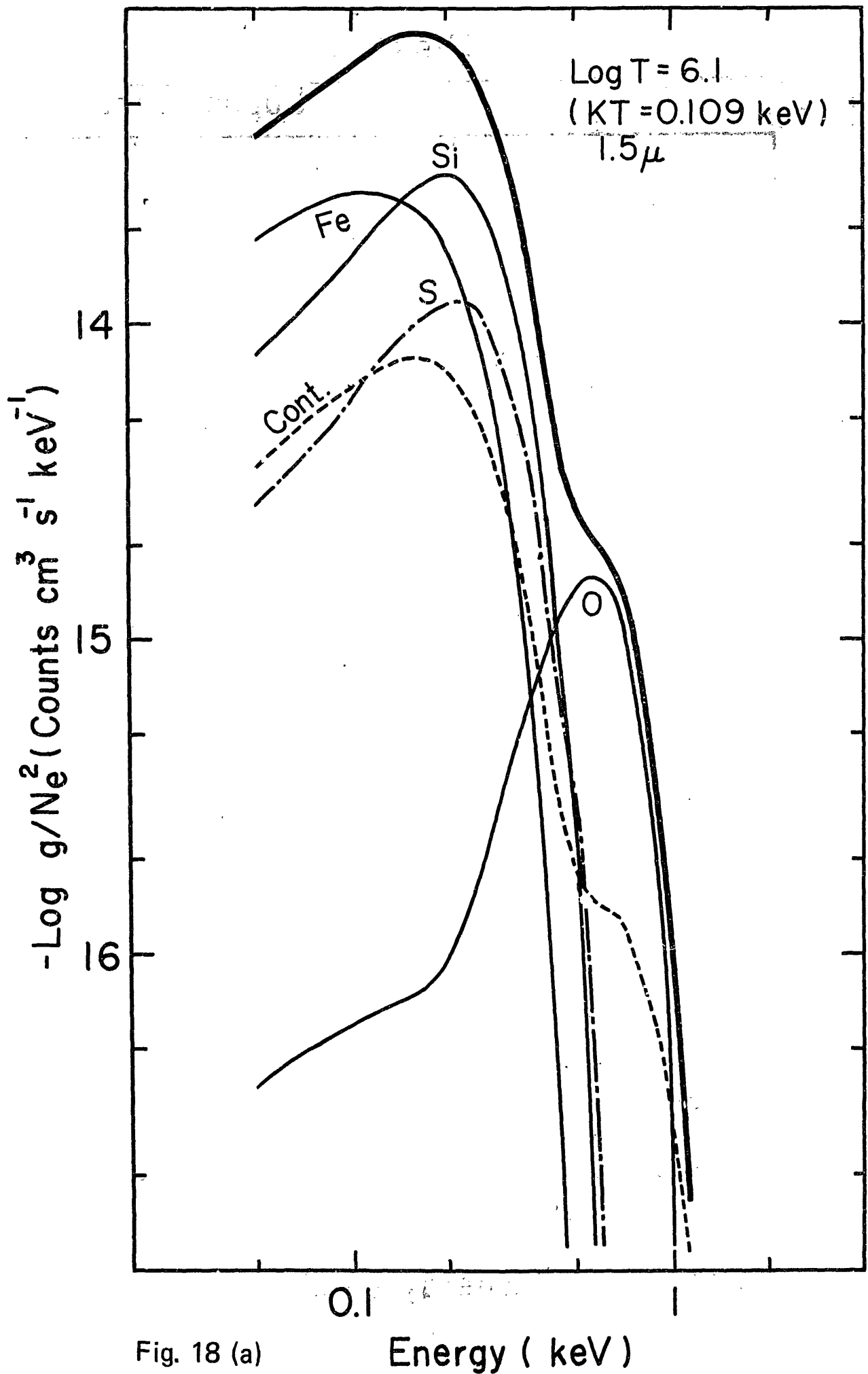


Fig. 18 (a)

Energy (keV)

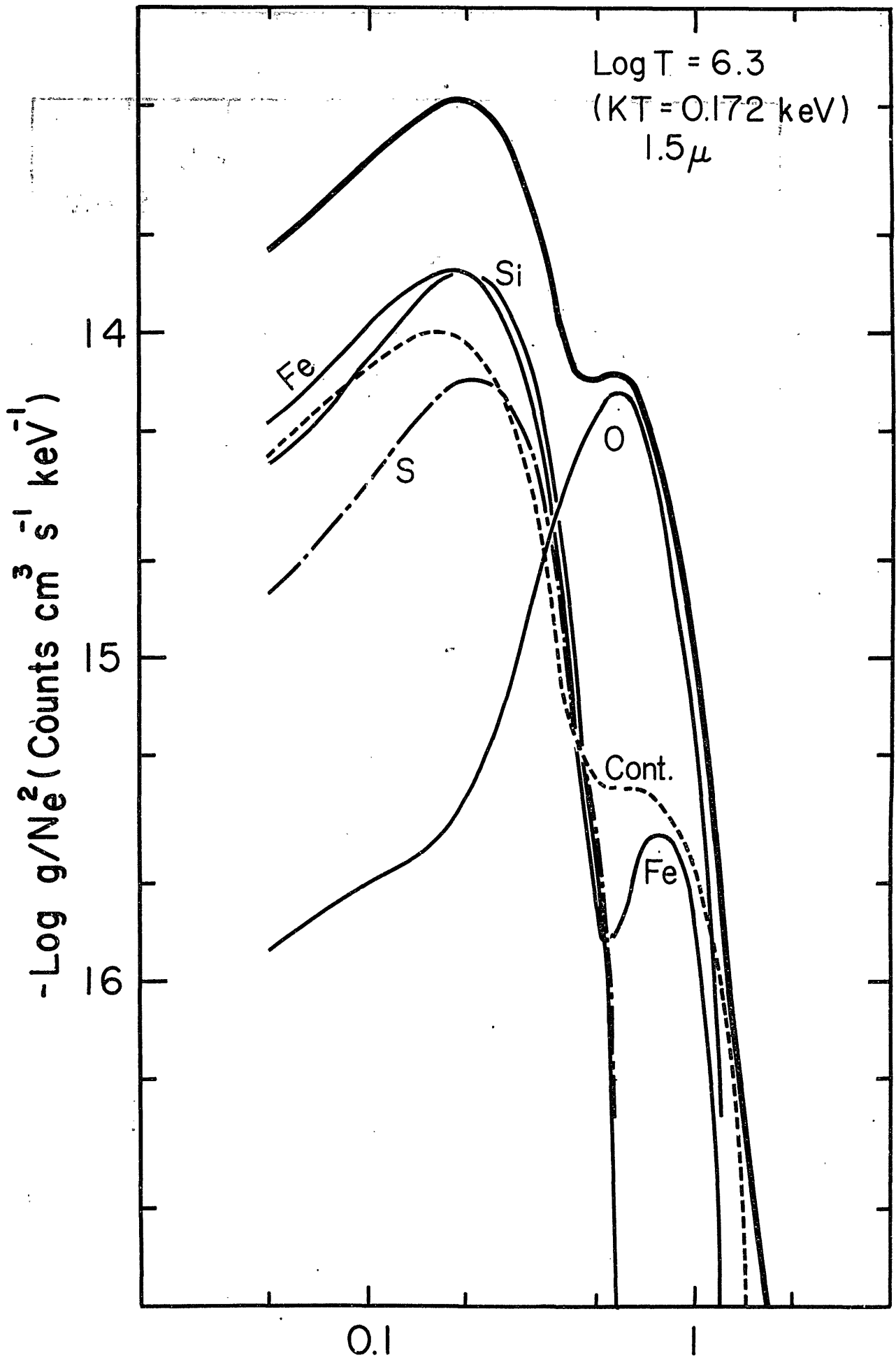


Fig. 18 (b)

Energy (keV)

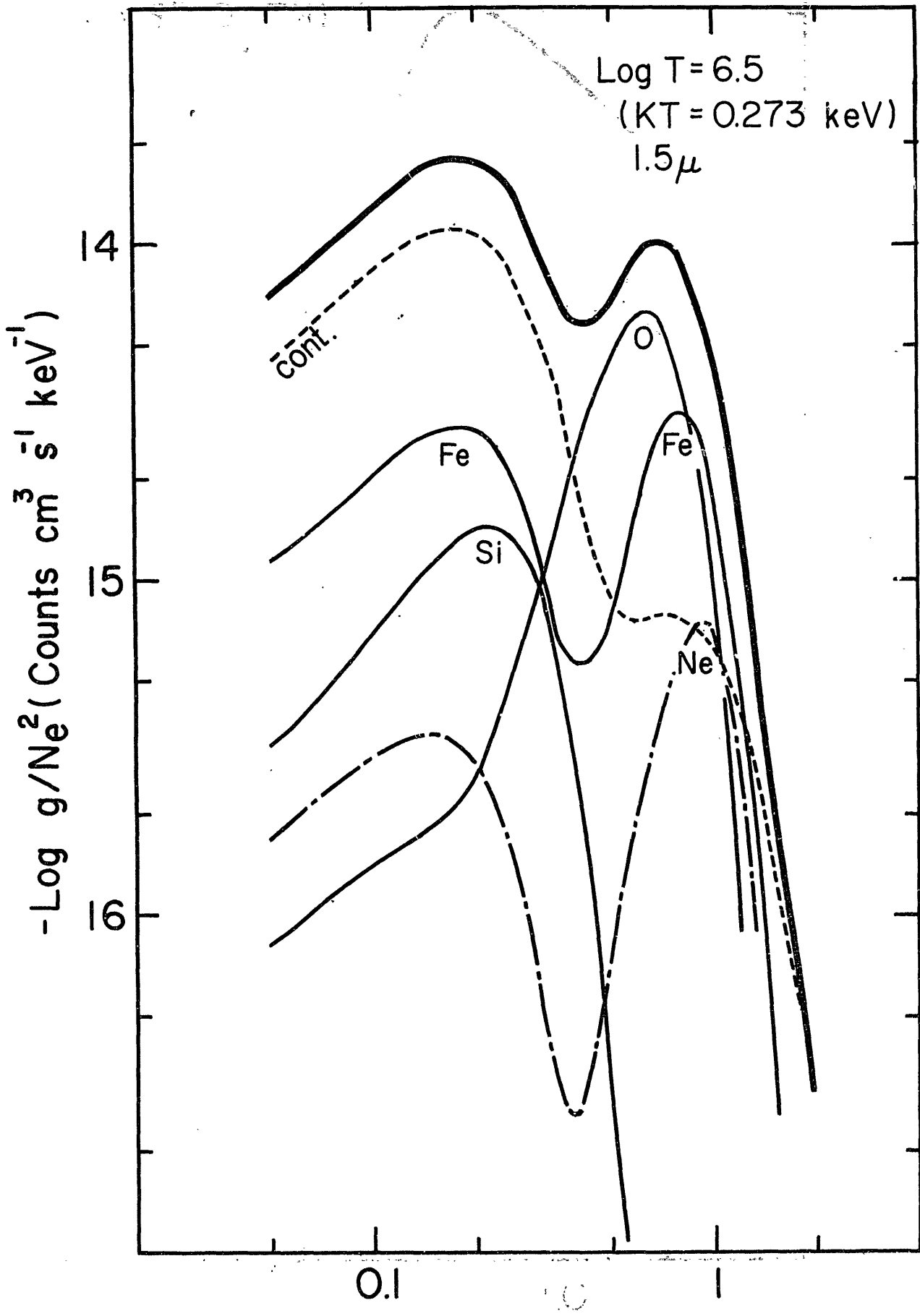


Fig. 18 (c) V_e vs Energy (keV) (c) 81 pp

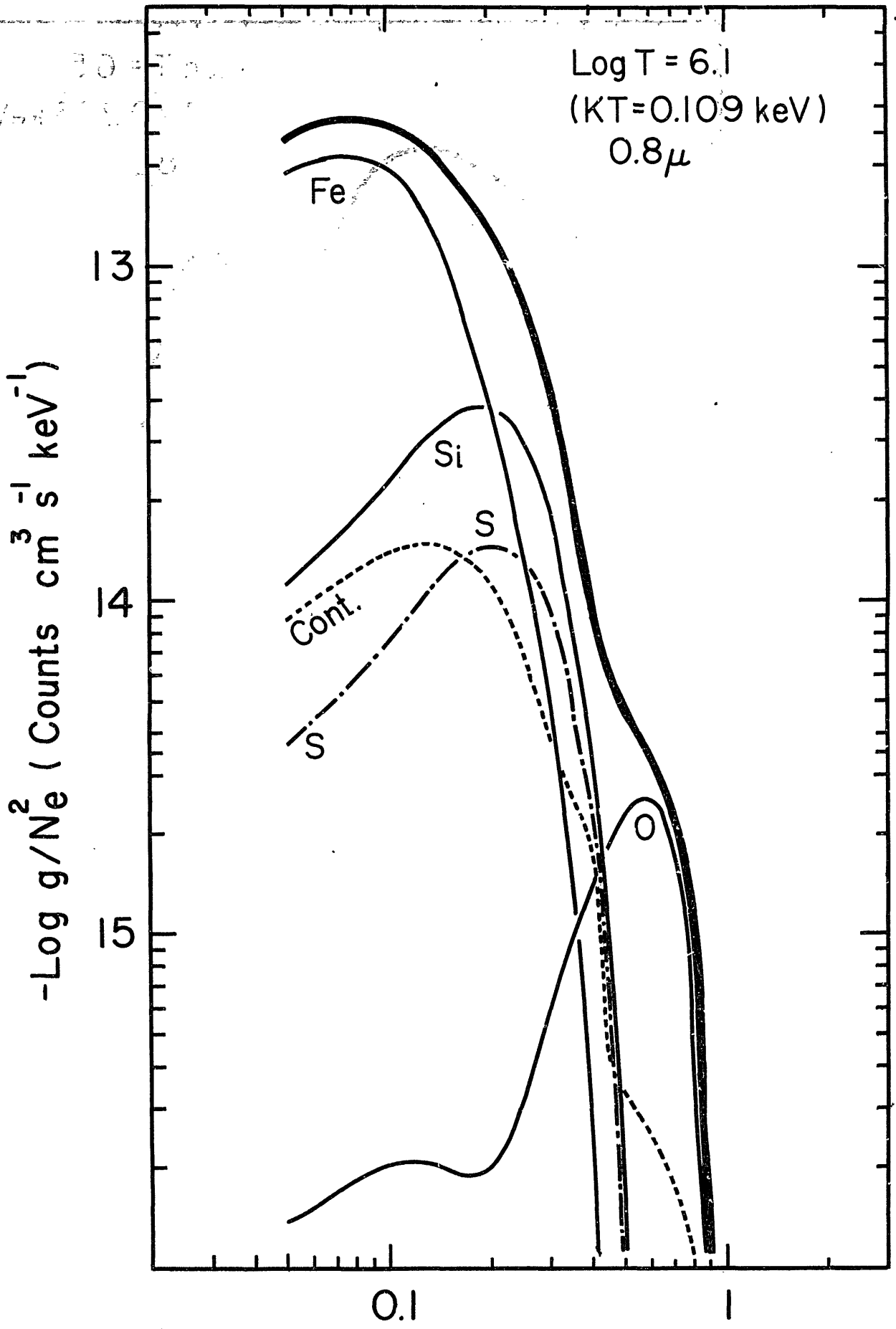


Fig. 18 (d)

Energy (keV)

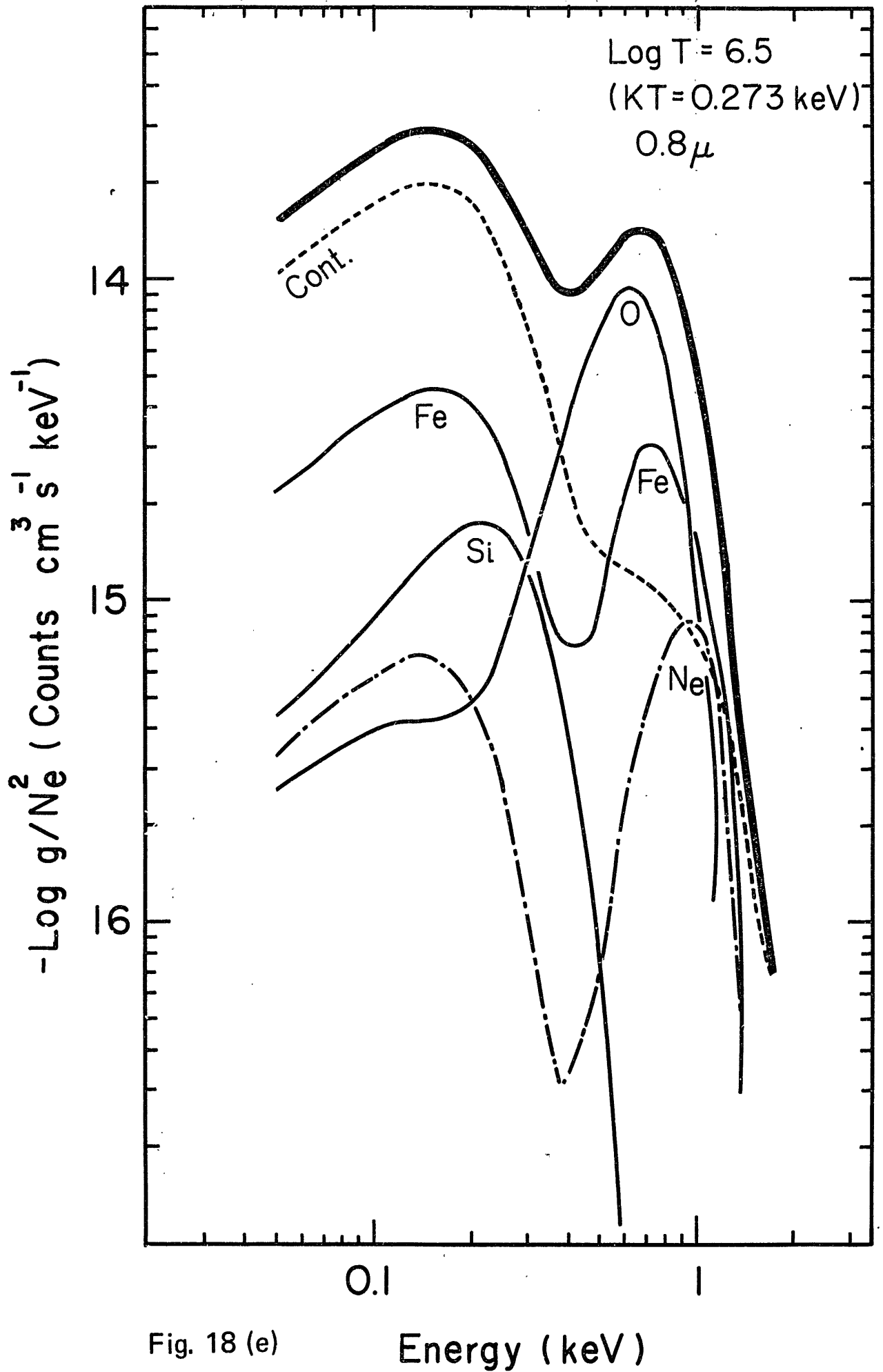


Fig. 18 (e)

Energy (keV)

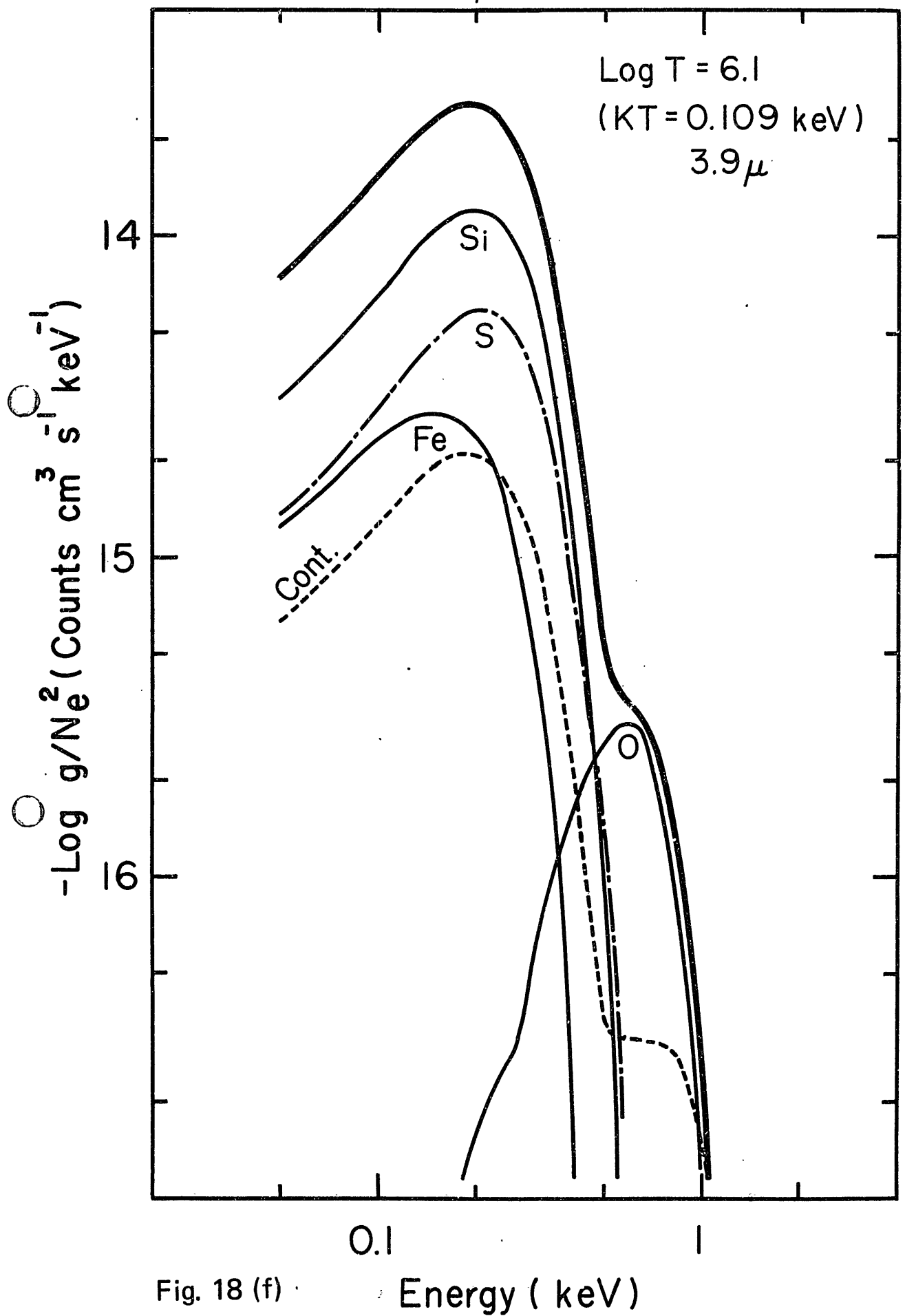


Fig. 18 (f)

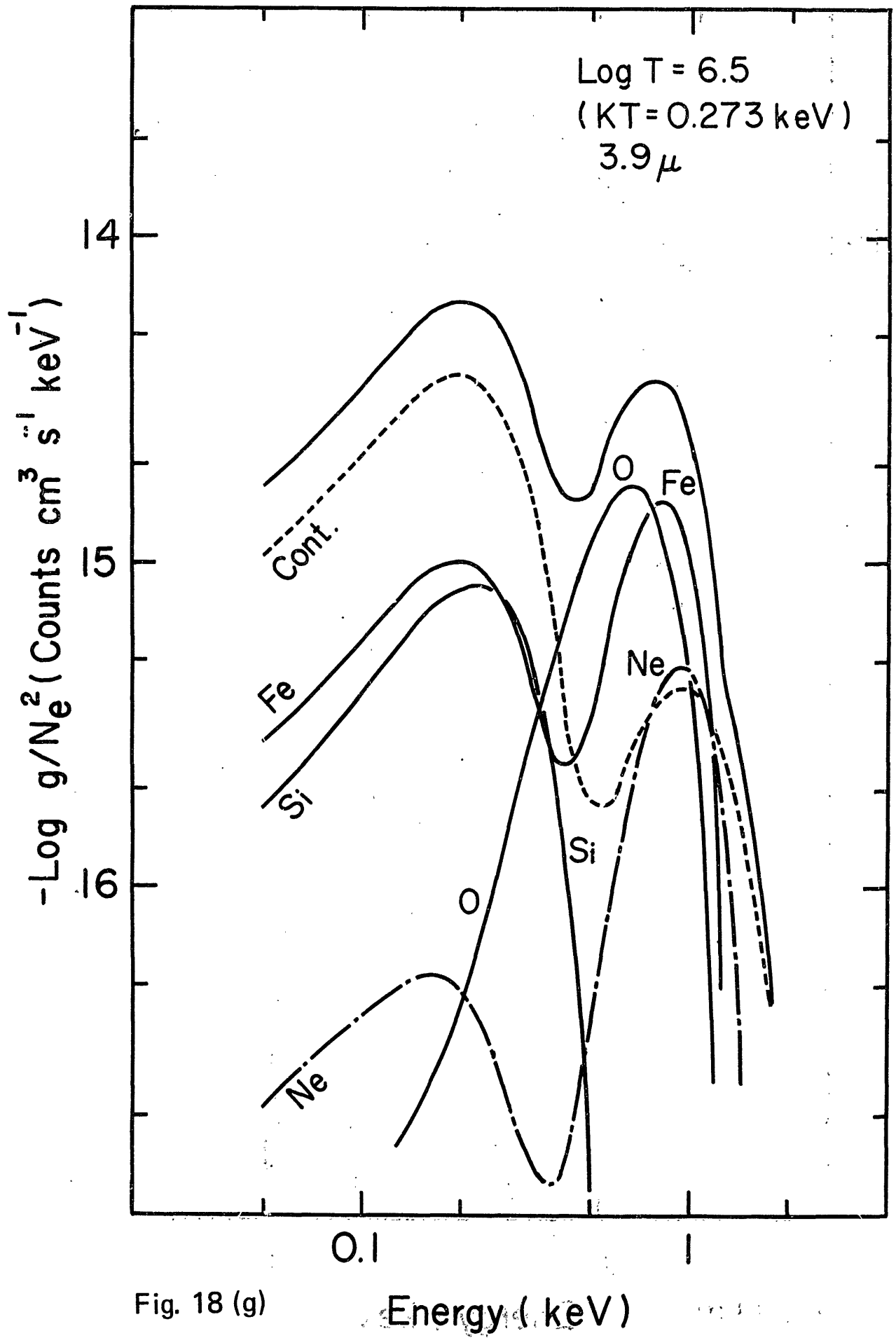


Fig. 18 (g)

Energy (keV)

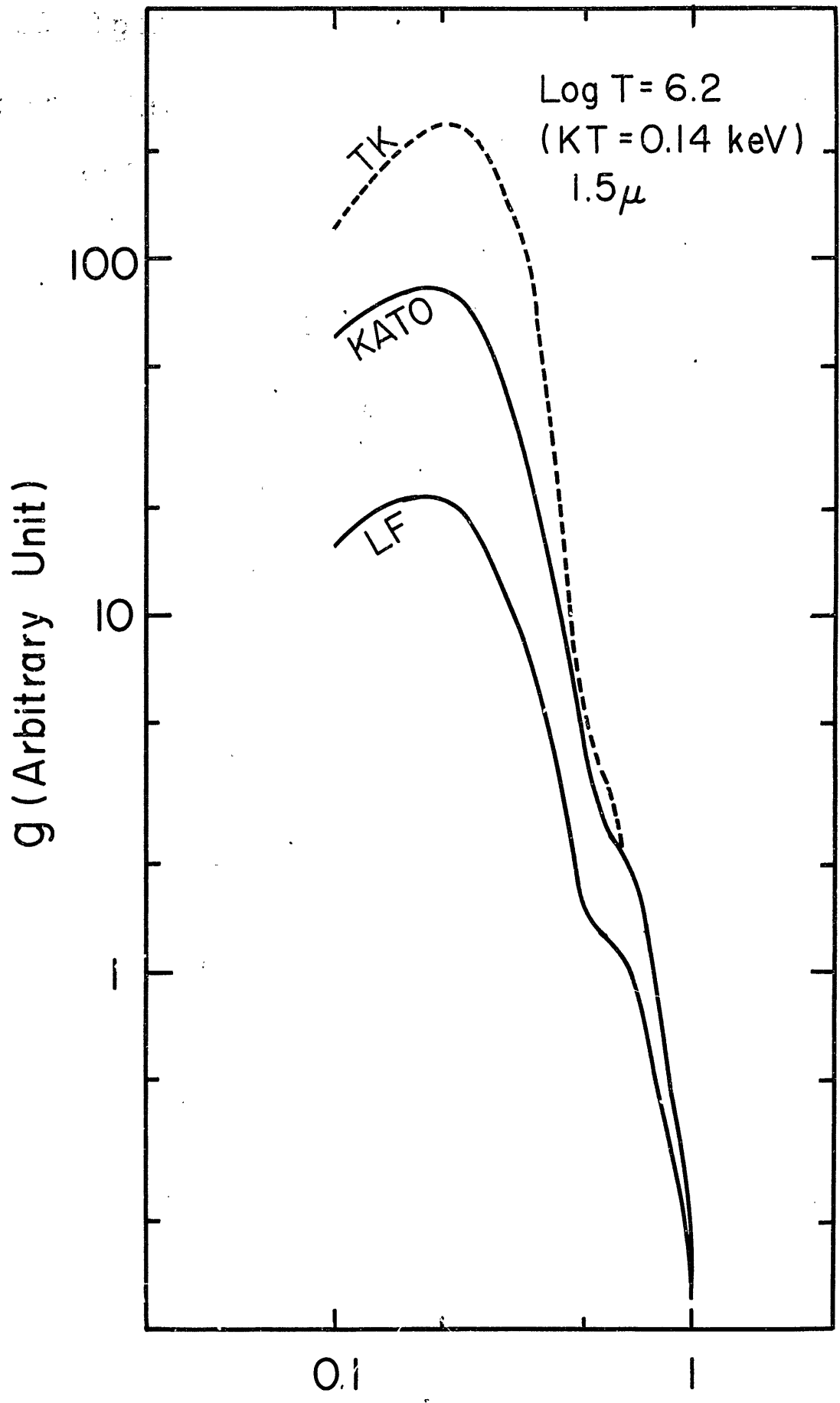


Fig. 19

Energy (keV)

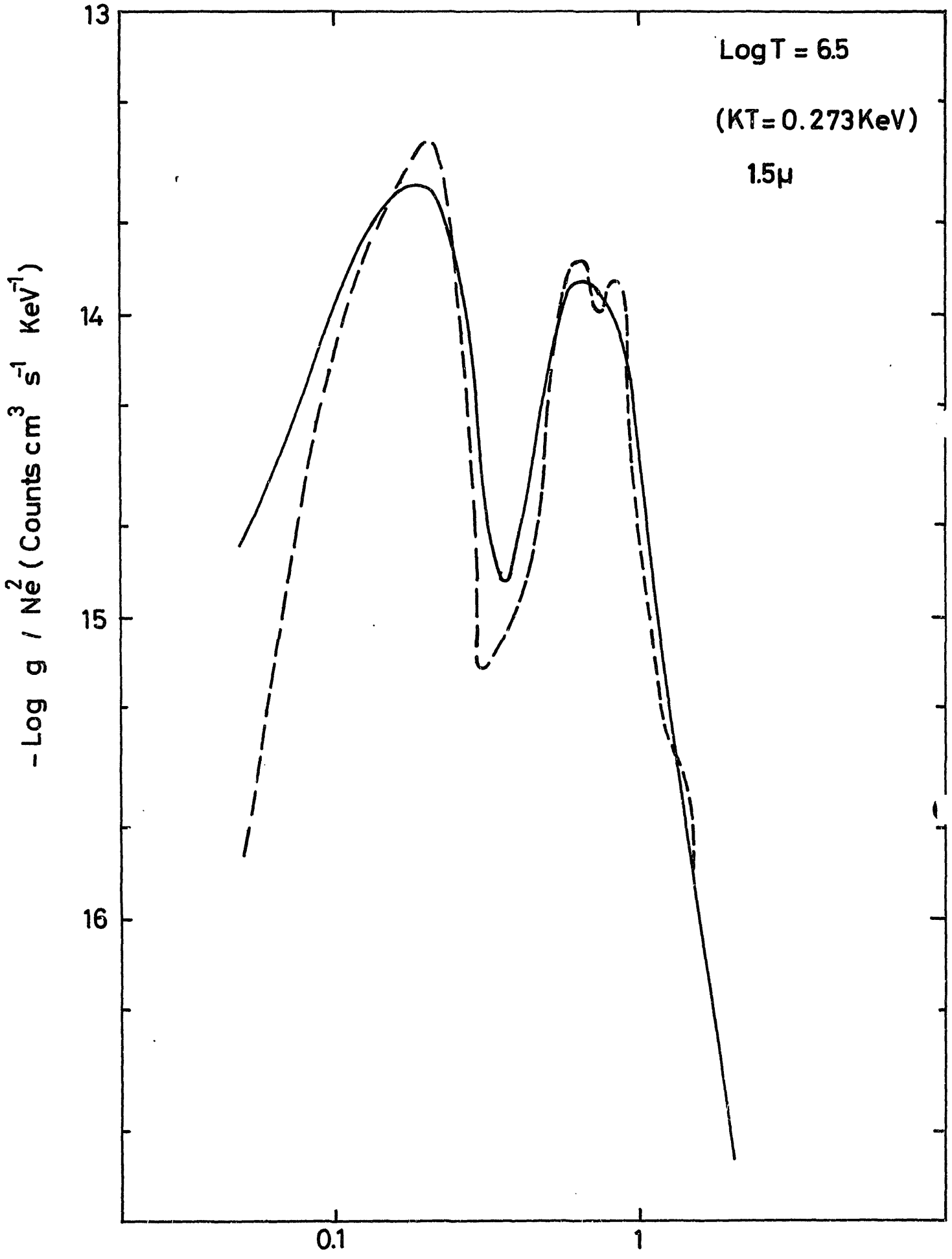


Fig. 20

Energy (KeV)

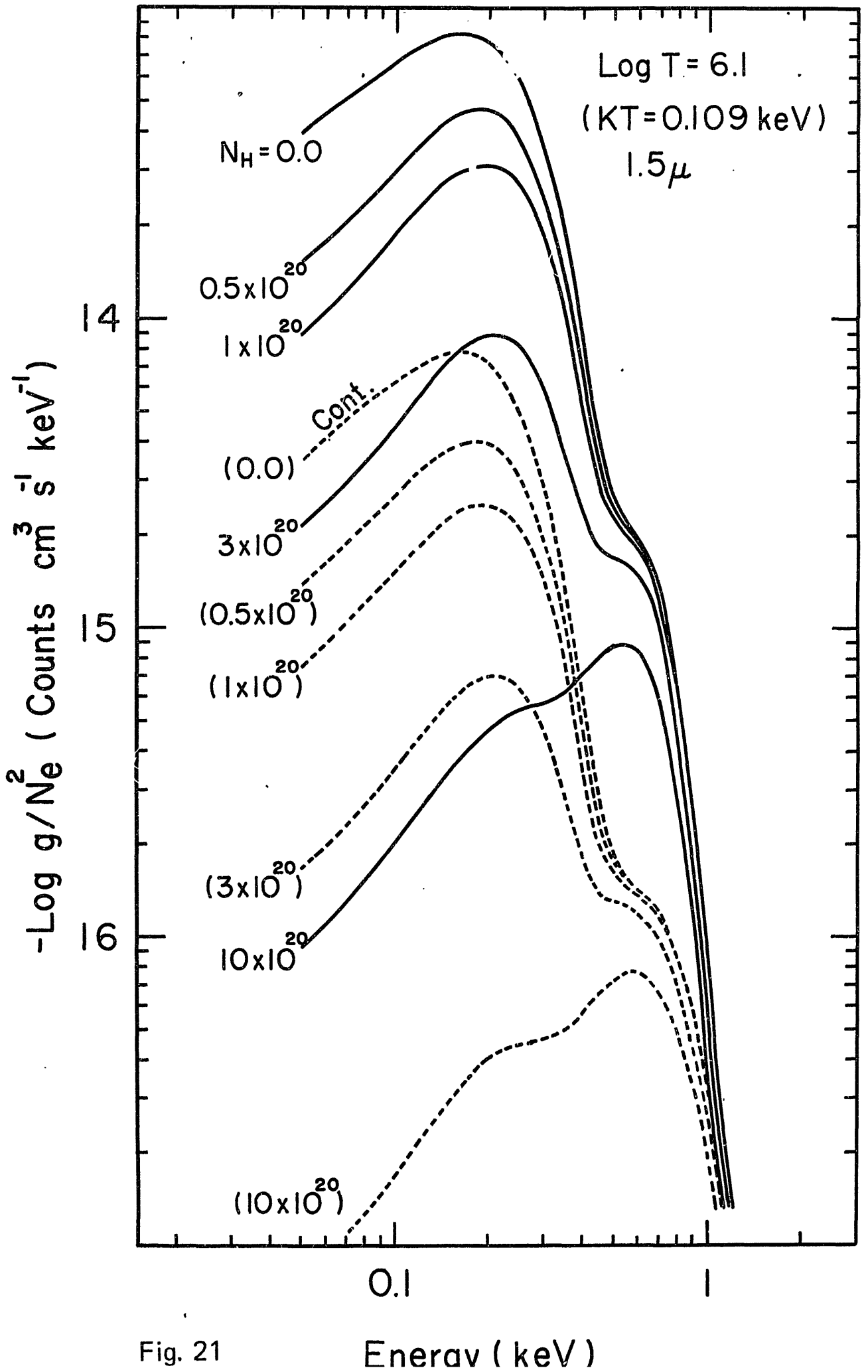


Fig. 21

Energy (keV)